AES/PE/14-36

Title: Petrophysical quantification of Utah reservoir sandstones and cap-rocks naturally exposed to CO_2 fluid fluxes by use of high-resolution Micro CT

Date: 30 October 2014

Name: Shailesh R. Kisoensingh

Title : **Petrophysical quantification of Utah reservoir sandstones and cap-rocks naturally exposed to CO_2 fluid fluxes by use of high-resolution Micro CT**

Author(s) : Shailesh R. Kisoensingh

Date : 30 October 2014
Professor(s) : Prof. P.L.J.Zitha
Supervisor(s) : Dr. A.Barnhoorn
TA Report number : AES/PE/14-36

Postal Address : Section for Petroleum Engineering
Department of Geoscience & Engineering
Delft University of Technology
P.O. Box 5028
The Netherlands
Telephone : (31) 15 2781328 (secretary)
Telefax : (31) 15 2781189

Preface & Acknowledgement

This report has been written as a graduation thesis of the master track Petroleum Engineering of Delft University of Technology. After following curses in Petrophysics, conducting my BSc. thesis in Petrophysics and assisting in the BSc. field development project, I have developed personal interest in Petrophysics. Due to my personal interest in Petrophysics, I talked to Dr. Auke Barnhoorn. He offered me an interesting project regarding artificial CO_2 storage by use of Micro CT technique on naturally precipitated CO_2 in eolian sandstones. Dr. Auke Barnhoorn became my supervisor, while Prof. Dr. Pacelli Zitha is the committee professor. I am thankful to the supervisors for all the input and feedback. Dr. Auke Barnhoorn is in my opinion an ideal supervisor and I enjoyed working with him and recommend him as a supervisor. I would also like to thank all others who supported this project in their own way like Karel Heller (lab), Dik Delforterie (cores), Joost van Meel (Avizo), Wim Verwaal (Micro CT), Ellen Meijvogel-de Koning (Micro CT) and Dr. Karl-Heinz Wolf (general input). My parents and girlfriend also deserve my thankfulness for their support. Thank you all for this interesting and fun research. Note that various graphs will not appear clear if printed out in black and white.

Index

Abstract

CO_2 emission is increasing globally, resulting in a global increase in temperature and as a result climate change. CO_2 storage in the subsurface is an option/ transitional measure to reduce CO_2 in the atmosphere and mitigate the climate change issue. Generally, for CO_2 storage to be a viable option, it must be ensured that the stored gasses should be at least 10.000 years safe in the subsurface. Simulating long-term storage of CO_2 in the laboratory for 10.000 years in storage experiments is not feasible and therefore a good option is to analyze rock samples that have naturally been exposed to CO_2 for such a large time frame. Such a CO_2 aquifer can be found in eolian sandstones in Utah, USA. Due to the occurrence of fractures in these sandstones, CO_2 bearing water has flown through these sandstones resulting in possible reaction and carbonate precipitation in the pores. In this study, the main points of interest are the determination of volume fractions of various components like porosity, carbonate precipitation close to and far from the fractures, by the use of Micro Computed Tomography (Micro CT). Micro CT results are compared to conventional lab (macroscopic) technology. The ultimate goals of this research are gaining actual insight/ data on what the result is if CO_2 storage is conducted and insight and recommendation regarding the use of Micro CT technology. The first conclusion on results regards calibration. Calibration difficulties in Micro CT technique generate noise. If calculating the fraction of components, noise has no influence on the fraction result. If connectivity analysis is conducted, noise will influence the result and should therefore be filtered. Sensitivity analysis for resolution shows that 2.5 μm is a suitable resolution to image these eolian sandstones and the smaller the samples are the higher resolution can be acquired. Lab based methods for porosity (Pycnometer, Wet Test and Hg Shell Test) generally agree with each other. The image based methods (2D and 3D) also agree with each other. The lab based methods and image based methods do not exactly agree with each other. The correlations regarding permeability, porosity and particles per volume show exponential relations. After conducting 3D grain analysis, the effect of carbonate precipitation is quantified. Because of the precipitation between grains, the grains tend to 'deform', which creates higher surface area and volume. *The exact influence of a fracture on carbonate precipitation can be summarized to be minimal. In the case of sample car614 the influence is clearly seen, but in all other samples the fracture seems to have had no influence or overruled by other (depositional) phenomena.*

Introduction

CO_2 emission is increasing globally, resulting in climate change i.e. global temperature increase (Technical Summary IPCCAR4 (2007)). Figure-1 illustrates the annual CO_2 change versus time, while figure-2 illustrates the mean temperature and difference versus time. Both figures show an increasing trend of CO_2 concentration and mean temperature with time.

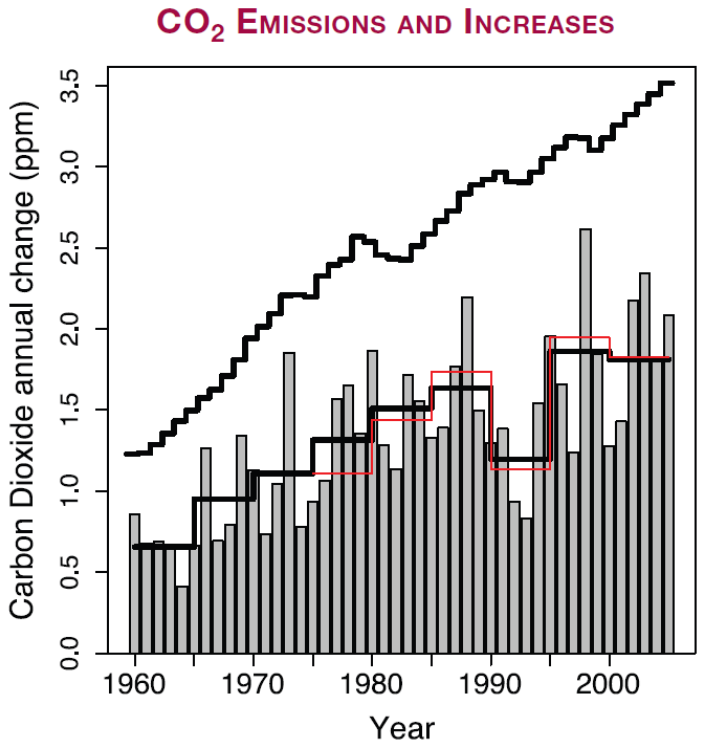

Figure-1: Carbon dioxide annual change vs. time (Technical Summary IPCCAR4, 2007)

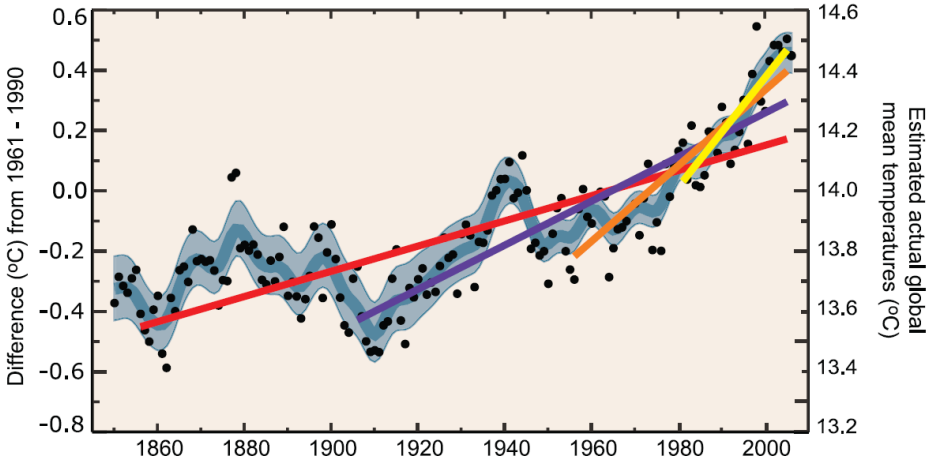

Figure-2: Estimated mean temperature and difference vs. time. Different trend lines indicate different domains of time (Technical Summary IPCCAR4, 2007)

Various climate protocols prescribe that the general solution is to decrease CO_2 emission. Decreasing CO_2 emission is generally not easy, because this implies global reduction of energy intensity, which is not easy with the global growth of population. Alternatively, CO_2 storage in the subsurface is an option. By storing the emitted CO_2 under controlled conditions in the subsurface, less CO_2 will be present in the atmosphere. Netherlands as one of the many countries has to reach a goal regarding sustainable energy and climate issues. CO_2 storage is therefore seen as a transitional measure in order to achieve certain sustainable and climate goals (co2-cato.nl). Ongoing projects regarding gas (fossil gasses) storage in the Netherlands are the TAQA gas storage project in Bergermeer (gasopslagbergermeer.nl). The world's first commercial CO_2 storage project is the Sleipner CO_2 storage project (Benson et al. (2003)). Located in the North Sea in the Norwegian part, Statoil as the national state oil company of Norway produced natural gas from the Sleipner gas field. The gas contained up to 9% of CO_2, which exceeds the 2.5% rule to be allowed to escape in the atmosphere. Statoil started research in order to inject CO_2 in the produces field, which finally led to the storage of 10 million tons of CO_2 (Benson et al. (2003)).

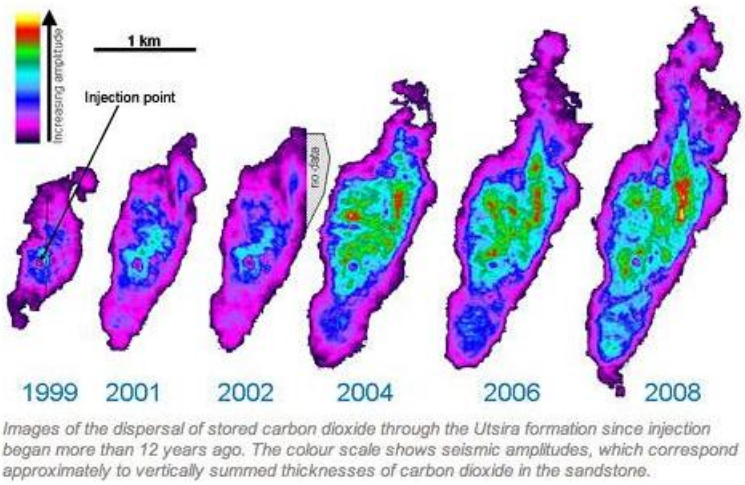

Figure-3: CO_2 storage models in the Sleipner field with time (http://www.energy-pedia.com/news/norway/statoilhydros-sleipner-carbon-capture-and-storage-project-proceeding-successfully)

Figure-3 illustrates the result of CO_2 storage in the Sleipner field for about 9 years (10 million tons).

Various minerals are formed during the storage process. The main mineral formed is calcium carbonate. Due to CO_2 storage, water and calcium minerals in water follow a certain equation, which represents the calcium carbonate formation (Barke et al. (2012)).

$$CO_2 + 3H_2O + Ca^{2+} -> CaCO_3 + 2H_3O^+$$

Generally, for CO_2 storage to be a viable option, it must be ensured that the stored gasses should be at least 10.000 years (Holland & Gilfillan (2002)) safe in the subsurface. Simulating long-term storage of CO_2 in the laboratory for 10.000 years in storage experiments is not feasible and therefore a good option is to analyze rock samples that have naturally been exposed to CO_2 for such a large time frame. Such an aquifer can be found in eolian sandstones in Utah, USA.

In June 2012 drilling activities have been initiated nearby Green River city in the Colorado plateau in the state of Utah. In this context, non hydrocarbons reservoirs are the main focus i.e. CO_2 'bearing' sandstones. Due to the occurrence of fractures in these sandstones, CO_2 bearing water has flown through these sandstones resulting in possible carbonate precipitation.

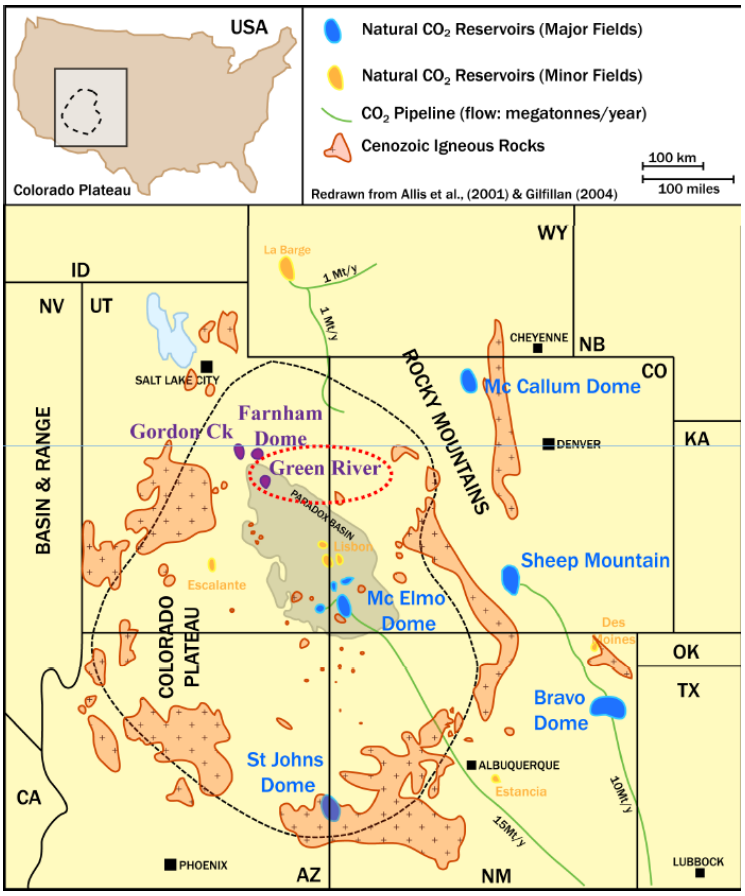

Figure-4: Location of the Colorado plateau, Utah, USA (Courtesy of Kampman, Niko)

Figure-4 shows the location of the Colorado plateau, natural CO_2 reservoirs and CO_2 pipelines in this area. The blue spots are major CO_2 reservoirs, while the yellow ones are small CO_2 reservoirs.

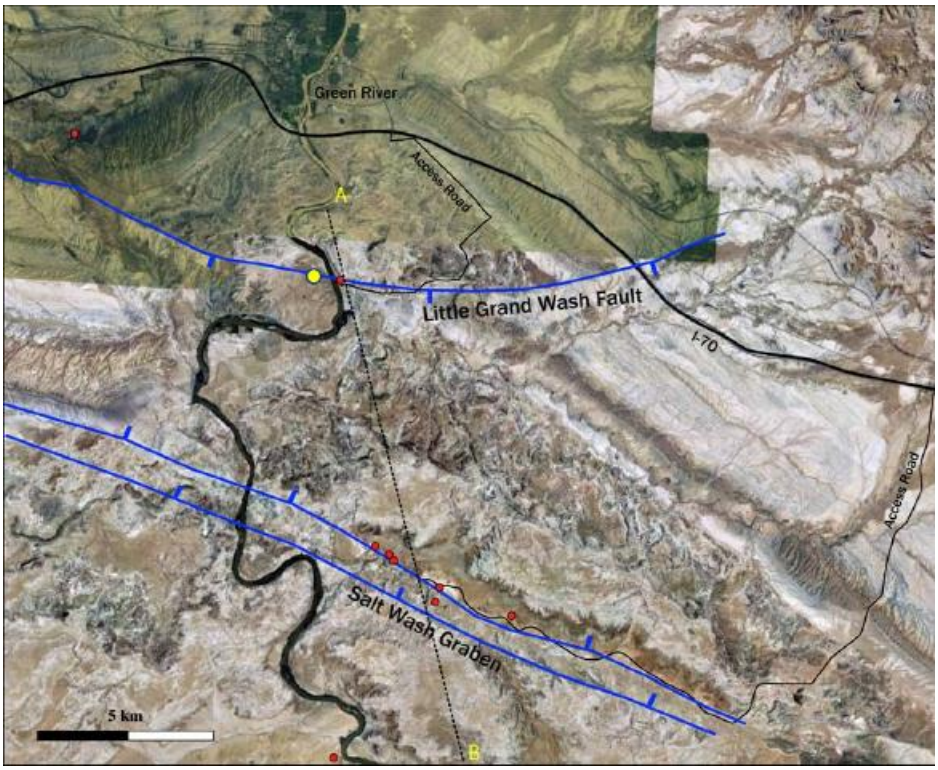

Figure-5: Location of the drill site in the Colorado plateau. Utah, USA (Courtesy of Kampman, Niko)

Figure-5 shows the location of the drill site (yellow spot) in the Colorado plateau. The black meandering line is the Green river. The drill site is near a normal fault called the 'Little Grand Wash Fault', which is indicated in blue and dips in southern direction. Mainly through this fault, CO_2 has been escaping for hundreds of thousands of years.

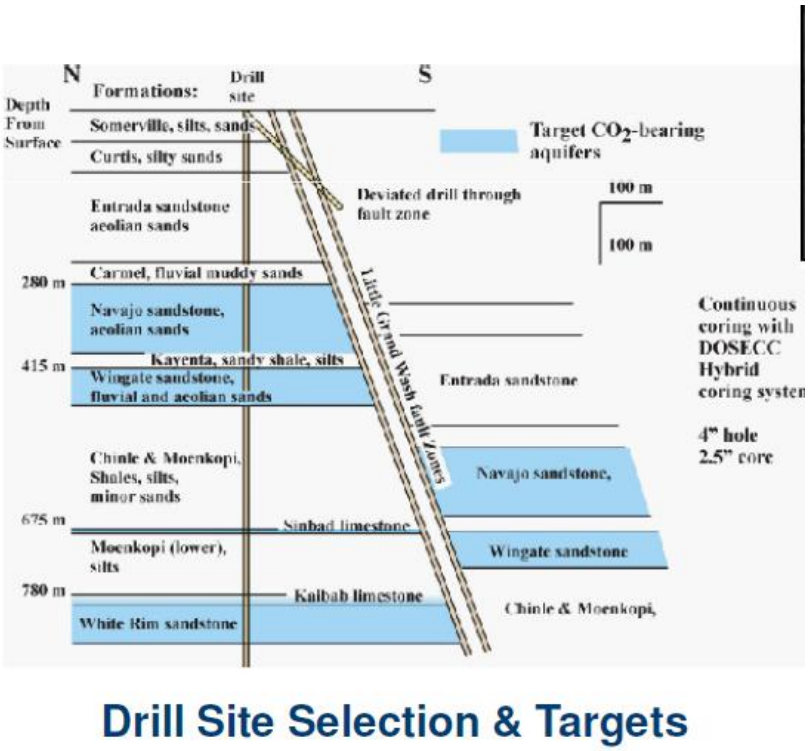

Figure-6: Cross section of well path drilled in June 2012 (Courtesy of Kampman, Niko)

Figure-6 shows the cross section of the well path. The main formations of interest are the Entrada formation and the Navajo Formation. The blue colour indicated possible CO_2 bearing reservoirs.

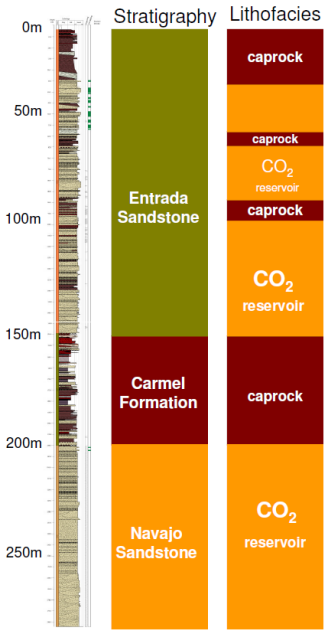

Figure-7: Formations of interest in Colorado Plateau, Utah, USA (Courtesy of Kampman, Niko)

Figure-7 gives the 300 m long core of the formations of interest. The Navajo Formation is a CO_2 bearing reservoir, while the Entrada Formation is an alteration of CO_2 bearing reservoir and cap rock. The Carmel Formation is a cap rock in between the Entrada and Navajo formations.

All data generated from the drilling activities is analyzed by a cooperation of stakeholders. Every stakeholder has a speciality and analyzes the data based on its speciality. This is schematically seen in figure-8.

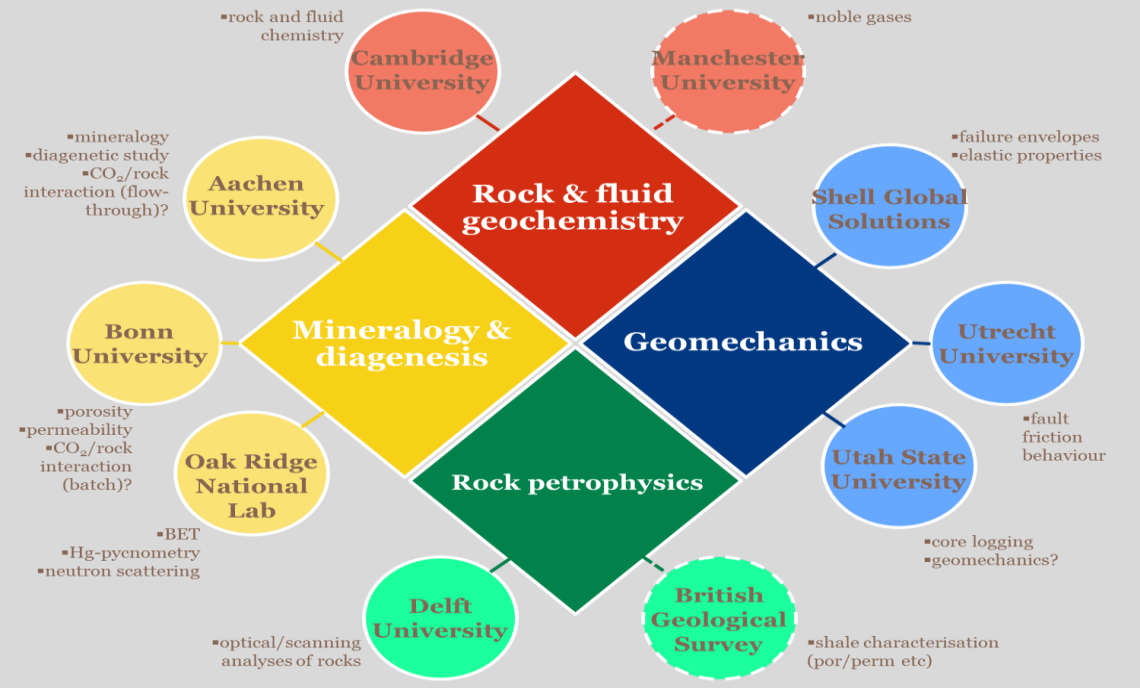

Figure-8: Cooperation Scheme with various specialities (Courtesy of Kampman, Niko)

The main task of this thesis is to petrophysically quantify these 3 formations, based on cores which have been collected at various stratigraphic depths. The distribution of the available cores is seen in figure-9.

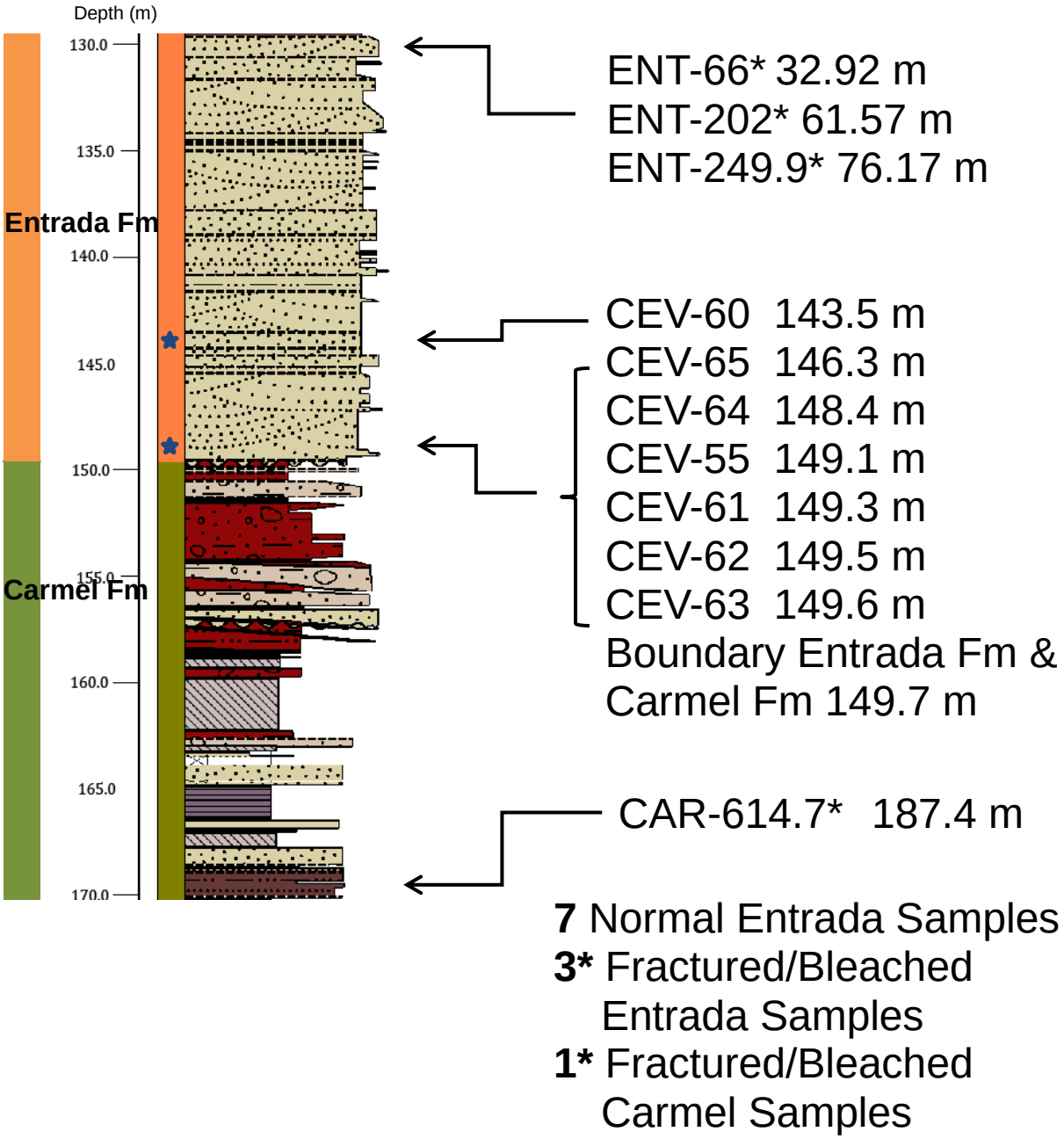

Figure-9a: Sample distribution for Entrada & Carmel Formations (Kampman et al., 2013)

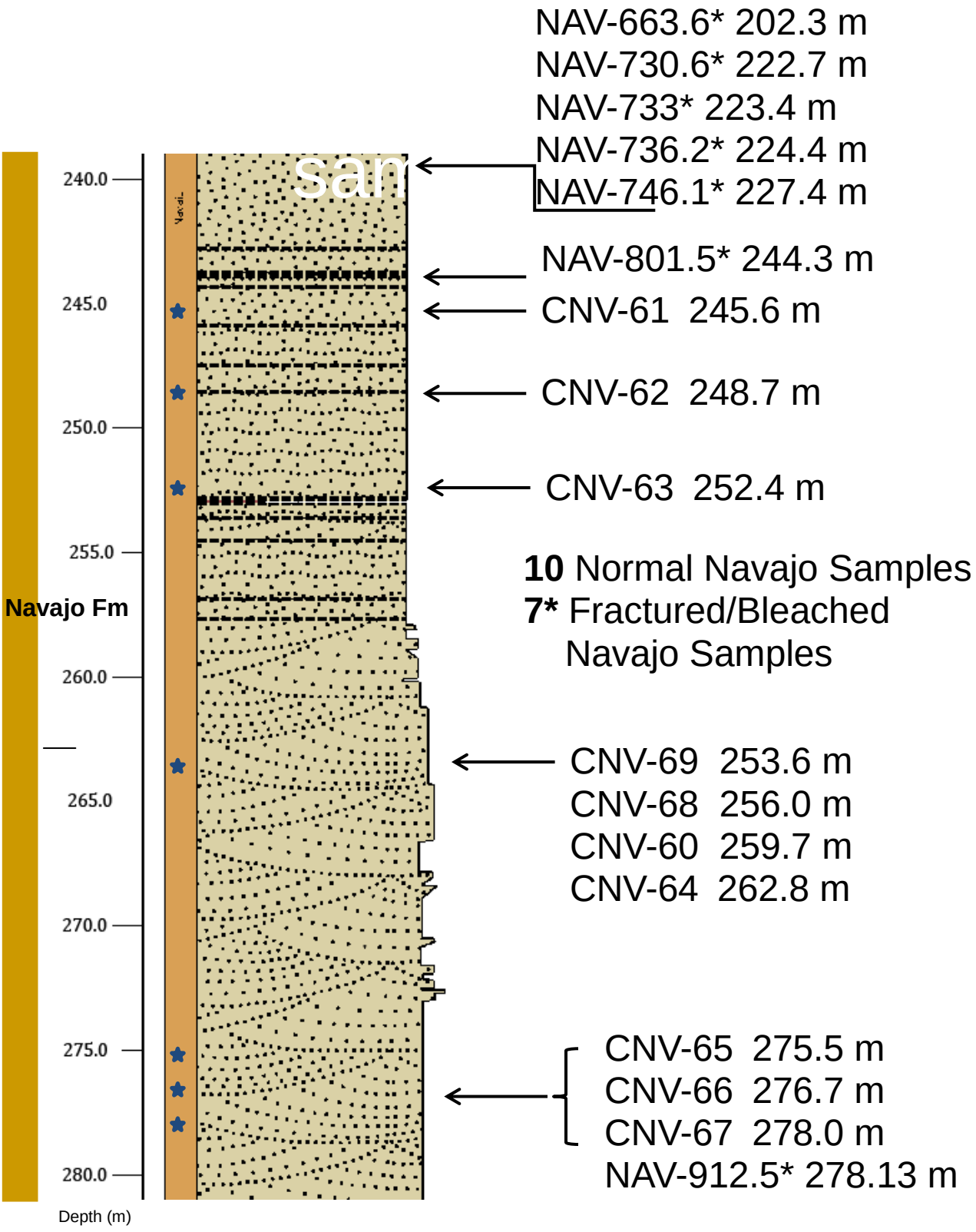

Figure-9b: Sample distribution for Navajo Formation (Kampman et al., 2013)

Totally there are 17 normal samples (batch-1). With normal samples is meant that the samples have no irregular surfaces and neat core plugs can be obtained from them in order to conduct macroscopic bulk experiments in the lab.

Figure-10: 'Normal' samples which are not altered by fracture planes

The 11 other samples (batch-2) are fractured and/or bleached and have surface irregularities. To obtain 'neat' cores for macroscopic lab experiments is not possible. These samples will only be used for microscopic analysis. Attachment_Pictures_Irregular.doc contains all the photos of the irregular samples.

Research objectives/ goals

The ultimate goals of this research are:

- The actual insight on what the result is if CO_2 storage is conducted.
- Insight and recommendation regarding the use of Micro CT technology.

Points of interest are:

- Fractions of various components like porosity, carbonate etc.
- Carbonate precipitation close to and far from the fractures.
- Use of relative new technology: Micro Computed Tomography (Micro CT) to analyze samples on microscopic scale.
- Comparing conventional lab (macroscopic) technology with Micro CT technology.

Chapter-1: Geological Quantification

Introduction

The 300 meter long Jurassic core is interpreted by a geologist and gives an idea about the depositional environment and facies (courtesy of Kampman, Niko).

Theoretical Description

The first top of the core (0-149.7 m) is called the Entrada Formation. The depositional environment can be characterized as eolian dune deposits. This formation generally contains siltstones, sandstones, inter-bedded siltstones by sandstones. The sandstones can be distributed in cross-bedded sandstones and ripple-bedded sandstones and can be characterized as a reservoir, based on the sandstone content (Courtesy of Kampman, Niko).

The middle part of the core (149.7-200 m) is called the Carmel Formation. The depositional environment can be characterized as fluvial. This formation generally contains siltstones, gypsum beds, shales & brecciated siltstones (with sandstone matrix) and can be characterized as a cap rock, based on the shale and gypsum content (Courtesy of Kampman, Niko).

The lower part of the core (200-300 m) is called the Navajo Formation. The depositional environment can be characterized as eolian. This formation generally contains cross-bedded sandstones, massive sandstones, silt and sands inter-bedded & ripple-bedded sandstones. This formation can also be characterized as a reservoir, based on the sandstone content (Courtesy of Kampman, Niko).

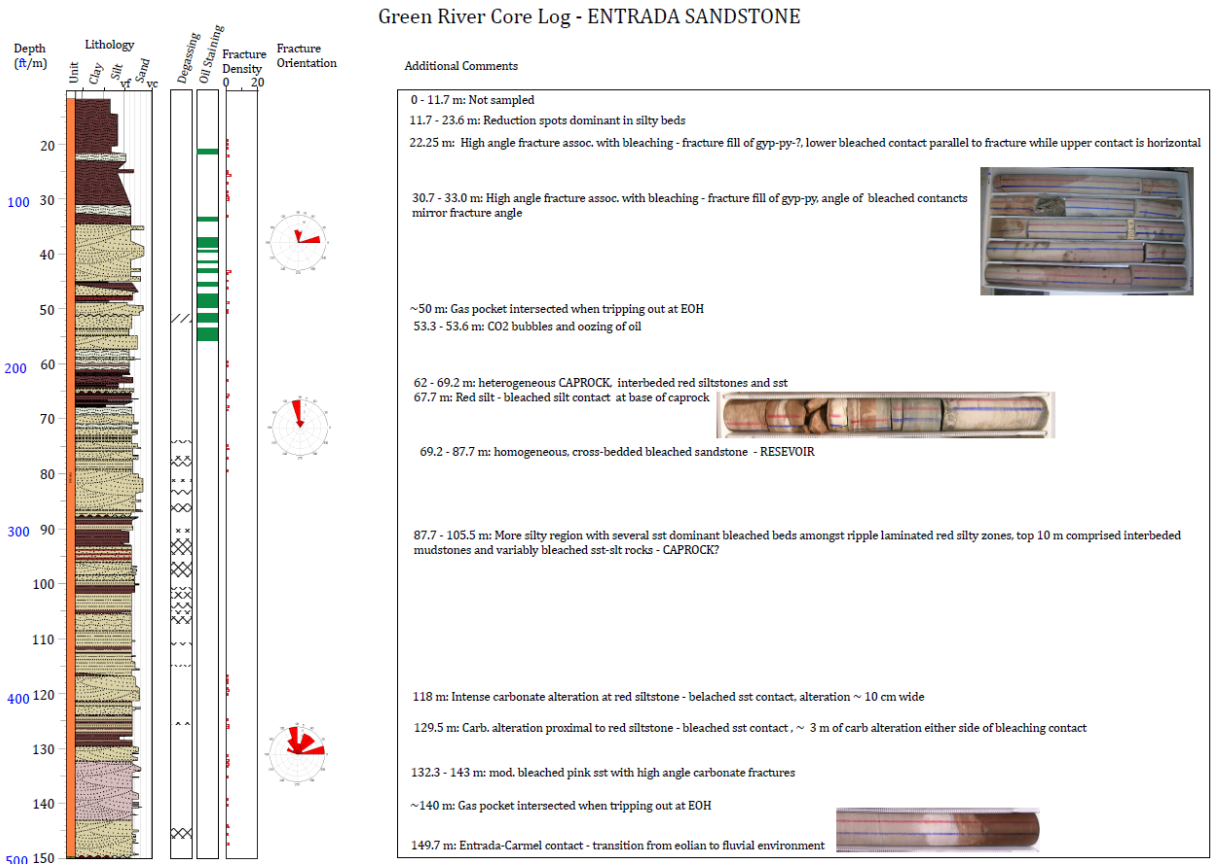

Figure-11: Detailed facies interpretation of Entrada Formation (Kampman et al., 2013)

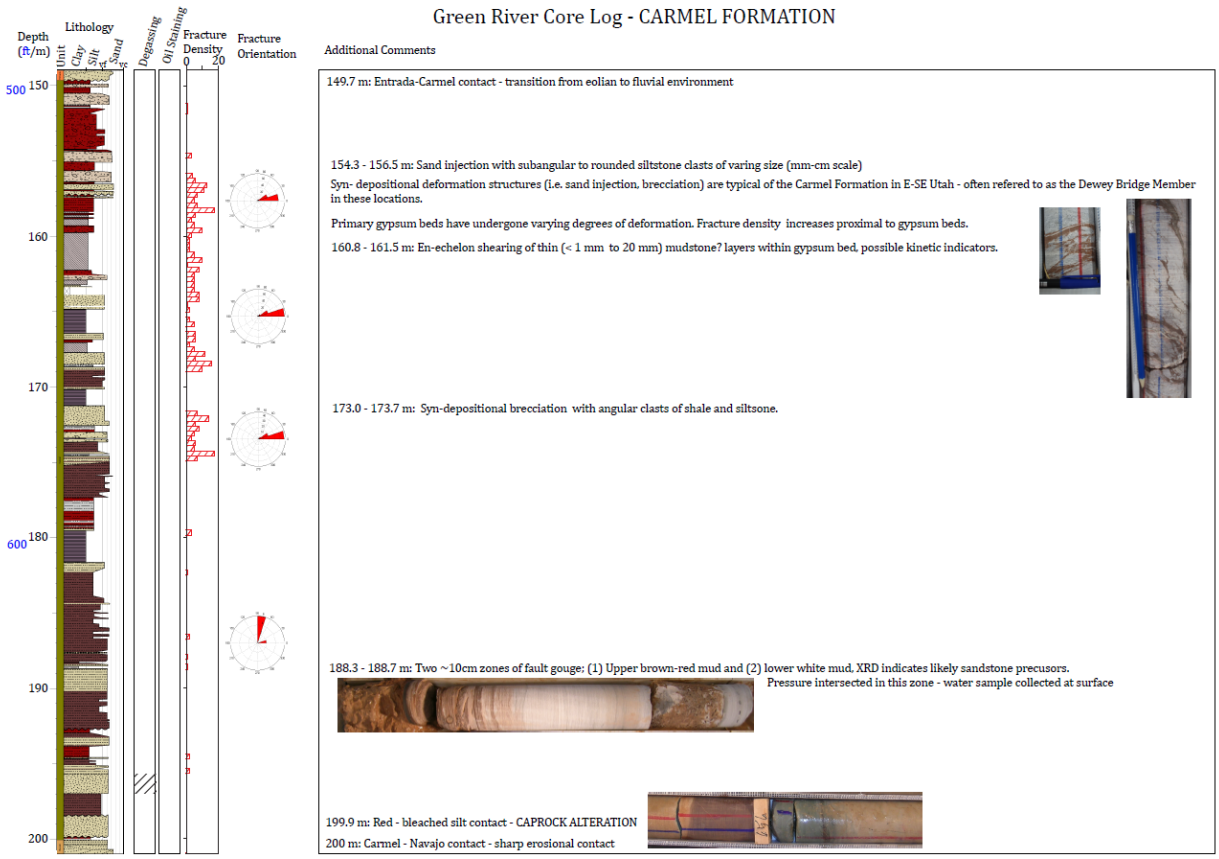

Figure-12: Detailed facies interpretation of Carmel Formation (Kampman et al., 2013)

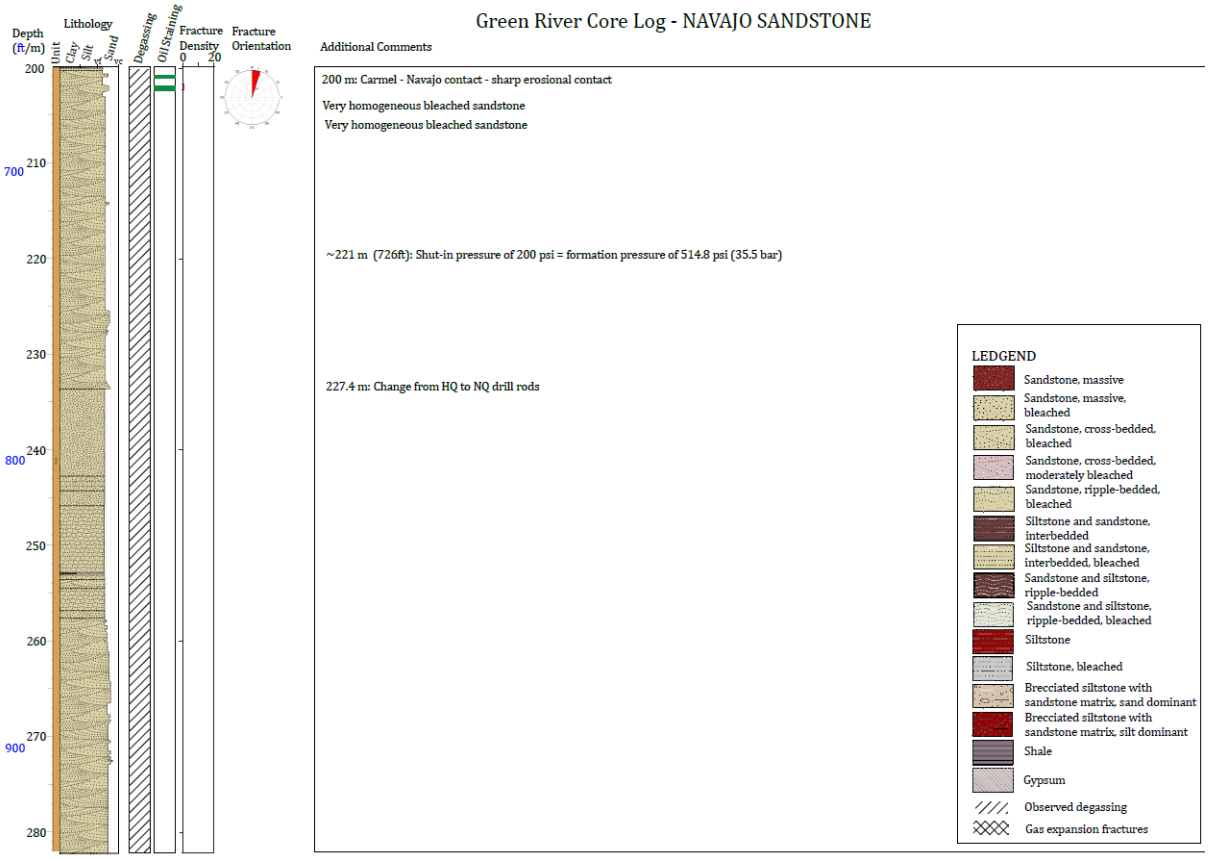

Figure-13: Detailed facies interpretation of Navajo Formation (Kampman et al., 2013)

Figure-10-13 illustrates the facies interpretation. Based on these figures, the Navajo Formation is a more homogenous formation if compared to the Entrada Formation. The cap rock is the most heterogeneous formation. These formations have been bleached by CO_2 bearing fluids (water) along the faults, which caused possible precipitation in the pores.

Based on the facies interpretation, every core can be assigned to a facies. This is illustrated in table-1.

Sample Code:	Sample Depth [m]:	Sample Depth [ft]:	Formation:	Facies:
CEV-60	143.50	470.80	Entrada	Ripple-bedded sandstone
CEV-55	149.10	489.17	Entrada	Ripple-bedded sandstone
CEV-61	149.30	489.83	Entrada	Ripple-bedded sandstone
CEV-62	149.50	490.49	Entrada	Ripple-bedded sandstone
CEV-63	149.60	490.81	Entrada	Ripple-bedded sandstone
CEV-64	148.44	487.00	Entrada	Cross-bedded sandstone
CEV-65	146.33	480.10	Entrada	Cross-bedded sandstone
CNV-60	259.72	852.10	Navajo	Cross-bedded sandstone
CNV-61	245.60	805.77	Navajo	Massive sandstone
CNV-62	248.70	815.94	Navajo	Ripple-bedded sandstone
CNV-63	252.40	828.08	Navajo	Ripple-bedded sandstone
CNV-64	262.80	862.20	Navajo	Cross-bedded sandstone
CNV-65	275.50	903.87	Navajo	Cross-bedded sandstone
CNV-66	276.70	907.81	Navajo	Cross-bedded sandstone
CNV-67	278.00	912.07	Navajo	Cross-bedded sandstone
CNV-68	256.06	840.10	Navajo	Ripple-bedded sandstone
CNV-69	253.62	832.10	Navajo	Ripple-bedded sandstone

Table-1a: Facies interpretation per core for normal samples (Kampman et al., 2013)

Sample Code:	Sample Depth [m]:	Sample Depth [ft]:	Formation:	Facies:
ENT-108*	32.92	108	Entrada	Ripple-bedded sandstone & siltstone (bleaching around fracture)
ENT-202*	61.57	202	Entrada	Siltstone & sandstone interbedded (Carbonated high angle fracture)
ENT-249.9*	76.17	249.9	Entrada	Cross-bedded sandstone (thick vein)
CAR-614.7*	187.36	614.7	Carmel	Siltstone & sandstone interbedded (bleached fracture)
NAV-663.6*	202.27	663.6	Entrada	Cross-bedded sandstone
NAV-730.6*	222.69	730.6	Entrada	Cross-bedded sandstone (high angle fracture)
NAV-733*	223.42	733	Entrada	Cross-bedded sandstone (high angle fracture)
NAV-736.2*	224.39	736.2	Entrada	Cross-bedded sandstone (high angle fracture)
NAV-746.1*	227.41	746.1	Navajo	Cross-bedded sandstone (high angle fracture)
NAV-801.5*	244.30	801.5	Navajo	Massive sandstone (high angle fracture)
NAV-912.5*	278.13	912.5	Navajo	Cross-bedded sandstone (high angle fracture)

Table-1b: Facies interpretation per core for *bleached/fractured samples (Kampman et al., 2013)

Chapter-2: Methodology

Paragraph-2.1: Porosity & Matrix Density determination based on Ultra Pycnometer

Introduction

The Ultra Pycnometer is an accurate device if compared to other water based devices. It is used to determine the matrix density and the matrix volume, which is used to calculate the porosity. This device is based on Boyle's Law, which utilizes gas flow (helium) through the core. Gas is much more mobile than liquid, which enables the gas to flow into the smallest pores present in the core.

Theoretical Description

Calibration of this device is done by homogenous solid spheres. The device has 3 sizes of cells (small, medium and large). Based on the dimension of the samples which had to be analyzed, the medium and large cells were used.

Figure-14: Ultra Pycnometer 1000, used to determine porosity

The initial step is to measure the length and the radius of the core. With these parameters the bulk volume of the core can be calculated.

Afterwards the dry mass of the core is measured. By running the gas through the core, the matrix volume is acquired from the Pycnometer. The Pycnometer saturates the cell with gas under a certain pressure and measures the amount of gas in the cell. By subtracting this amount of gas from the total cell volume, the matrix volume is obtained. By simply dividing the dry mass by the matrix volume, the matrix density is acquired, as illustrated with equation-1.

Eq-1: $\rho_m = \frac{M_d}{V_m}$, with ρ_m the matrix density, M_d the dry mass and V_m the matrix volume.

By subtracting the matrix volume from the bulk volume, the pore volume is obtained, resulting in the porosity, as illustrated by equation-2.

Eq-2: $\varphi_p = 1 - (\frac{V_m}{V_b})$, with φ_p the Pycnometer porosity, V_m the matrix volume and V_b the bulk volume.

The total workflow is illustrated by the below diagram:

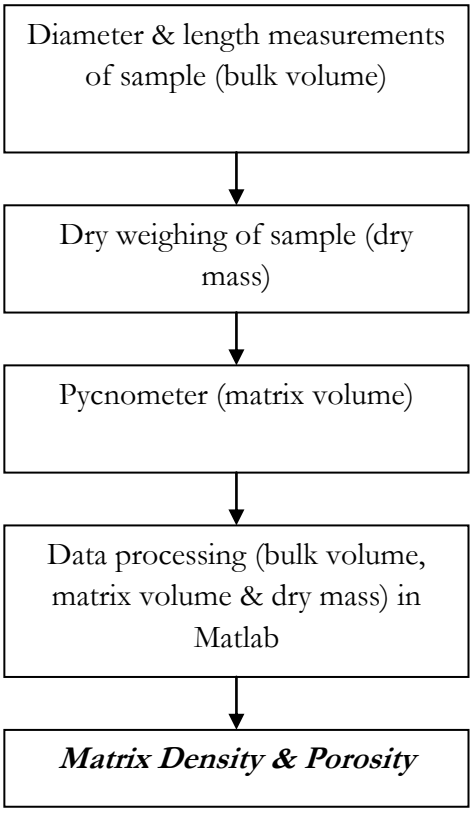

Diagram-1: Total workflow from dimension measurements to output

Paragraph-2.2: Porosity determination based on Archimedes (Wet Test)

Introduction

In contrast to the Pycnometer measurement, which is a dry process, the Archimedes test, also called the wet porosity test is conducted under submersed conditions. This method uses the dry mass, submerged mass of saturated sample, density of fluid and bulk volume of the core to generate a porosity value.

Theoretical Description

In order to conduct this method, the cores must be vacuumed, meaning that all air should be sucked out of the pores. If that has taken place the cores must be saturated with water in the vacuum tank. This enables water to go into the pores which are not filled with air anymore, causing the water saturation process to be more accurate then when saturating without pre vacuumed cores.

Figure-15: Wet test alignment, based on submersed samples to determine porosity

The above figure shows the tank in which cores are vacuumed. On top, the pump is connected and sucks the air out of the cylinder and thus the pores. The white cylinder is filled with water and is rotated if the cores are sufficiently vacuumed in order to saturate the cores. Afterwards the submerged mass of saturated sample is measured by weighing the cores under submersed condition with a mass balance on top of the tank tied to a core in the tank under water. This is illustrated in the figure below.

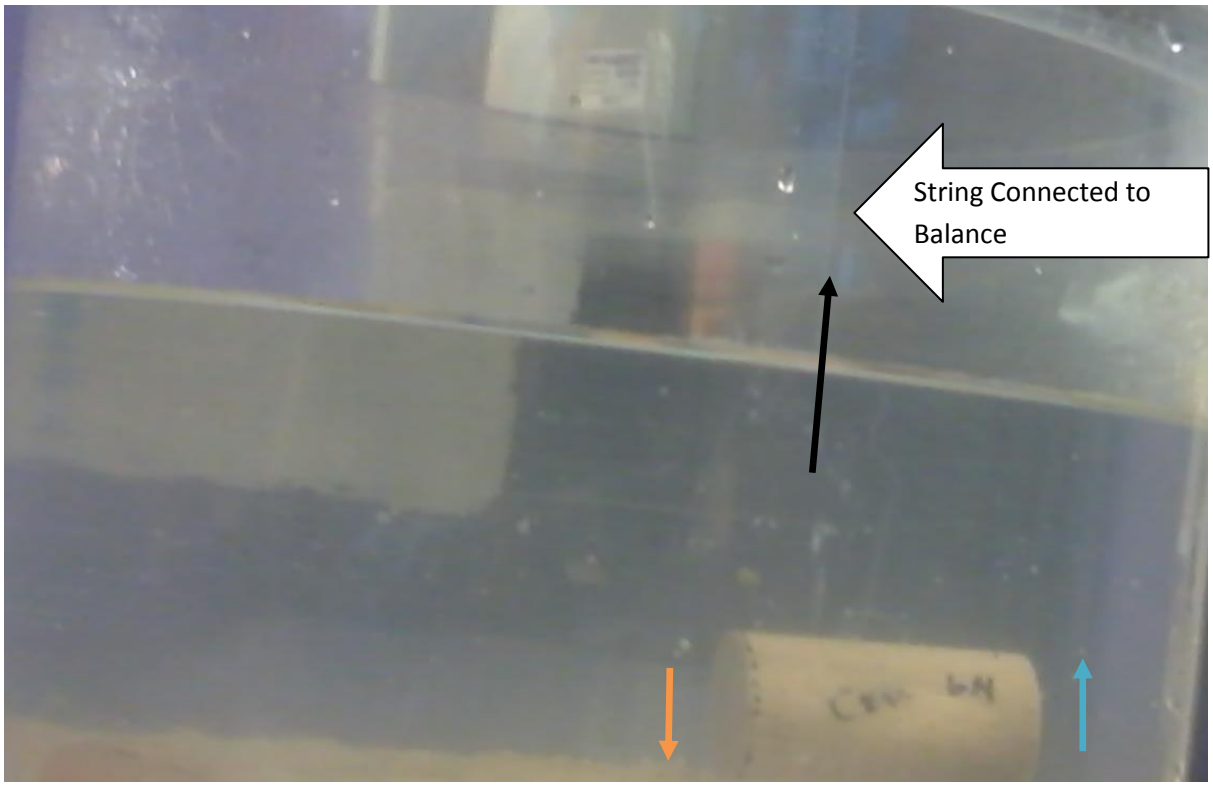

Figure-16: Weighing of cores under water to acquire submersed weight to determine porosity

In the weighing process the law of Archimedes plays an important role. This law states that the buoyancy force which works on the mass must be equal to the force of the replaced fluid. This must then be corrected for porous media. As seen in the above figure, there is a balance between the gravity force (F_g, orange), the buoyancy force (F_b, bleu) and the tensile force (F_t, black), resulting in equation-3.

Eq-3: $F_b + F_t = F_g$

Simple mechanics and Archimedes gives the definition of these forces, resulting in equation-4, 5, 6 and 7.

Eq-4: $F_b = \rho_w V_m g$

Eq-5: $V_m = (1-\varphi)V_b$

Eq-6: $F_t = M_w g$

Eq-7: $F_g = M_d g$

Combining these 4 equations, result into equation-8.

Eq-8: $\varphi_w = 1 - \frac{M_d - M_w}{\rho_w V_b}$, with φ_w the wet test porosity, M_d the dry mass, M_w the submersed mass of saturated sample, V_m the matrix volume and V_b the bulk volume.

The total workflow is illustrated by the below diagram:

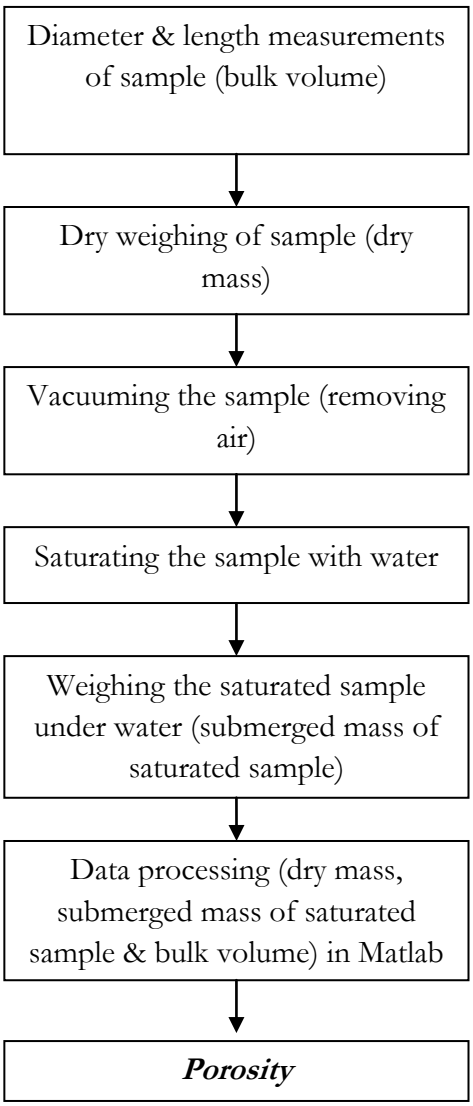

Diagram-2: Total workflow from dimension measurements to output

Paragraph-2.3: Porosity determination by Shell

Introduction

Royal Dutch Shell, as one of the stakeholders, has conducted porosity measurements in the same way as how the wet test (Archimedes) has been conducted. The difference is that Shell has used mercury instead of water and chloroform instead of a vacuum tank.

Paragraph-2.4: Porosity & other components determination based on 2D and 3D imaging in Avizo

Introduction

In order to acquire 2D and 3D image data, the Micro Computed Tomography (Micro CT) technique is used. This technique provides three dimensional images of the internal structure of an object, in this case rock samples.

Theoretical Description

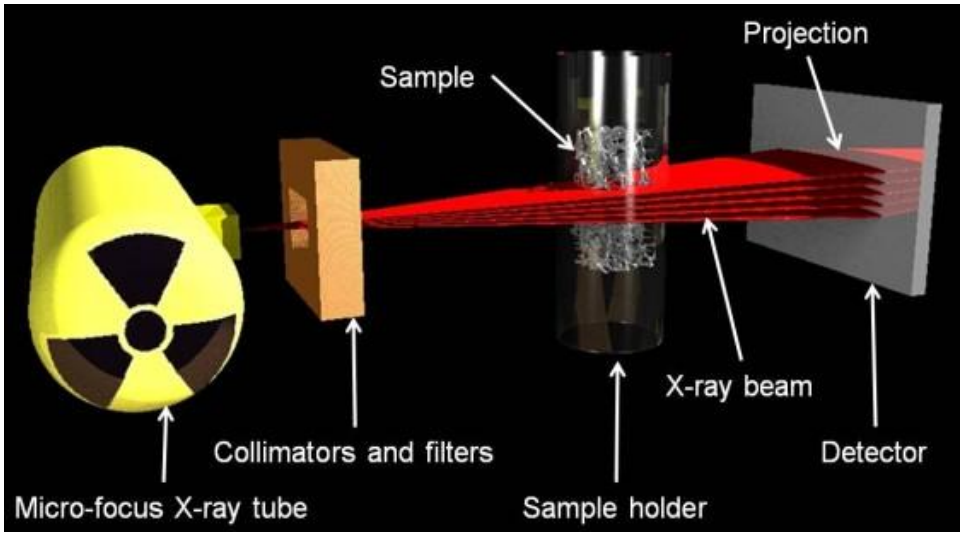

Figure-17a: Schematic of main components micro CT scan (www.b-cube.ch)

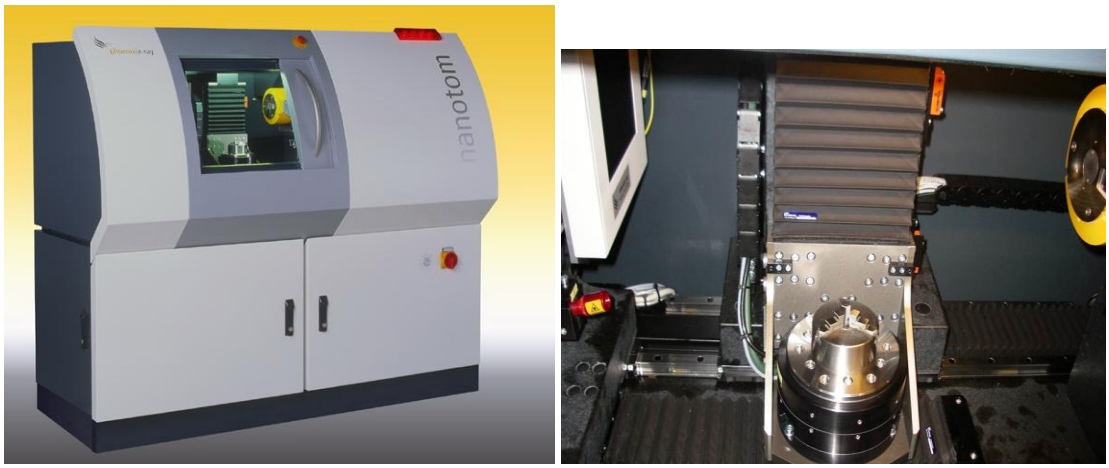

Figure-17b: Schematic of Nanotom scanner (courtesy of Wim Verwaal)

The Nanotom scanner can scan up to a maximum of 0.5 microns. Depending on volume size 5 minutes to 2 hours is needed for acquisition and reconstruction. The scanner is designed to scan

samples of maximum 1 kg, maximum 120 mm diameter and maximum 150 mm in height. The voltage and power of the X-ray tube is respectively 180 kV and 15 W.

The interaction of ionizing radiation like X-ray with matter is the basic physical principal of micro CT. This results in density contrasts. The rock sample is put between filters and a projection screen. In this situation 2D projections can be generated. The sample is then rotated along its axis and every degree or two a new projection is made. With this and a (median) filtering mechanism the 3D projections can be reconstructed. The result is the inner structure in 2D (pixels) and 3D (voxels).

The idea is to acquire a high resolution. As is known from the chapter of geology, the samples are eolian deposits, meaning very fine grained samples. Before the start of this thesis, a few scans were already made on a resolution of $2.5\ \mu m$, meaning that one single pixel (2D) and one single voxel (3D) is equal to $2.5\,\mu m$. For the cylindrical cores, diameters of $8\,mm$ are scanned and for more irregular samples, diameters of $4-5\,mm$ are scanned in order to acquire the $2.5\ \mu m$ resolution. To obtain high resolutions, the sample should be as small as possible. The smaller the sample, the easier it is to obtain high resolutions. For example, samples of 25 mm diameter will not be useful to create 2.5 microns resolution. In this case the highest possible resolution may be in the order of magnitude of 20 microns. There is a clear relationship between sample volume and resolution. This is depended on the size of the recording screen in combination with the width of the samples (Peterson, 2005).

The scans are made under certain scan settings. The detailed scan settings are documented in the attachment: Attachment_Scan_Settings.txt.

Reconstruction

As soon as the scans are made, the reconstruction process follows. This is done with reconstruction software, Phoenix Datos 2.0 Reconstruction Pro. The main tasks in this part are to select the sample volume that should be reconstructed and accounting for beam hardening, the so called beam hardening correction. Beam hardening is the most commonly encountered artefact in CT scanning, which results in more bright appearance of the edges of the sample in comparison to the centre. This is due to the distance the beam travels; the higher the distance is travelled, the more energy is lost. This energy loss is also dependent on the absorption of the used sample. High absorptive samples will lead to high energy lost. Firstly, the edges of the sample are encountered by the beam, resulting in high brightness. When the centre of the sample is encountered by the beam, the beam has already lost energy to the edges, resulting in less brightness. This contrast in brightness is referred as beam hardening. The applied beam hardening correction used is *9.5*. This is determined visually in combination with trial and error by checking the detection mechanism. As long the detection mechanism is not reasonable the trial and error process goes on. Fig. 17b shows the effect of beam hardening. The border lights up (high energy) in contrast to the middle part.

The reconstruction is done under certain settings. The detailed settings are documented in the attachment: Attachment_Reconstruction_Settings.txt.

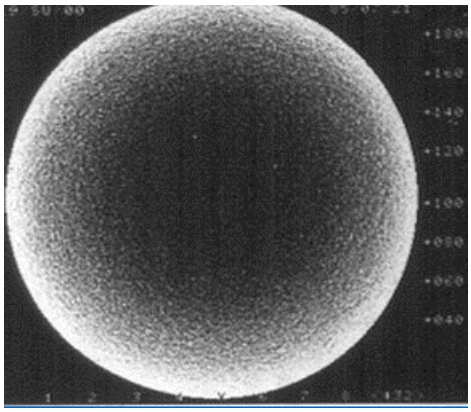

Figure-17c: Beam hardening effect. Border lights up in contrast to middle part.

Filtering

After the reconstruction process has taken place, the filtering process can be initiated. This is done with the VGStudio MAX 2.0 software. The main tasks in this software are to acquire geometrically cut volumes (triangle, squares, cylinders etc.) and filtering. The used geometry is the cylinder. The beam hardening correction in the reconstruction process is not a 100% perfect correction. If using the volume including the edges which have been altered by beam hardening, the result for example porosity shows erratic/ unrealistic values. By sufficiently cutting out the edges of the sample, so by getting rid of the altered zone, the beam hardening effect is left out. This is an important recommendation in processing CT data.

Lastly, the filtering is done by using a *median-5* filter. This has also been selected visually in combination with trial and error. Typically the above described process results in the below figure.

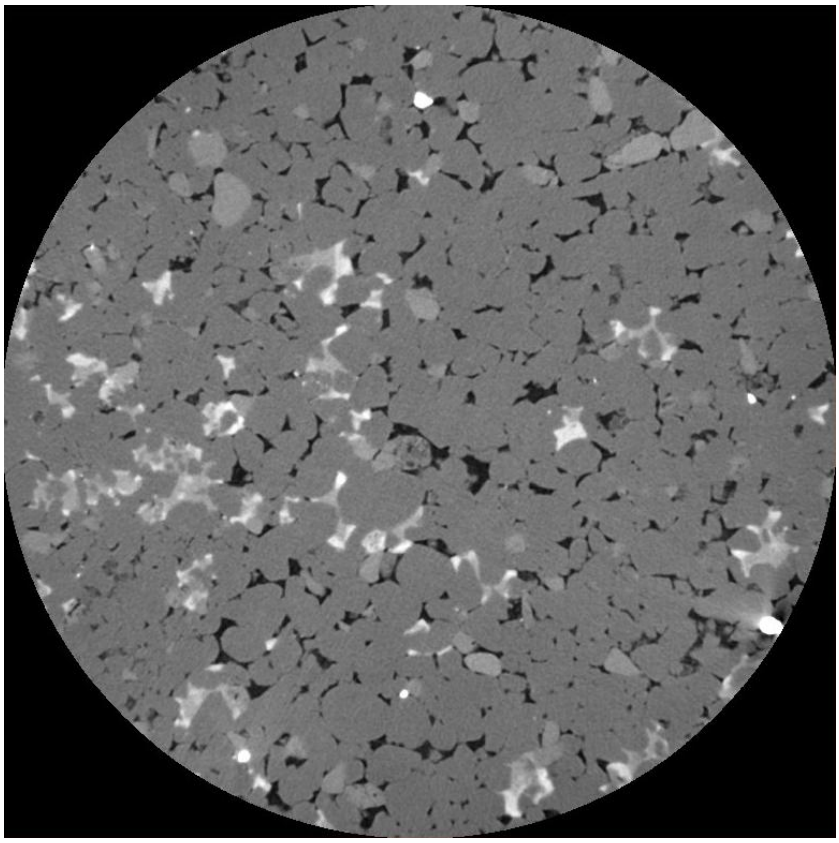

Figure-18: Result of micro CT scanning of 8 mm cores. This is a slice (2D).

As can be seen in figure-18, the colours range from white to black. Black means air, so very low density material, while white refers to metals, so extremely high dense materials. From this principle, the conclusions can be drawn, that black stands for porosity (air filled), dark grey stands for grains (silica), light grey for carbonate and white for heavy minerals (iron oxides, sulphides).

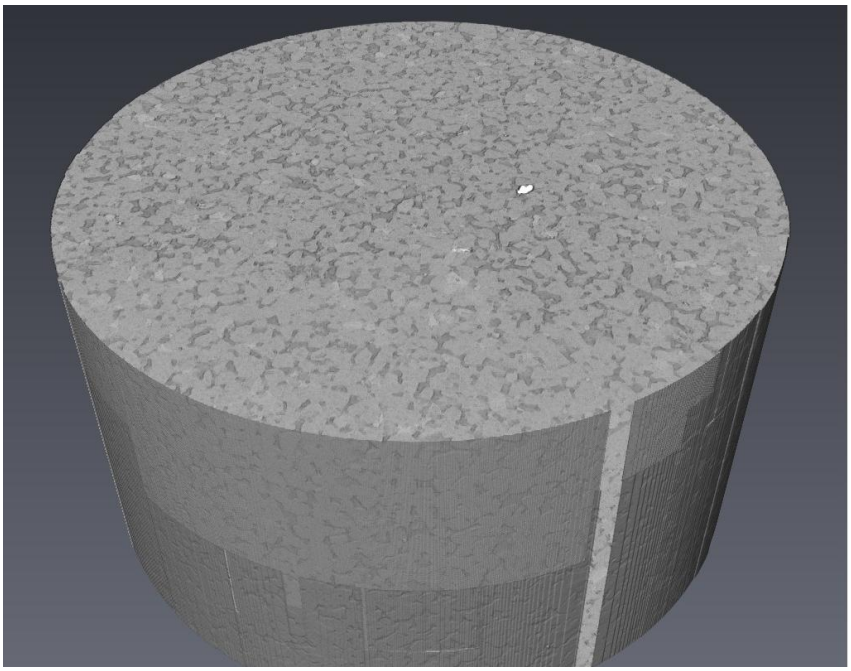

Figure-19a: Result of micro CT scanning of 8 mm cores. This is a volume (3D).

The next step is to acquire volume and area fractions for pore space, carbonate and heavy minerals. This is done in the imaging software program Avizo. After loading the micro CT scan reconstructions in Avizo, thresholding of specific ranges in greyscale levels has been done. Thresholding means detection of the components. Thresholding depends on the density, so on the colour (grey values). The grey values are represented in CT numbers in Avizo. When thresholding the pore space (black), all black material (same density) is detected. The same is valid for the thresholding of carbonate and heavy minerals. After the thresholding, the result is placed in a binary representation (binarisation) as seen in the figures below.

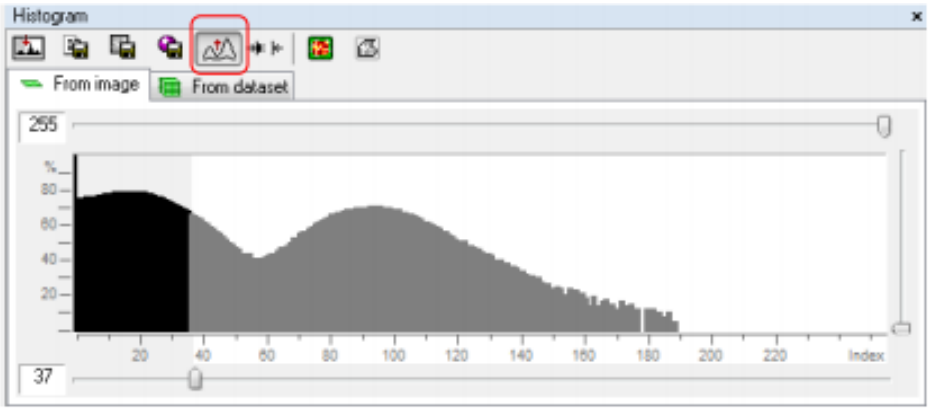

Figure-19b: Histogram of scanned samples. The peaks indicate the detection points of components. The first peak (left) indicates the detection point of the pore space, while the inverted peak indicates the carbonate detection point.

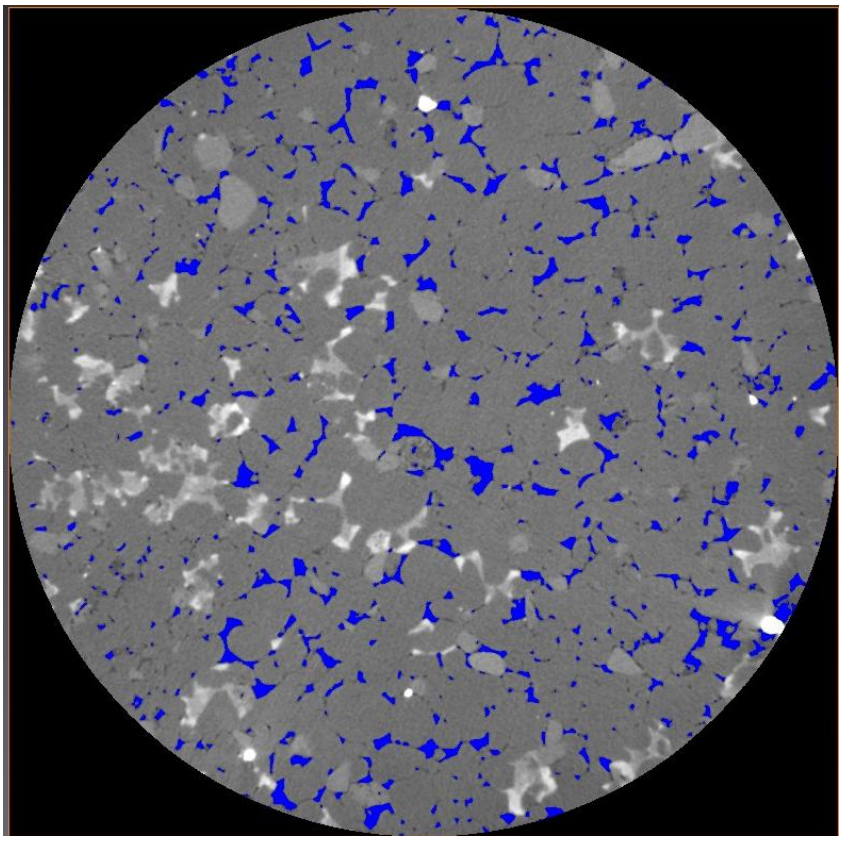

Figure-20: Result of pore space thresholding/ detection

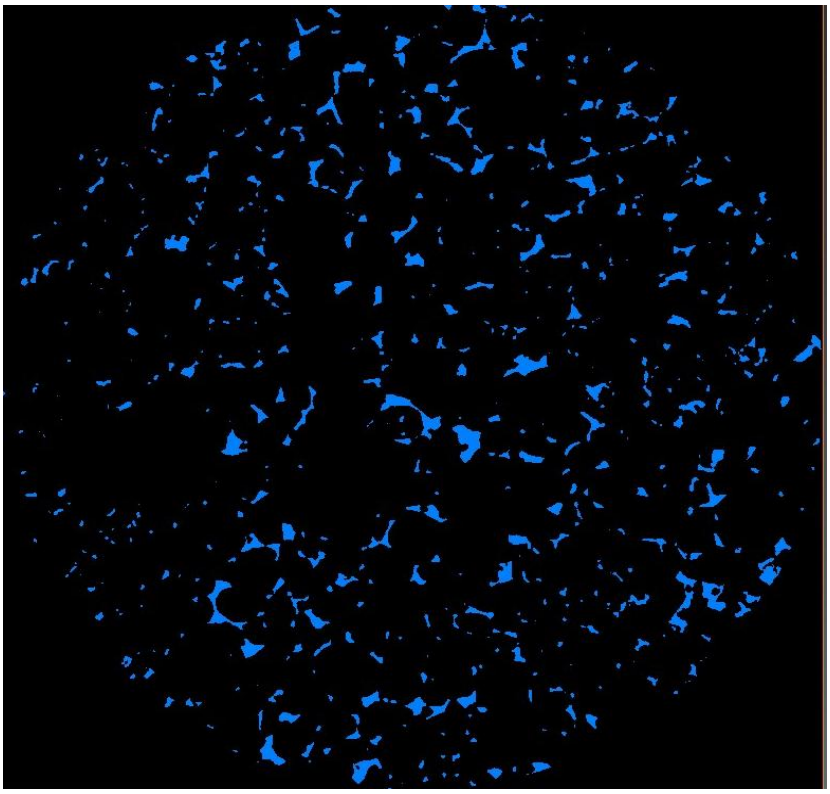

Figure-21: Binary of pore space after detection process

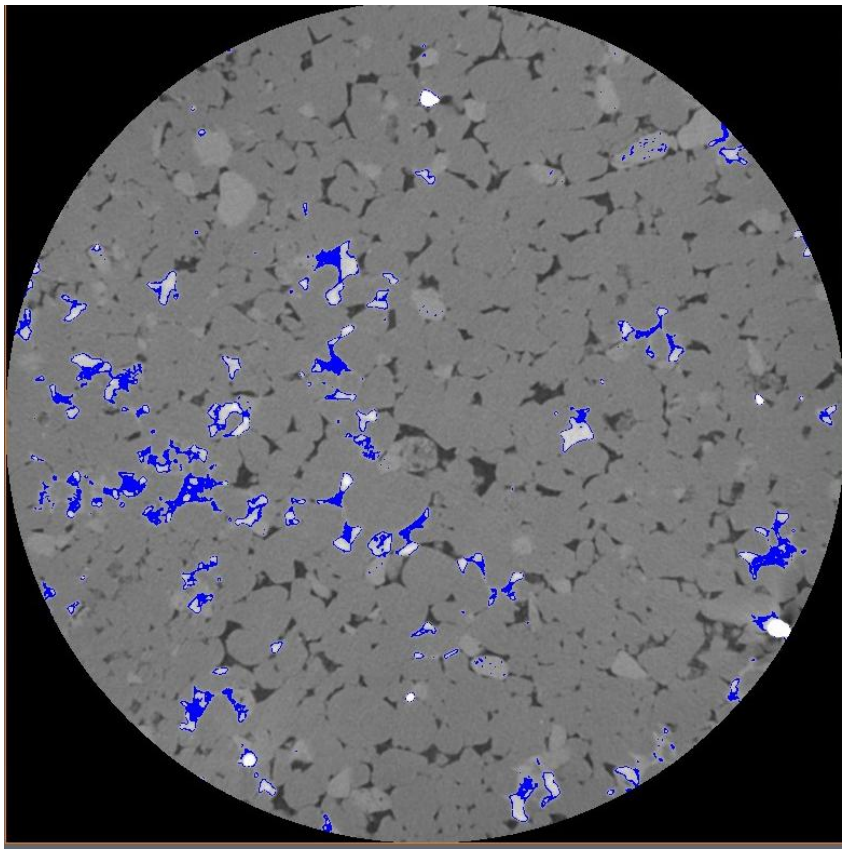

Figure-22: Result of carbonate thresholding/ detection

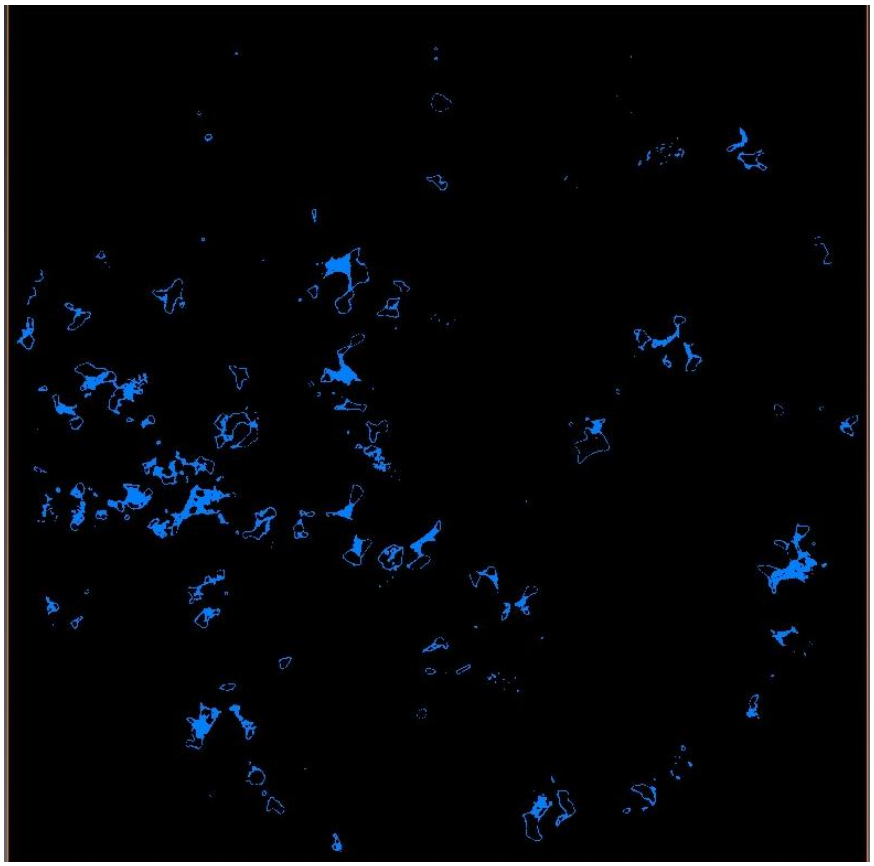

Figure-23: Binary of carbonate after detection process

3D Analysis

Once the binarisation has taken place, the difficult task is finished. By clicking on the label analyze function, the 3D volume and 3D area of the binary file is computed. This implies the individual volume and area in 3D (cylinder). By also detecting the whole volume (bulk) in combination with the sum of the individual results of volume per component, the volume fractions of the pore space, carbonate and heavy minerals can easily be calculated.

Eq-8: $\varphi = \frac{sum(indiv.porespace)}{bulkvol.}$

Eq-9: $cc = \frac{sum(indiv.calcite)}{bulkvol.}$

Eq-10: $om = \frac{sum(indiv.heavy\,\min.)}{bulkvol.}$

2D Analysis

The same can be done in 2D, but then only in terms of area. This implies the area per horizontal slice. The sample is sliced in about $500-1000$ pieces ($500-1000$ circles) and the 2D analysis is done per slice (per circle), resulting in $500-1000$ porosities, carbonate fractions and heavy mineral fractions.

Resolution Sensitivity

The samples are scanned on a resolution of 2.5 μm. The question arose: is this resolution high enough to see all pores in the samples? Are there pores which are smaller than this value? In order to test this, the binary images can be converted to lower resolutions by the resample function in Avizo. The additional resolutions are 5 μm and 10 μm. By calculating porosities for different resolutions, the sensitivity to resolution can be modelled.

Noise

The problem with image data is the generation of noise during the detection (thresholding) process. Small pixels are sometimes taken into the thresholding process, but do not belong there. In order to illustrate and quantify the role of noise, a certain noise threshold value is used. This threshold value illustrates that all object volumes below this value are seen as noise and therefore deleted. Initially, the question arose: what is the exact threshold value? To model the relation between threshold value and area/ volume fractions, a vector of threshold values is generated based on voxel size. The smallest voxel size is 1*1*1 voxels, which corresponds to 2.5 μm $*2.5$ μm $*2.5$ μm $=1.56e-8$ mm^3 in the case for 2.5 micron resolution. This implies that the smallest object that can occur has a volume of $1.56e-8$ mm^3. For respectively 5 and 10 micron resolution the smallest object volumes that can occur are $1.25e-7$ mm^3 and $1e-6$ mm^3. In the case of 2D, pixels apply (1*1 pixels). For all cases a vector is generated which it's minimum is the size of the smallest object volume (in 3D: 1*1*1 voxels and in 2D 1*1 pixels). The step size of these vectors is a factor of 10 and a cubic interpolation is used in between the points. The x-axis in fig. 25 illustrates the vector in 3D for 2.5 micron resolution and has a minimum of $1.56e-8$ mm^3.

For 2.5μm:

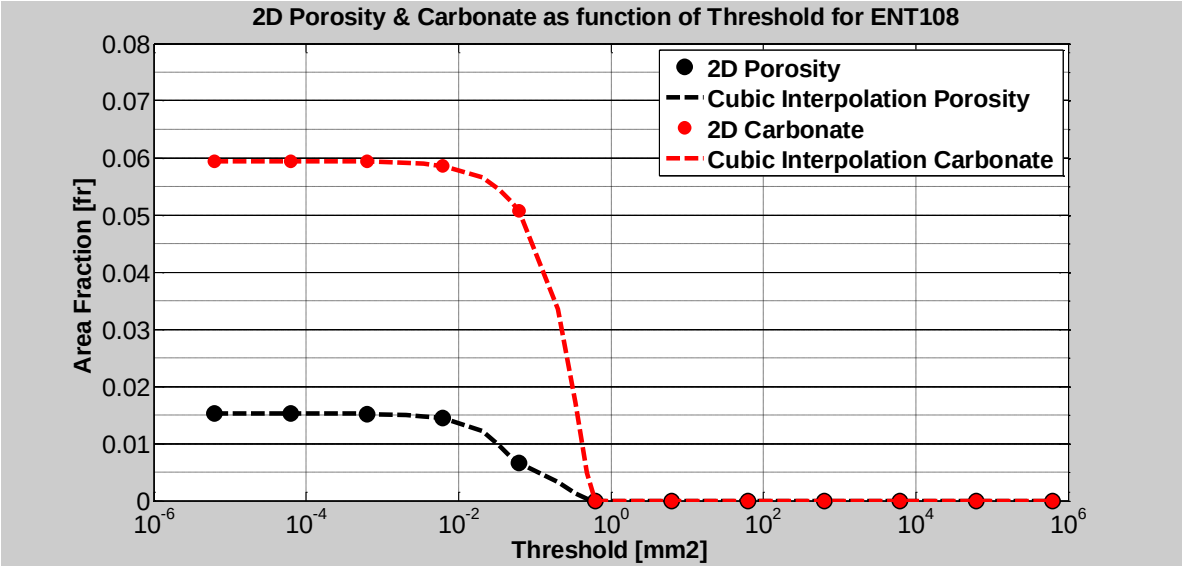

Figure-24: 2D porosity & carbonate as function of noise threshold for 2.5μm. To get an idea about pixel dimension, 10^{-6} corresponds to 1*1 pixels, 10^{-5} corresponds to 10*10 pixels etc.

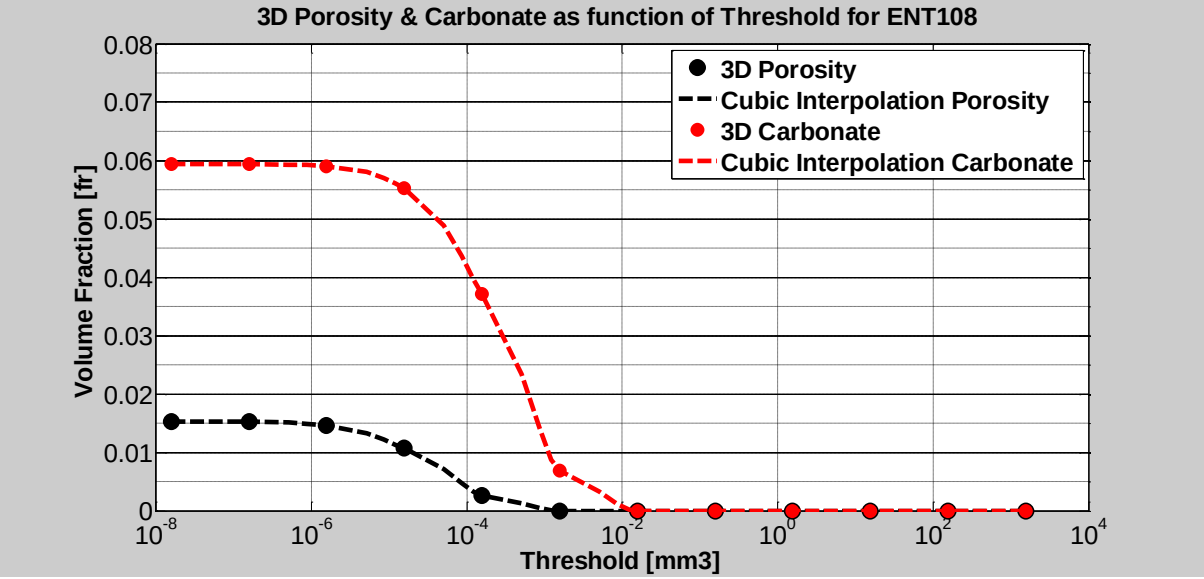

Figure-25: 3D porosity & carbonate as function of noise threshold for 2.5μm. To get an idea about voxel dimension, 10^{-8} corresponds to 1*1*1 voxels, 10^{-7} corresponds to 10*10*10 voxels etc.

For 5 µm:

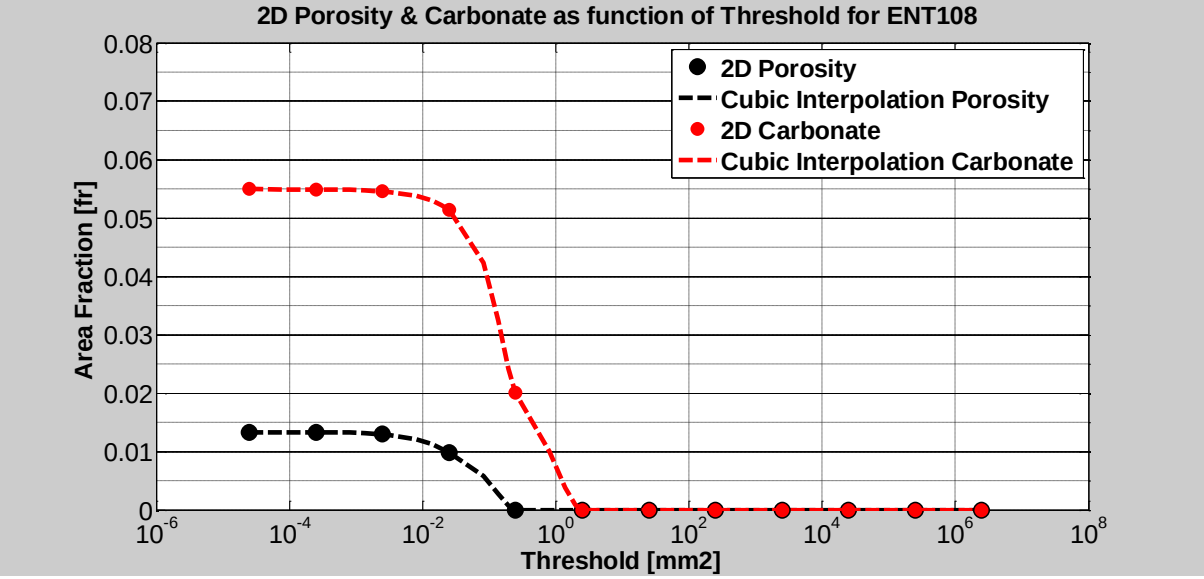

Figure-26: 2D porosity & carbonate as function of noise threshold for 5 µm

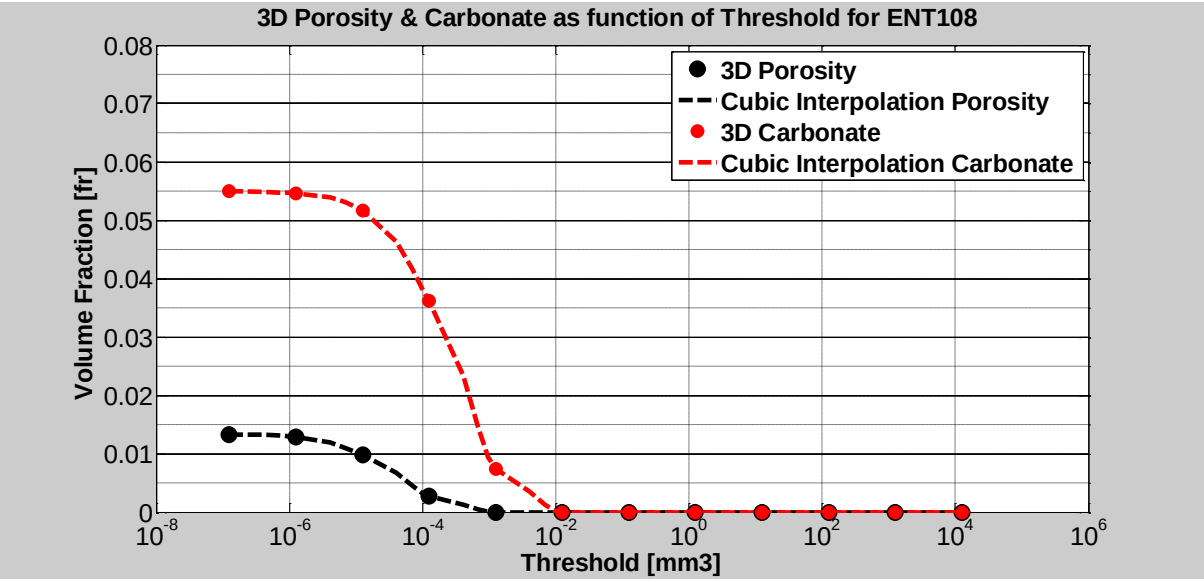

Figure-27: 3D porosity & carbonate as function of noise threshold for 5 µm

For 10 μm:

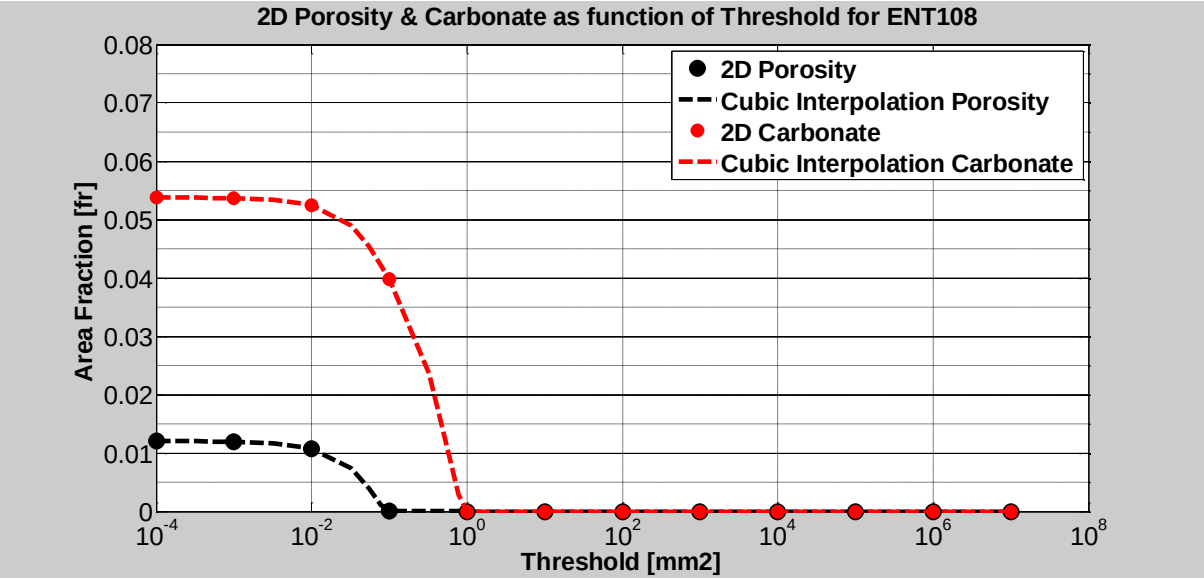

Figure-28: 2D porosity & carbonate as function of noise threshold for 10 μm

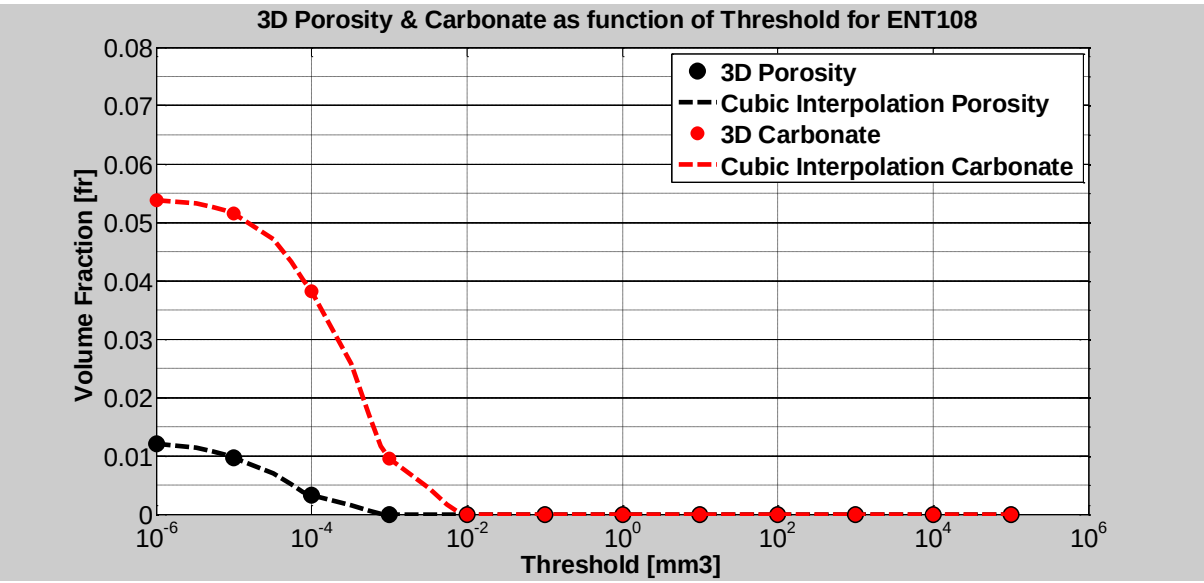

Figure-29: 3D porosity & carbonate as function of noise threshold for 10 μm

The previous 6 graphs (fig. 24-29) illustrate the 2D and 3D area and volume fractions for porosity and carbonate for 3 different resolutions as function of noise threshold. As is expected, the fractions decrease with increasing noise threshold, simply because area and volumes are removed.

The noise threshold value is required to be at the point where the fraction value tends to start to decrease, because that indicates that from this point on, real porespace is being removed. In other words, as long as the fraction stays constant, noise is removed. As soon as the fraction starts to decrease, the noise threshold value is acquired. Fig.30 illustrates this process.

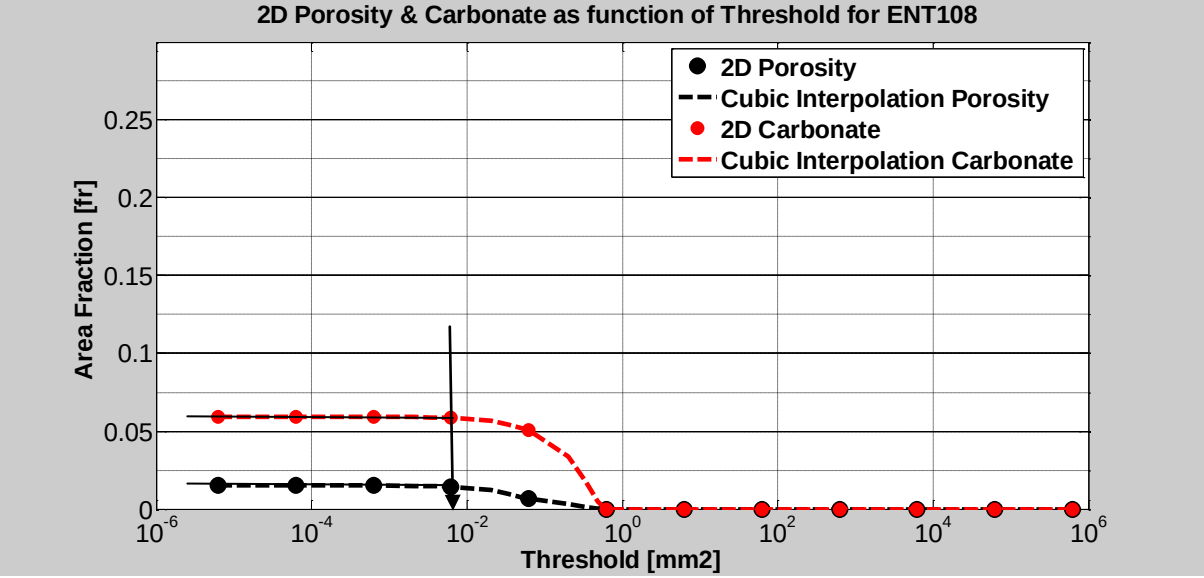

Figure-30: 2D porosity & carbonate as function of noise threshold for $2.5\,\mu m$

As is illustrated in fig-30, the first 4 points of porosity and carbonate are the same (see horizontal lines). After the 4th point, the values decrease, meaning that porespace and carbonate is being removed. This requires the noise threshold value to be $2.03e-2$ mm^2 (illustrated by vertical arrow), meaning that all individual areas below this noise threshold value are assumed to be noise. By conducting this for all samples, all components and all resolutions, histograms are generated to acquire the noise threshold values. The threshold sensitivity graphs illustrate more important features. As is seen in fig.30, the first 4 points are constant; but if comparing this to fig.29 there are no constant points, which makes it difficult to see the threshold point due to lack of constant points. Because of this difficulty, the resolution of 10 microns is not preferable. Based on this, the conclusion can be drawn that if the threshold dependency has more than one constant point, the scan resolution is usable and it also allows quantifying noise. The more constant points, the better the scan is, because of the presence of more detail.

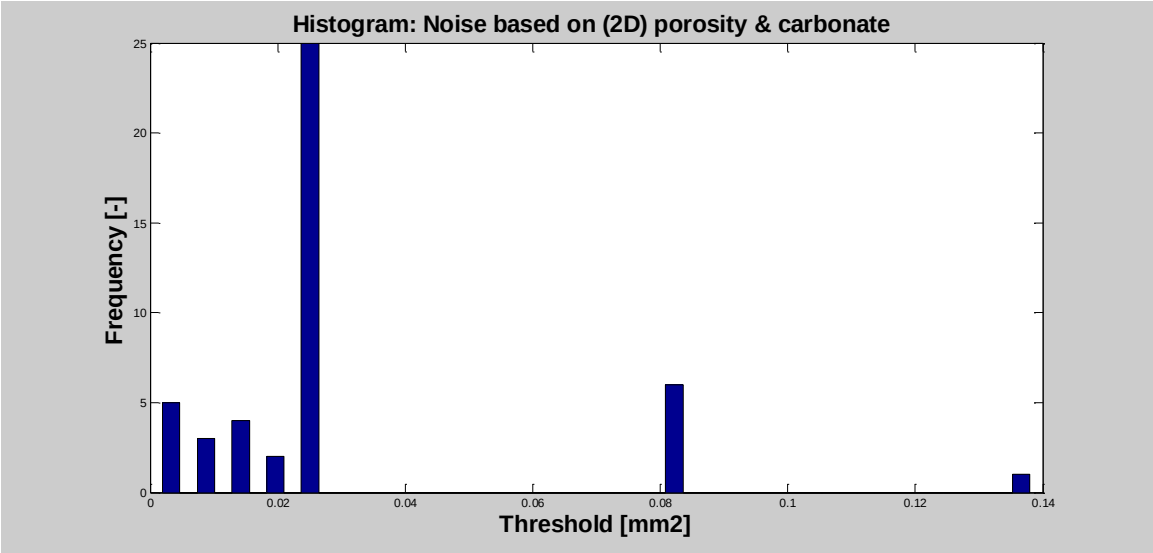

Figure-31: 2D porosity & carbonate histogram of noise threshold values for $5\,\mu m$

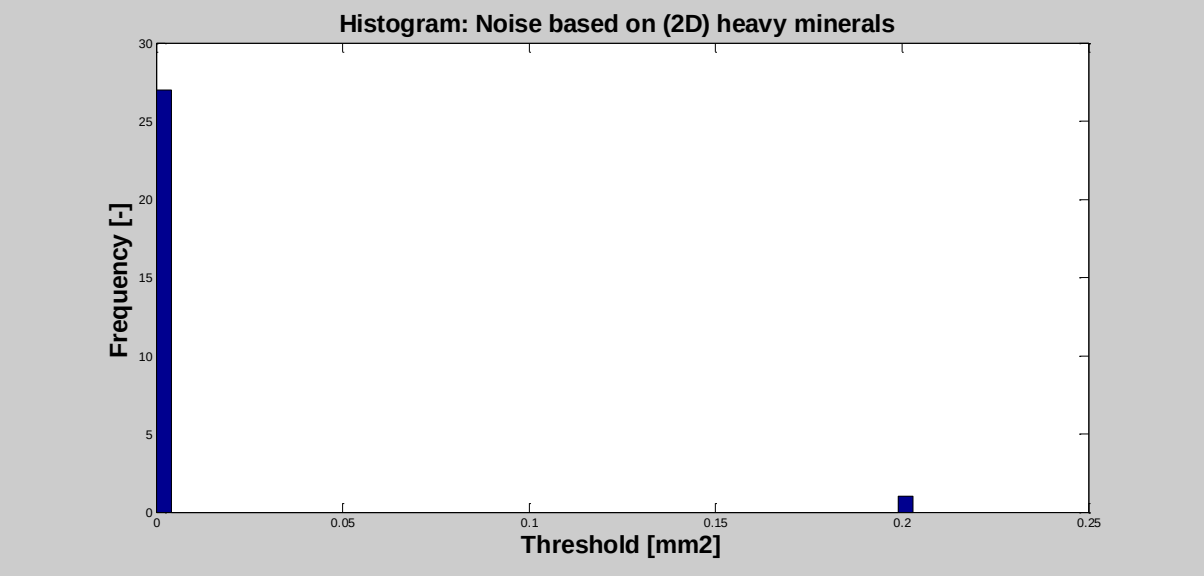

Figure-32: 2D heavy minerals histogram of noise threshold values for 2.5 µm

Conducting this in 2D and 3D, for all samples, all components and all resolutions, the most frequent noise threshold values are acquired:

2.5 µm	2.5 µm	2.5 µm	2.5 µm	5 µm	5 µm	5 µm	5 µm	10 µm	10 µm	10 µm	10 µm
2D	2D	3D	3D	2D	2D	3D	3D	2D	2D	3D	3D
Phi&Cb.	Hm.	Phi&Cb.	Hm.	Phi&Cb.	Hm.	Phi&Cb.	Hm.	Phi&Cb.	Hm.	Phi&Cb.	Hm.
6.25E-02	**6.25E-04**	**1.56E-05**	**8.58E-07**	**2.50E-02**	**2.50E-04**	**1.25E-04**	**1.25E-06**	**1.00E-02**	**1.00E-03**	**1.00E-04**	**1.00E-05**

Table-2: Noise threshold values for all samples, all components and all resolutions in 2D and 3D. 2D dimensions are in mm^2 and 3D dimensions in mm^3.

Based on the noise threshold quantification, the fractions for all components in 2D and 3D can be obtained. This is one value and not as function of noise threshold anymore. Per resolution, one value is obtained. By extrapolating to 'zero' resolution by using the data of 2.5 µm, 5 µm, 10 µm and a stable spline interpolation, the fraction at 'zero' resolution can be achieved. This indicates the resolution sensitivity.

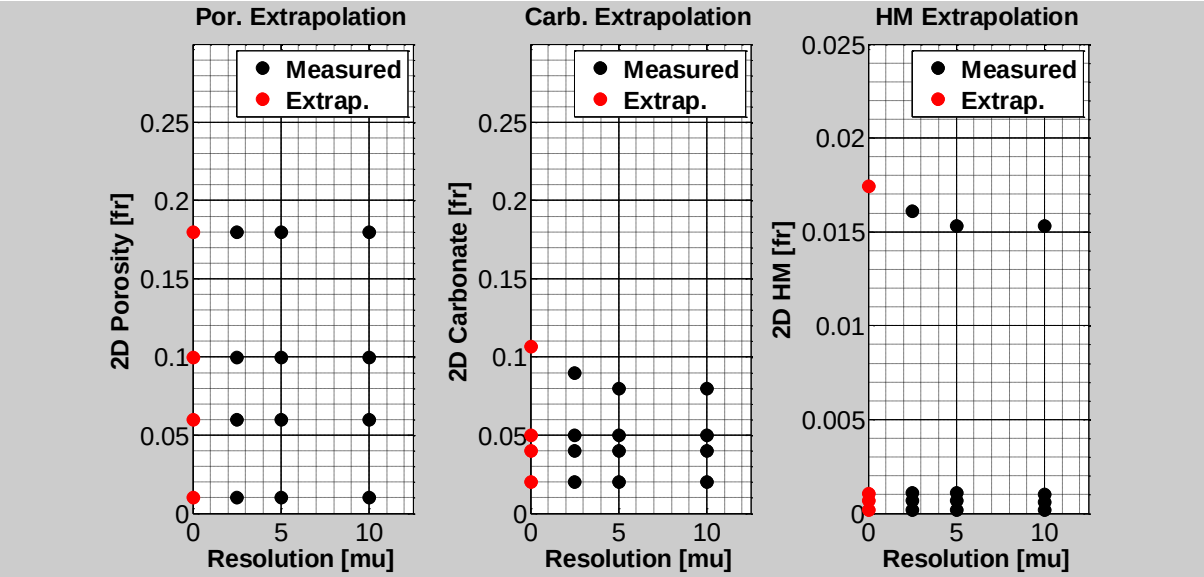

Figure-33: 2D components as function of resolution

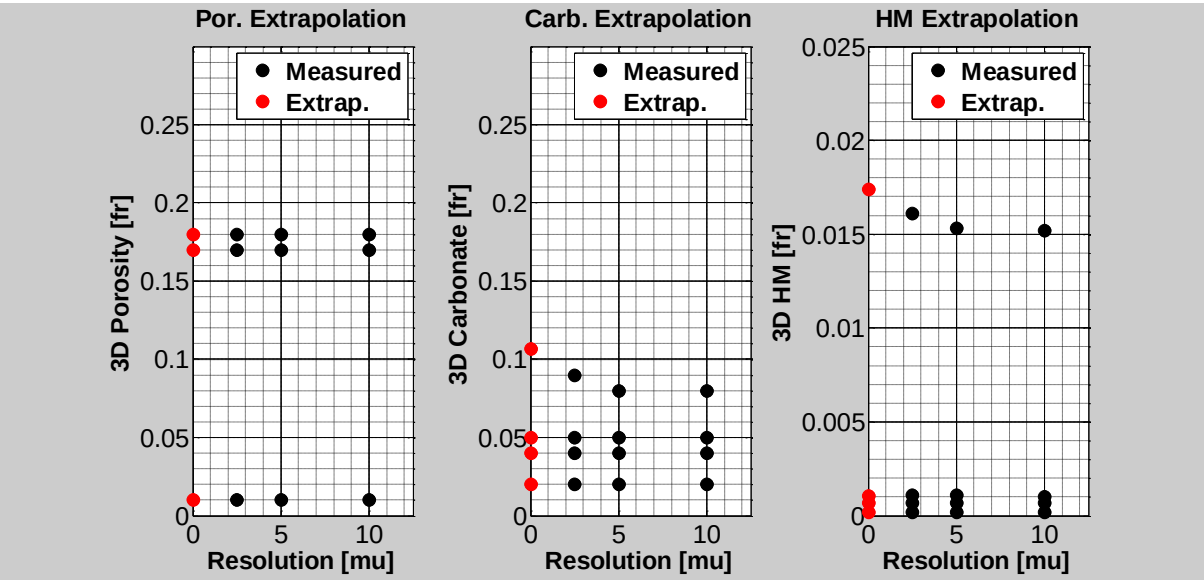

Figure-34: 3D components as function of resolution

As is illustrated in fig.33 and 34, the extrapolation to 'zero' resolution generally does not vary. In the case it varies, the variation is not large. By this sensitivity analysis, the conclusion can be drawn that the scanned resolution of $2.5\,\mu m$ is sufficient to see and quantify components. This is the last step to generate profiles with depth for all components in 2D and 3D. So in general pore space more robust in comparison to carbonate. At 2.5 microns a lot of irregular detail is captured as can be seen in fig. 23. This is removed by noise reduction, meaning that carbonate content is really a minimum value.

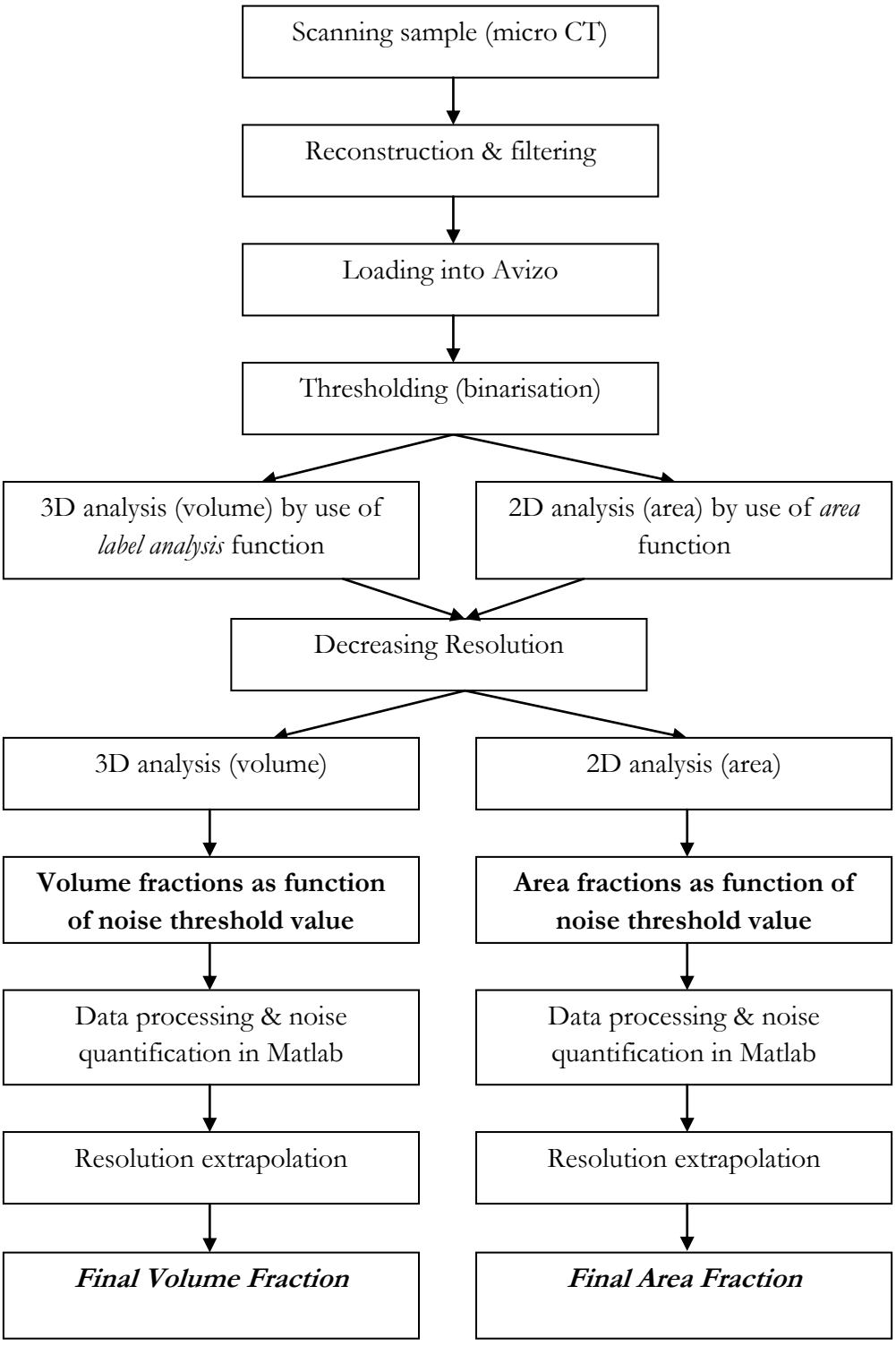

Diagram-3: Total workflow from scanning to output

Paragraph-2.5: Particles per volume

The number of particles per volume is an indicator of the connectivity. High amounts of particles per volume indicate that the particles are not connected to each other. This means that the more particles per volume, the lower the connectivity (permeability) is. Additionally, good sorted eolian reservoirs may have high amounts of particles per volume, but also high permeability because of the good sorting mechanism.

The number of particles per volume can be acquired by counting the numbers of individuals per components and dividing that by the total volume per component (see eq.-11-12). This can easily be done using Avizo. By conducting the 3D analysis, the porespace is acquired. During this analysis procedure, the number of particles is also counted.

Eq-11: $\varphi\_part = N_{\varphi}part / V_{\varphi}part$

Eq-12: $cc\_part = N_{cc}part / V_{cc}part$

With φ_part represents the pore particles per volume, $N_{\varphi}part$ represents the number of pore particles per volume and $V_{\varphi}part$ represents the volume of the pore particles. Eq-12 holds for carbonate instead of pore space.

Paragraph-2.6: Permeability determination by Shell

Royal Dutch Shell has conducted permeability measurements based on gas. Furthermore, the gas based permeability is corrected for gas slippage using the Klinkenberg correction. Initially, a Darcy based permeability experiment was built, using water to determine the permeability at the faculty. Tests concluded that the samples were not high permeable. This required higher pressures to pump the fluid through the samples. Unfortunately, these higher pressures (~4-6 bars) caused the flow lines to leak. Practically, the experiment was not feasible and needed much more sophistication. Because Shell is one of the stakeholders of this project, they offered to do the permeability measurements at their lab in Rijswijk.

Paragraph-2.7: Carbonate Irregularity

Introduction

Based on the carbonate deposited structure, grain analysis can be conducted in order to quantify the various carbonate deposited structures. The quantification can be done in 3D (volume and surface area).

Theoretical Description

Generally, 3 possible structures of carbonate deposition are visually and subjectively identified:

- No carbonate deposition at all
- Carbonate deposition in 'spot' structure, when imaging overall carbonate deposition
- Carbonate deposition in 'blob' structure, when imaging regional carbonate deposition

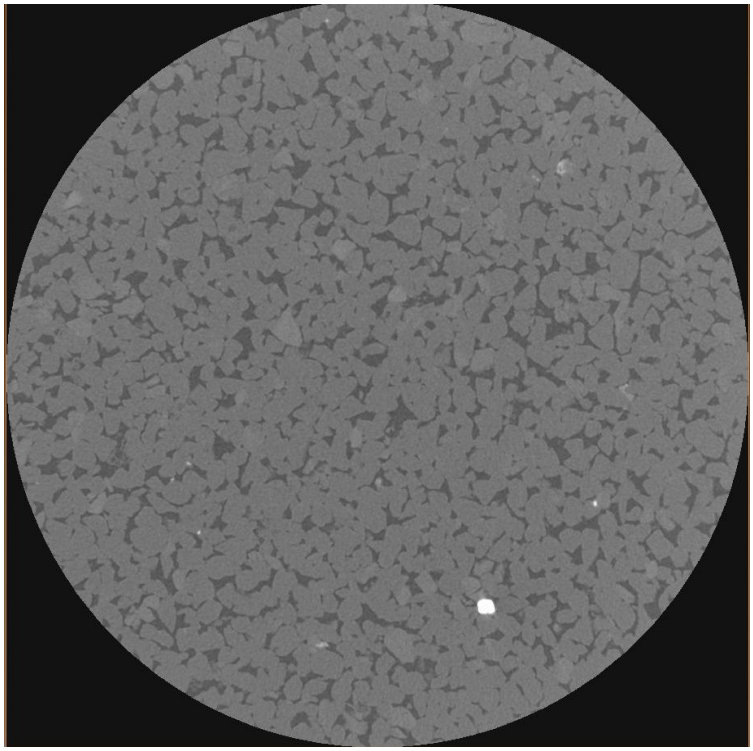

Figure-35: No carbonate deposition (CNV66). This sample has no carbonate deposition and can be used as a reference.

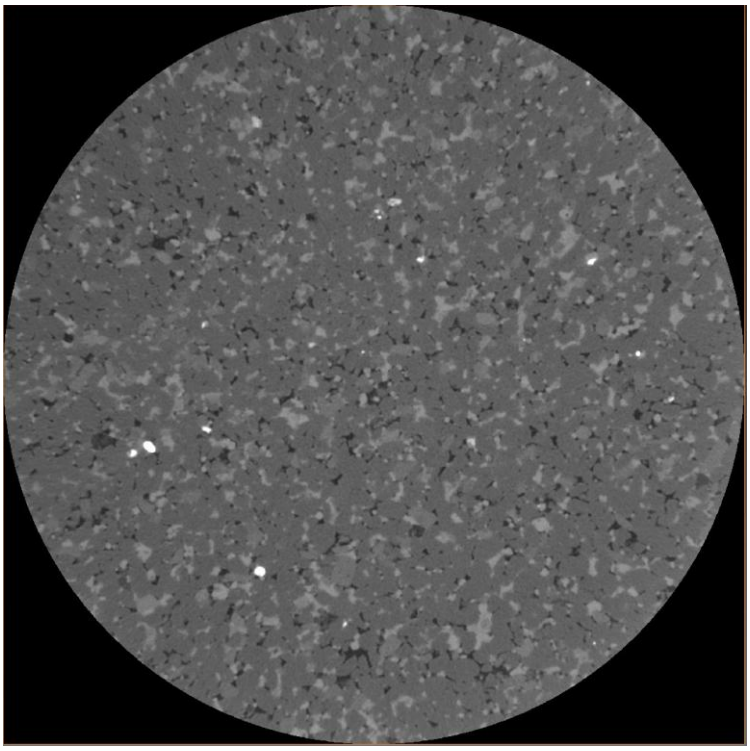

Figure-36: 'Spotty' carbonate deposition (light grey, CNV60), based on visual and subjective approach.

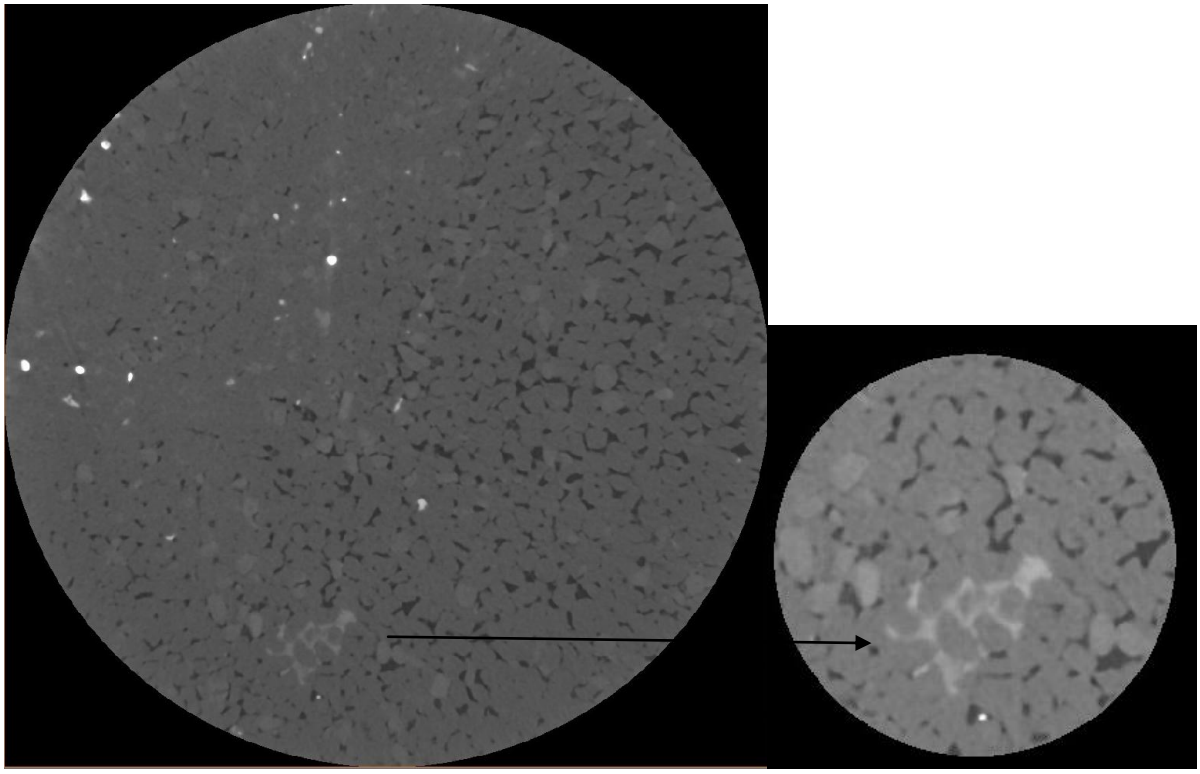

Figure-37: 'Blobby' carbonate deposition (light grey, CNV65), based on visual and subjective approach.

The idea is to analyze the grains in 3D for all 3 scenarios. Based on the binary of the grains, the initial conclusion can be drawn that the grains are grown and connected to each other.

Firstly, the grains should be detected (thresholding). In practice, this is a difficult task, because the grains are not equally dens. The density is not constant for all (silica) grains; even a small difference in density creates a major difference in grey values (for example pore space has grey values around 2000, while carbonate has grey values around 20000. Thresholding the grains is not the optimal solution, whereas thresholding the pore space, heavy minerals and carbonate is much better and smoother to do (this was done in chapter-2). By thresholding these components, summing the binaries, inverting this and slightly reducing the volume (volume edit), a binary of the grains is achieved. This is a simple operation, but results in a representation of the grains.

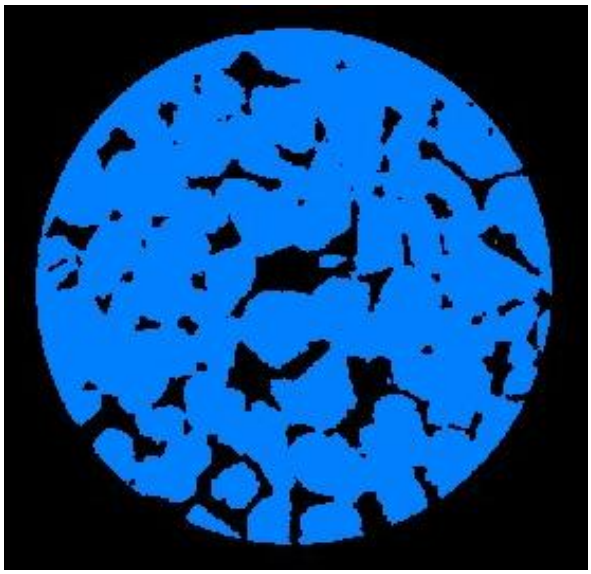

Figure-38: Binary of silica grains of 'no' carbonate deposition (blue)

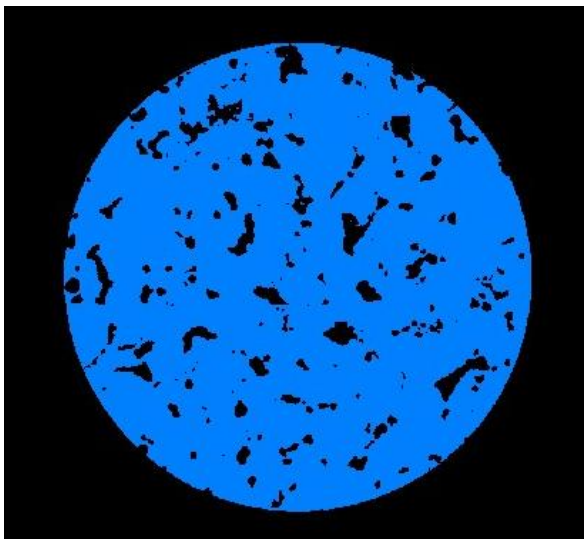

Figure-39: Binary of silica grains of 'spotty' carbonate deposition (blue)

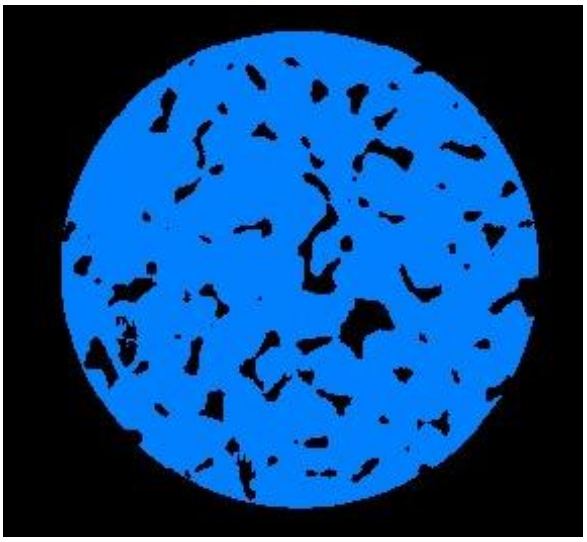

Figure-40: Binary of silica grains of 'blobby' carbonate deposition (blue)

The next step is to separate the grains from each other. This can be done with the fast watershed function. This function separates objects from each other based on the given input binary. It accounts for open spaces (porosity, carbonate and heavy minerals) and for the curvature of an object (for example a grain).

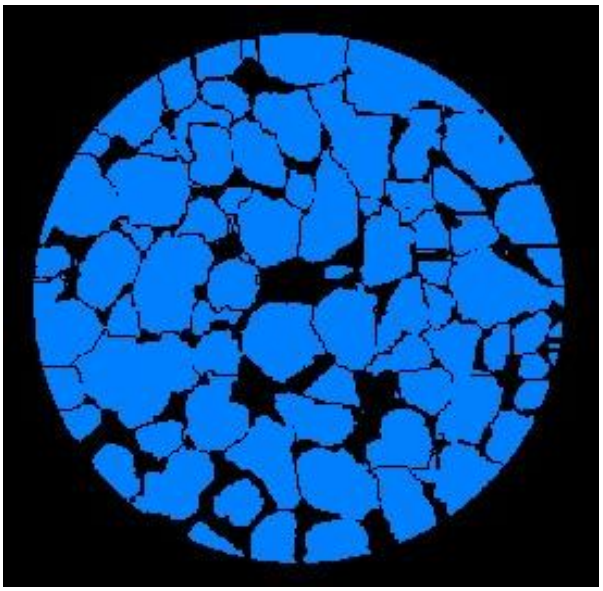

Figure-41: Separated grains of 'no' carbonate deposition (blue)

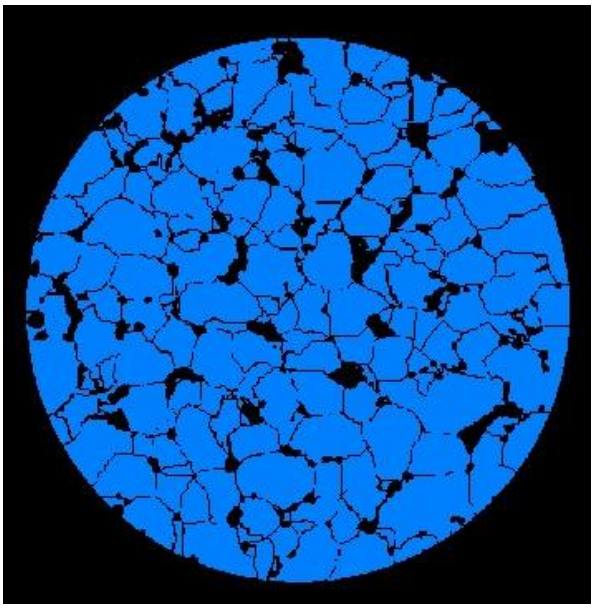

Figure-42: Separated grains of 'spotty' carbonate deposition (blue)

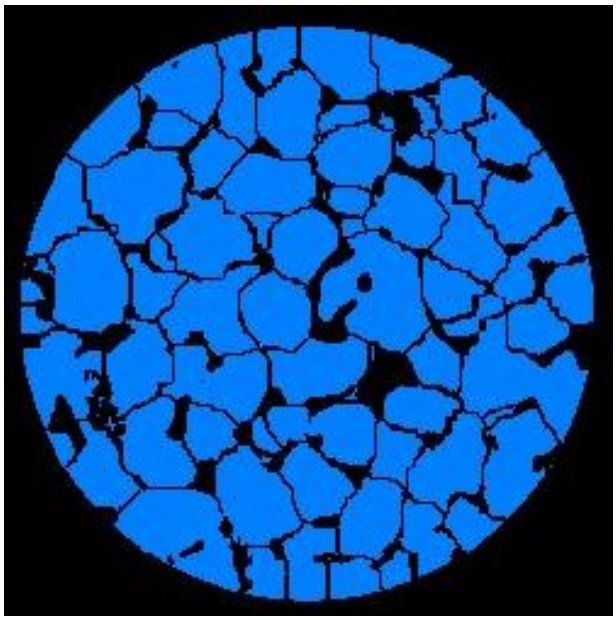

Figure-43: Separated grains of 'blobby' carbonate deposition (blue)

Finally, the 3D analysis can be conducted on the separated grains, resulting in 3D volume and surface area of the grains.

The final results follow in the result chapter.

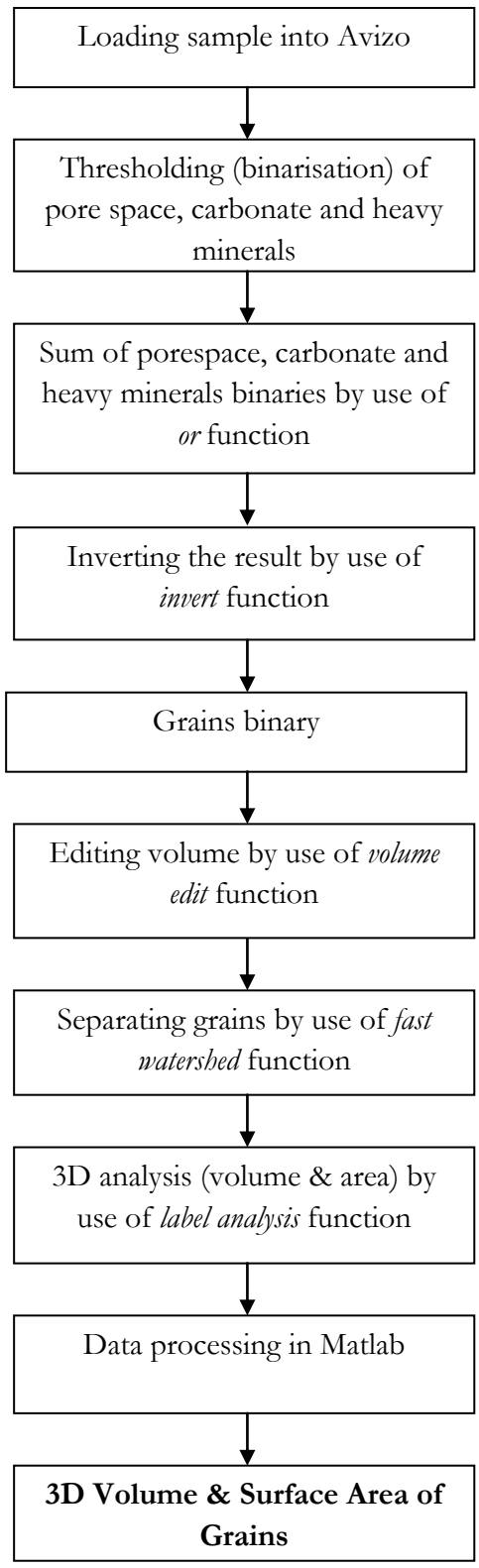

Diagram-4: Total workflow from loading into Avizo to 3D volume and surface area of grains

Paragraph-2.8: 2D fraction profiles of fractured samples

Introduction

The samples acquired during this project can be divided into 3 main categories: fractured (10), non-fractured (17) and bleached (1) samples. The fractured samples contain a fracture plain. By analyzing this fracture plain for various components (porosity, carbonate and heavy minerals), the effect of the fracture on these components were quantified.

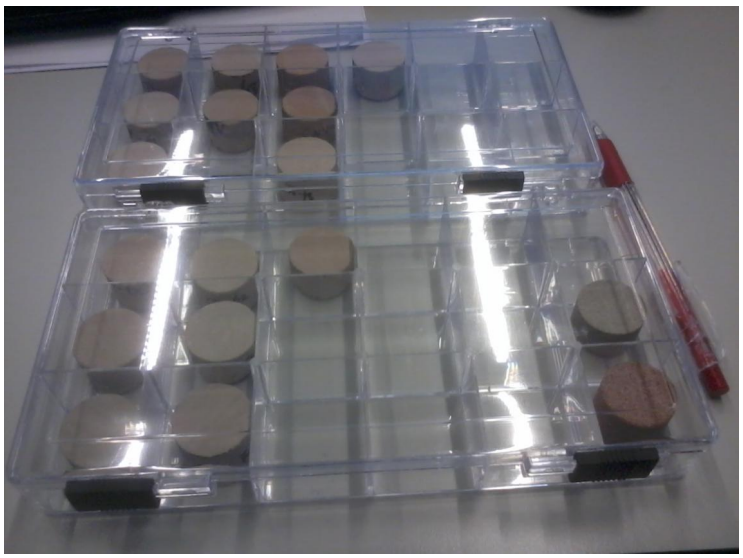

Figure-44: Series of non-fractured samples

Figure-45: Fractured sample; blue line indicates fracture plane

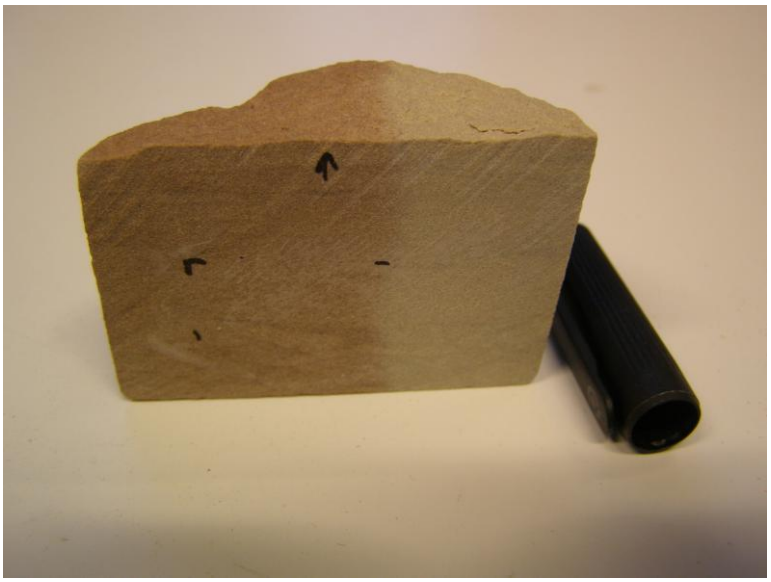

Figure-46: Bleached sample (ENT-108). Flushing of iron minerals by carbonate fluid fluxes.

Theoretical Description

Because a profile of the various components around and away from the fracture plain/ bleached zone is desirable, the 2D area function is used. This function is the optimal function to use, because the sample can be sliced in a certain number of slices and the slice direction can be adjusted parallel to the fracture/bleached plain. Following figure illustrates this process.

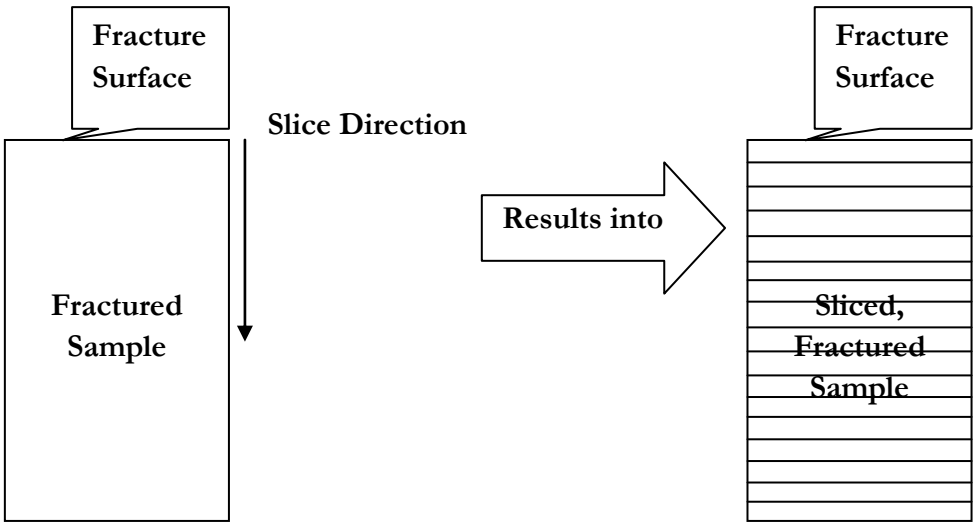

Figure-47: Theoretical explanation of slice system for fracture surface analysis

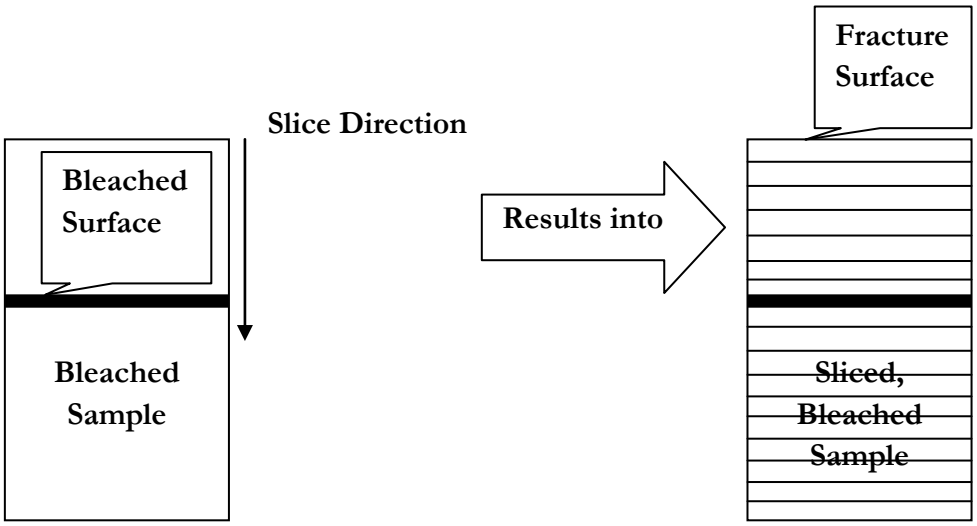

Figure-48: Theoretical explanation of slice system for bleached surface analysis

The 2D area function gives the 2D area per slice of the various components. In combination with the total area per slice, the fraction per slice of the various components can be determined. Based on chapter-2, the 2D fractions and 3D fractions are generally the same.

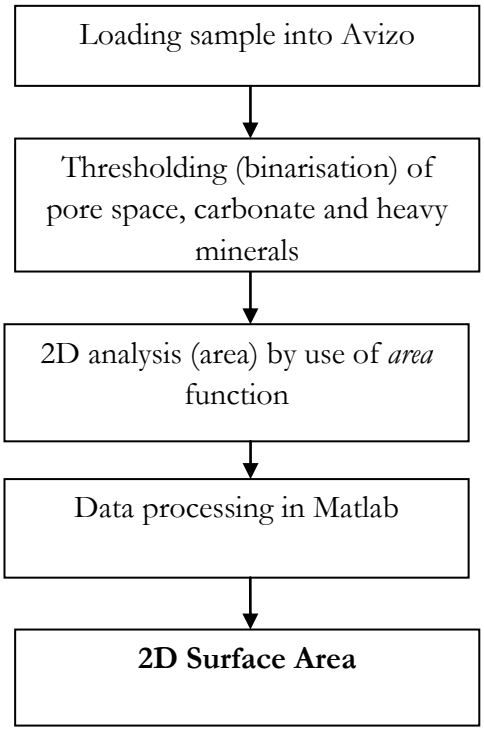

Diagram-5: Total workflow from loading into Avizo to 2D area

Paragraph-2.9: 3D connectivity profiles of fractured samples

Introduction

The fractured and bleached samples are also analyzed in 3D in order to quantify the connectivity. As was done in chapter-3, the number of particles gives information regarding the connectivity. The same procedure as in paragraph-3.1 is done, but now in a detailed section of the samples to acquire a connectivity profile.

Theoretical Description

In contrast to the 2D area function, the label analysis (3D) function is used. Basically, the particle volume and number is acquired. Additionally, the barycentre coordinates is also acquired. The coordinates (x, y and z) indicate where the centres (centre of gravity) of the particles lie in the sample.

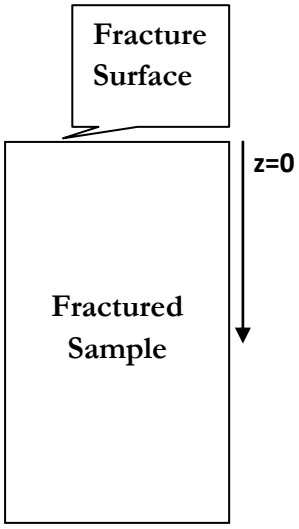

Figure-49: Theoretical explanation of 3D detection system

The label analysis function also indicates the coordinates of volumes. Because a profile of connectivity through the sample is wanted, the z-coordinate is the most preferable. First, the individual volumes per z-coordinate are sorted. By summing all individual volumes per z-coordinate, the total volume per z-coordinate is acquired. Then dividing the number of individual particles per z-coordinate by the summed volume per z-coordinate, the number of particles per volume per z-coordinate is obtained.

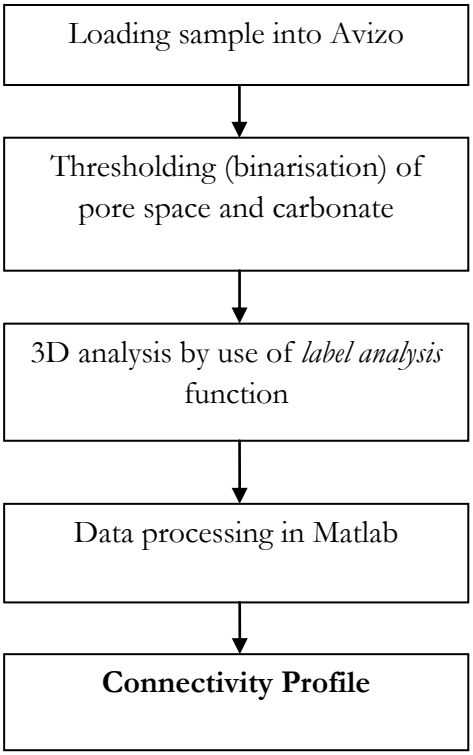

Diagram-6: Total workflow from loading into Avizo to connectivity profile

Chapter-3: Results & Visualization

Paragraph-3.1: Porosity comparison between various methods

In this section various porosity, carbonate and heavy minerals methods are compared to each other. 3 lab based methods and 2 image based methods have been used. The lab based methods are the Pycnometer, the Wet test and the Hg Shell test methods, while the image methods are the 2D and 3D Avizo methods. Generally, the difference between lab based and image based methods is that the lab based methods give an average representation of the parameter, whereas by the use of image based methods the variability can be quantified.

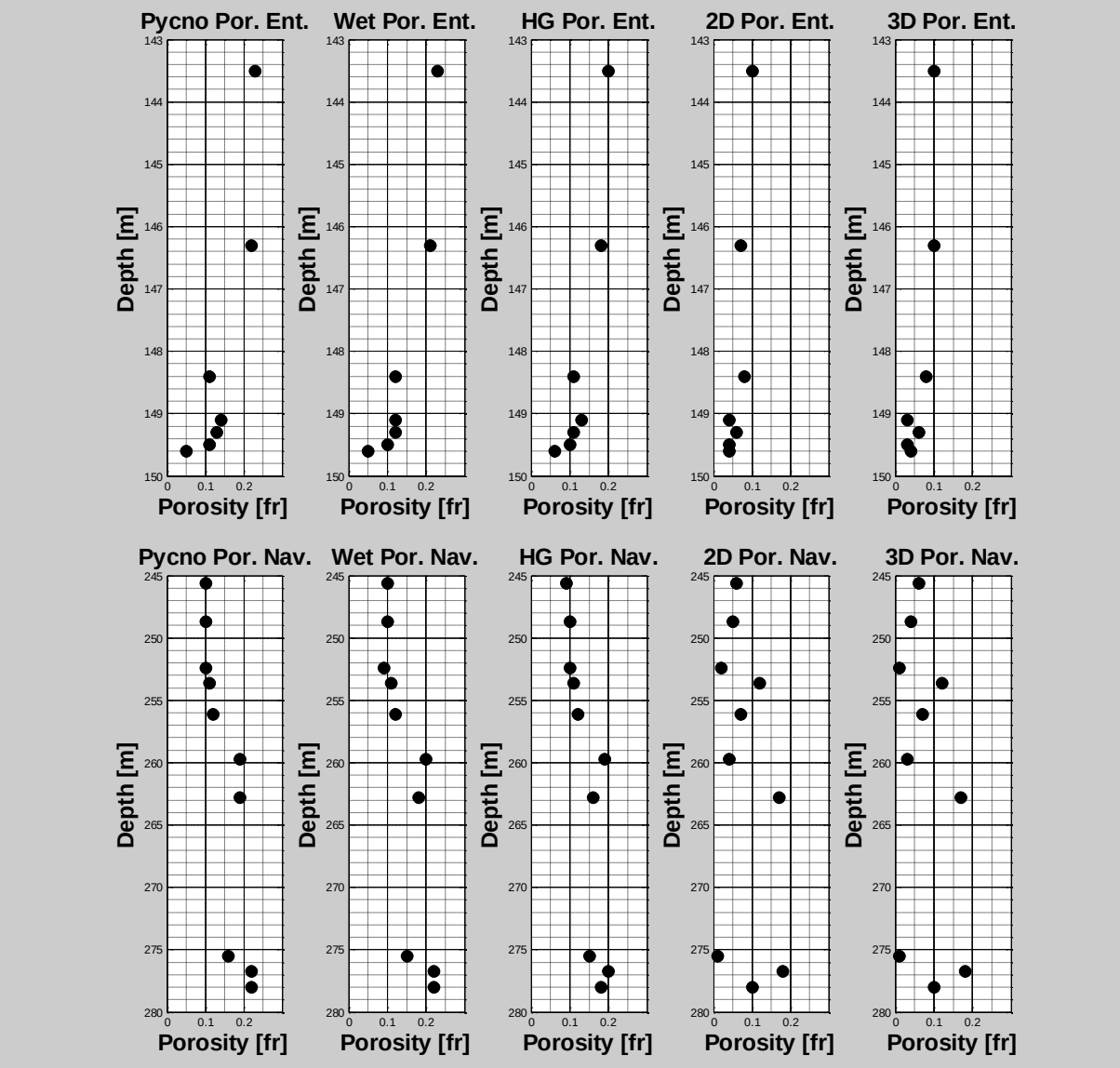

Figure-50: Porosity profiles for lab and image methods (Entrada & Navajo formation)

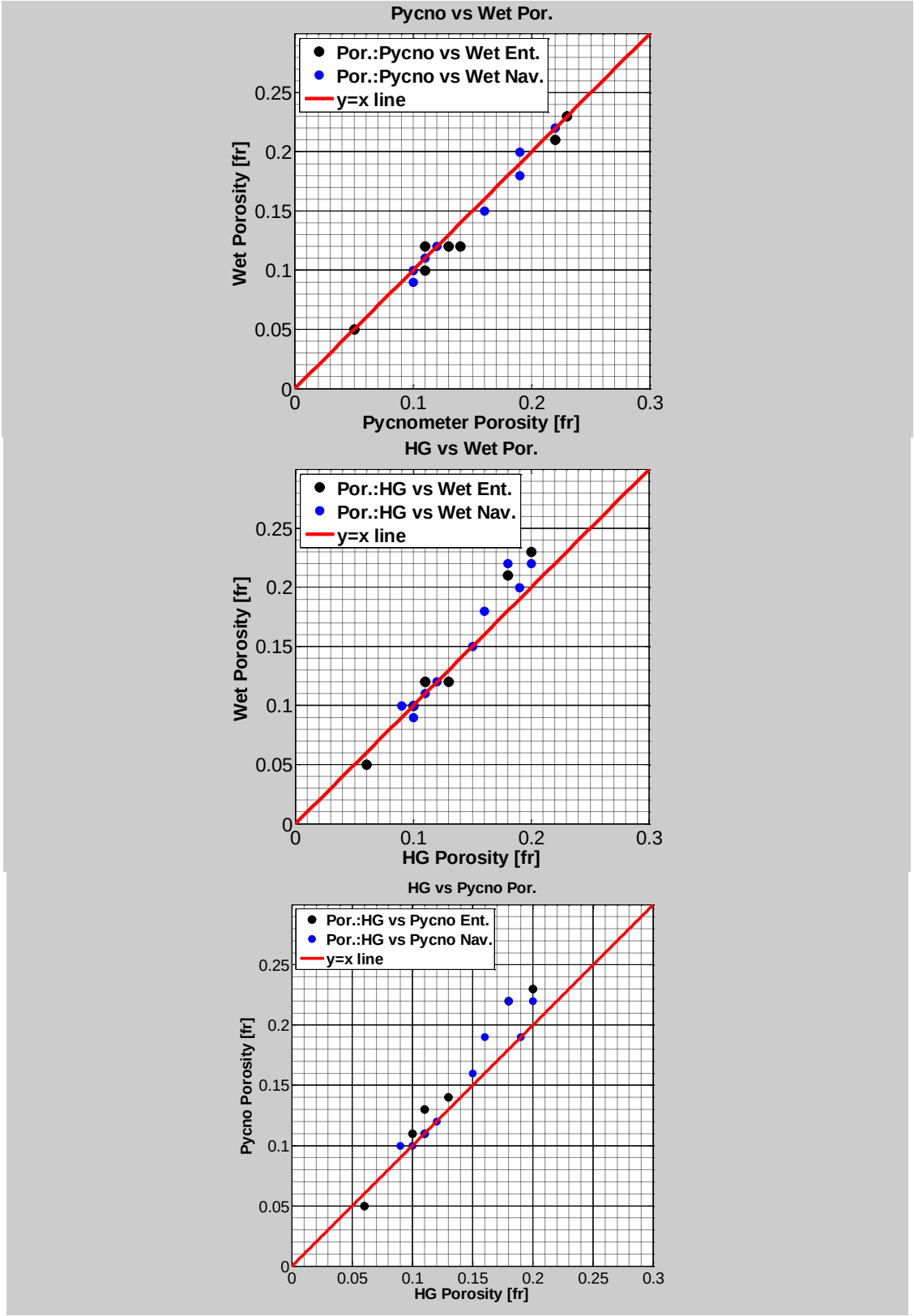

Figure-51: Porosity comparison Wet, Hg & Pycno tests

Fig.50 illustrates the profiles of the 5 various porosity methods for the Entrada and Navajo formations, in which can be seen that the profiles of the 3 lab methods (Pycnometer, Wet test & Hg Shell) are similar. Although 3 different fluids (helium, water & mercury) have been used in these lab tests, which imply 3 different regimes of penetration, the results are the same. This can also be seen in fig.51, in which the 3 various methods are compared to each other by plotting against each other.

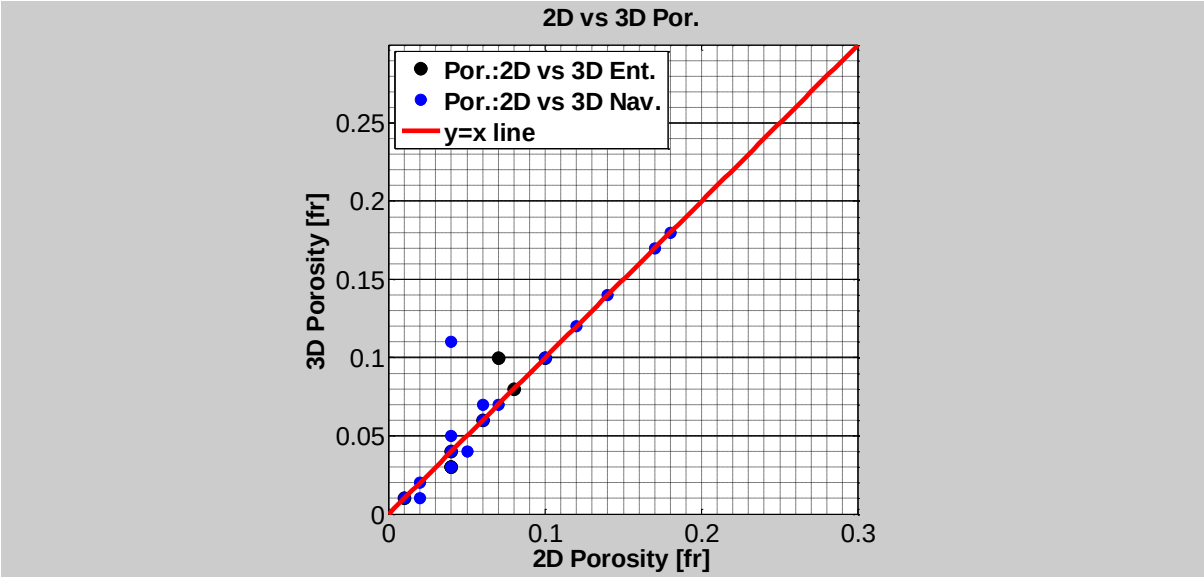

Figure-52: Porosity comparison 2D & 3D image methods

Fig.50 also illustrates the profiles of 2 image based methods (2D & 3D). The main difference lies in the dimension, meaning pore objects measured in area (2D-slices) and volume (3D-volumes). These 2 profiles agree with each other and are also illustrated in fig.52. The image based methods are also used to quantify the carbonate and heavy mineral content. For both of these components, the same conclusion holds (see next section).

If now comparing one of the image methods with one of the lab methods, then the lab based methods and image based methods do not agree with each other. The difference is illustrated in fig.53.

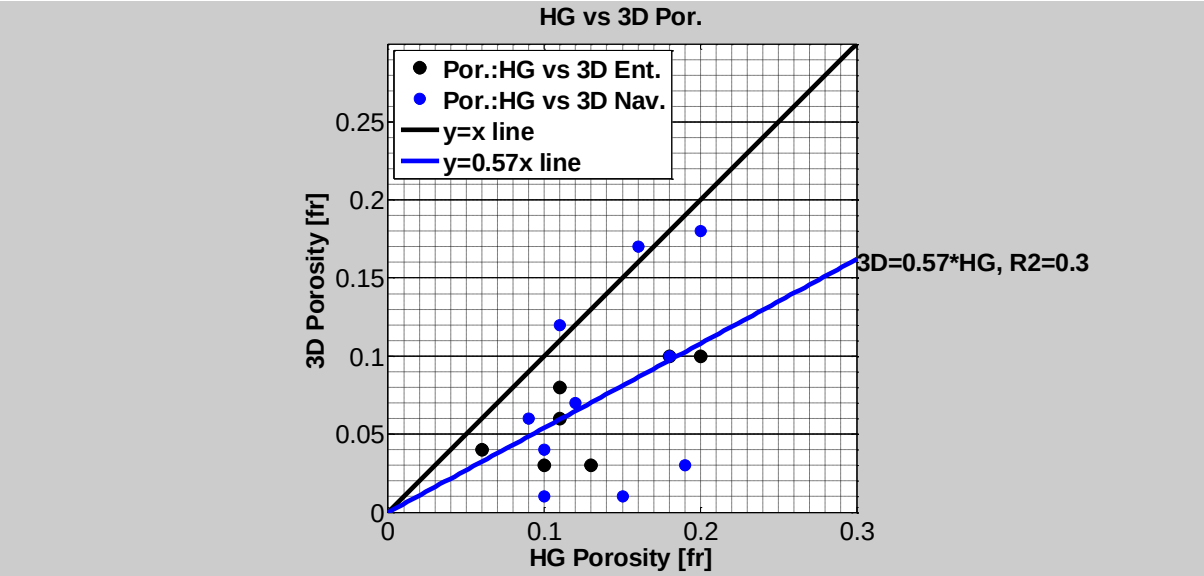

Figure-53: Porosity comparison Hg & 3D. Blue points indicate Navajo samples, whereas black points indicate Entrada samples.

By plotting (fig.53) one of the lab methods, in this case the Hg Shell Test, versus one of the image methods, in this case the 3D, then a linear relationship can be acquired. The overall fitting is 0.3 and generally the image based methods is half the quantity of the lab based methods. Note that a fitting of 0.3 cannot be seen as a good fitting, because in a perfect case the fitting coefficient should be 1. Unfortunately, the high scattering of the data points, which illustrates high heterogeneity, does not allow a suitable/ usable trend relation between the lab porosity and image porosity. As has been stated earlier, the lab methods are based on penetration of fluids in the pores, whereas the image methods are based on pixel/ resolution features. Fig.53 shows that the majority of the data points are below the y=x line, meaning that the image results are lower than the lab results in other words, the image results are underestimated to the lab results. This phenomenon may lie in resolution and/ or volume features. It may be that the scanned resolution is not high enough to see all pores. The image results are based on 2.5 micron resolution and means that pores below this resolution cannot be seen. Another reason can be the volume of the sample. If the sample is highly heterogonous, it may be that data points are affected by sample volumes which have been extracted from high or low porous parts. This explanation may apply for the 2 points in fig.53 which lie above the y=x line.

By stating that the resolution may influence the underestimation of the image based results may be in contrast to the illustration in fig.33-34 in section 2.4. These graphs conclude that the scanned resolution of $2.5\,\mu m$ is sufficient to see and quantify components. It is then more likely to assume high heterogeneity and sample volumes which have been extracted from high or low porous parts. Additionally, one has to keep in mind, that possible pores/ object below the resolution of 2.5 microns cannot be imaged. So big pores are well images, but small ones are completely missed.

Paragraph-3.2: Permeability

The main purpose of this section is to calculate the permeability based on Darcy and Klinkenberg. The input parameters are area, length, gas viscosity, pressure and flow rate. The output parameter is permeability.

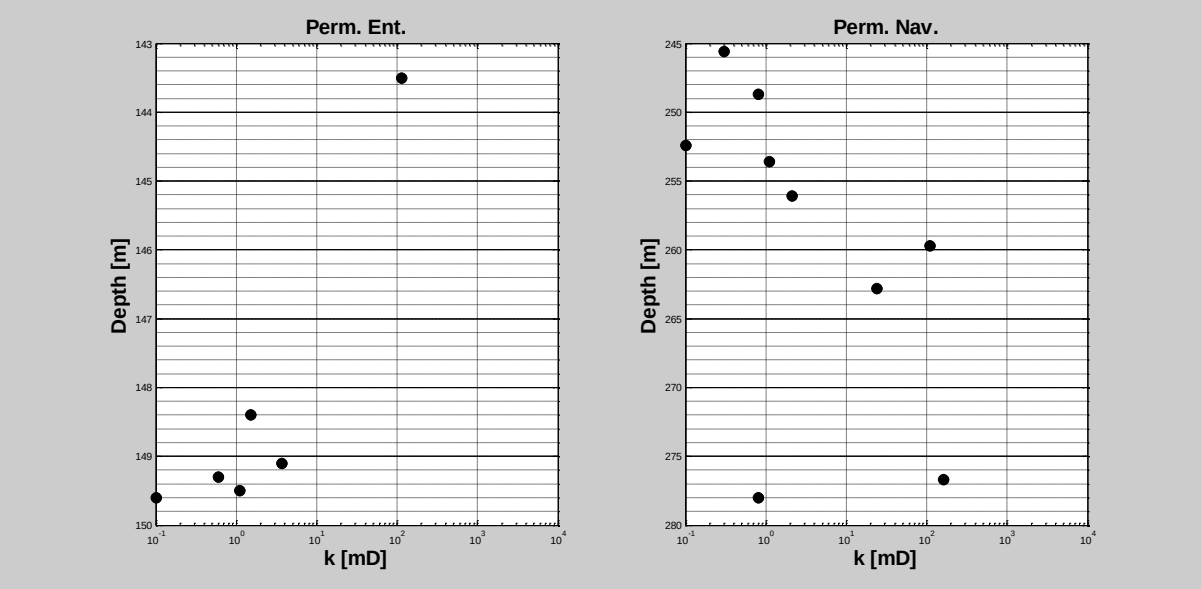

Figure-54: Permeability per depth (Entrada & Navajo formation)

Fig.54 illustrates the permeability profiles for the Entrada and Navajo formation. The Navajo formation permeability shows a slight increasing trend for permeability with depth. For the Entrada formation no clear trend can be established. Permeability is a very sensitive parameter to the smoothness of the cores, the pores which are not connected to the gas pathways are not measured, the smoothness of the sleeve containing the core (sufficient radial pressure) and non leaking flow lines.

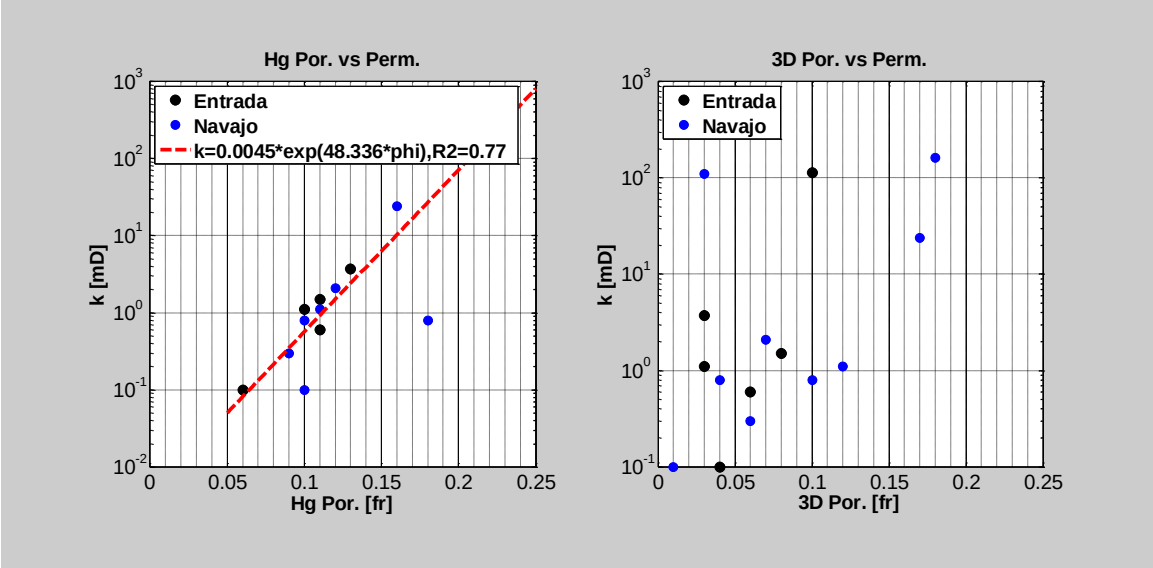

Figure-55: Correlation between permeability and porosity for lab and image methods

The porosity-permeability relationship based on the lab porosity has an exponential relationship. Due to the log-log axis the relationship appears to be a straight line. The fittings coefficient is 0.77, in which the perfect case it would be 1. In contrast to the abundant trend for permeability to lab porosity, the correlation of permeability to micro CT based 3D porosity is not abundantly present. As has been stated earlier, the lab based porosity differs from the image based porosity (see fig.53 in section 3.1). This difference was explained by volume extractions in high heterogeneous samples and in lesser extent resolution features. Based on these reasons, the lab based permeability will not correlate to the image based porosity. Image based permeability methods would more likely correlate to the image based porosity.

Paragraph-3.3: Quantification of CT data

3.3.1: Microstructures

In this section micro structural features like pore shape, carbonate deposition will be touched upon. Fig.56 shows a horizontal 2D slice of one of the normal samples (CNV66). Pore space (black), grains (grey) and heavy minerals (white) occur in this sample. There is no carbonate deposition in this sample as is seen in fig.56. The figure also shows that the grains are more or less interconnected to each other, whereas the heavy mineral deposition is very little and randomly situated.

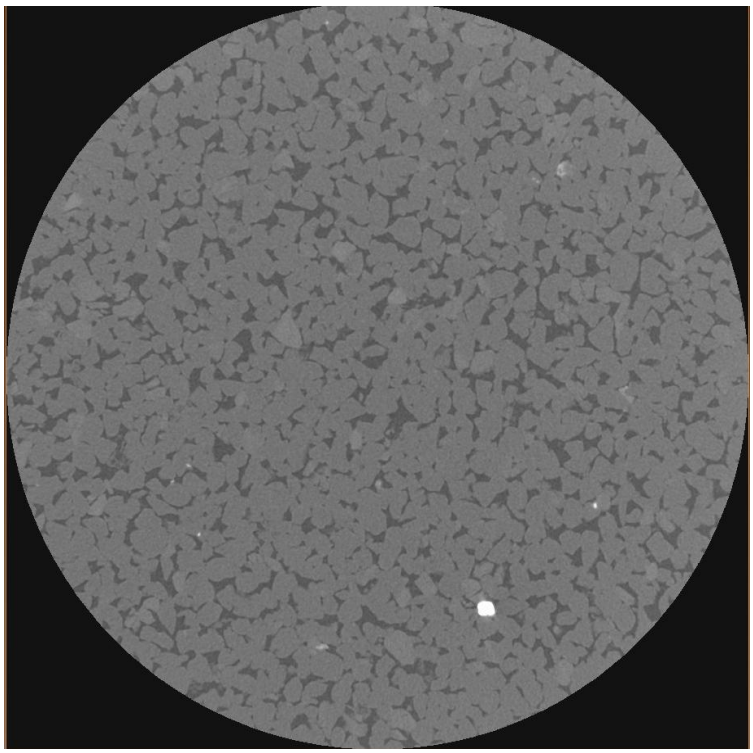

Figure-56: No carbonate deposition (CNV66)

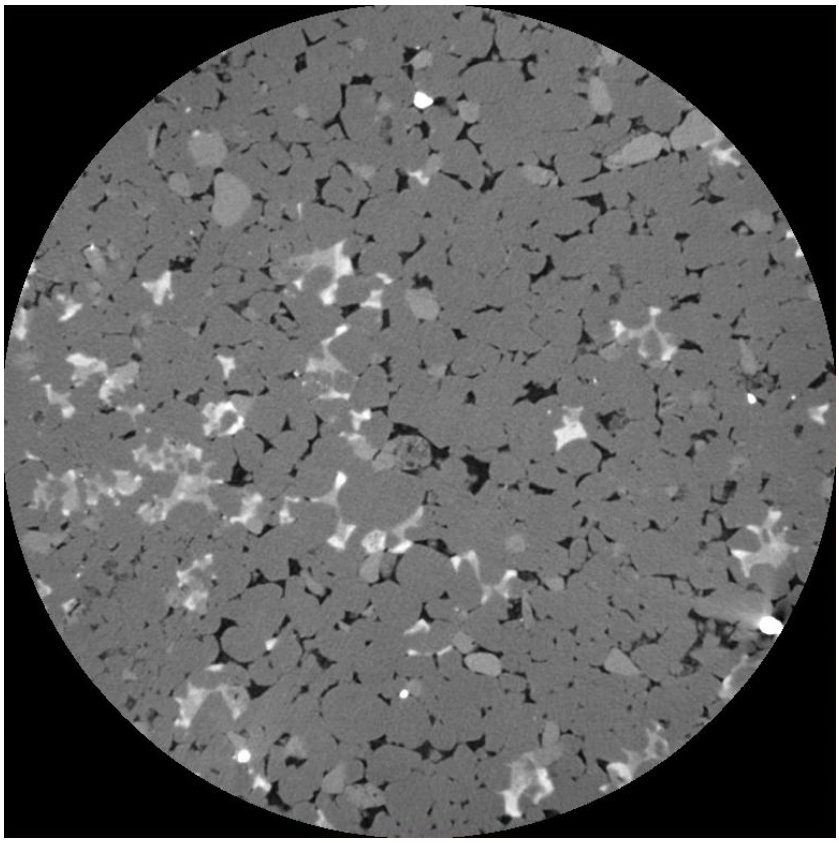

Figure-57: Result of micro CT scanning of 8 mm cores

Fig.57 shows a horizontal 2D slice of one of the normal samples. Pore space (black), grains (grey) and heavy minerals (white) occur in this sample. In this sample carbonate deposition did occur (light grey). The structure of the carbonate deposition is 'blobby', meaning that it is not randomly distributed over the whole slice, but more in the big pores. Based on this figure, the big pores especially are almost filled up.

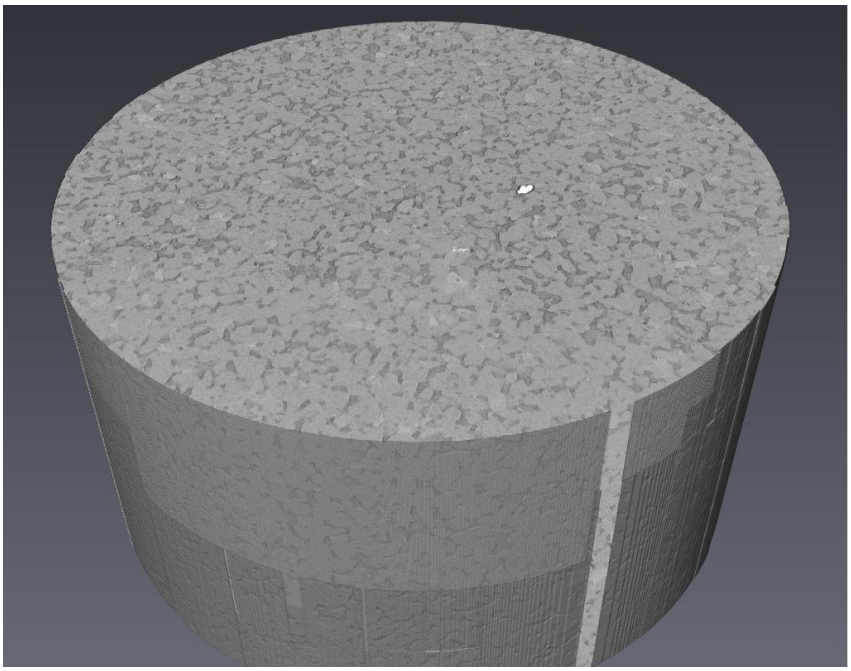

Figure-58: Result of micro CT scanning of 8 mm core

Fig.58 shows a 3D representation of a scanned sample.

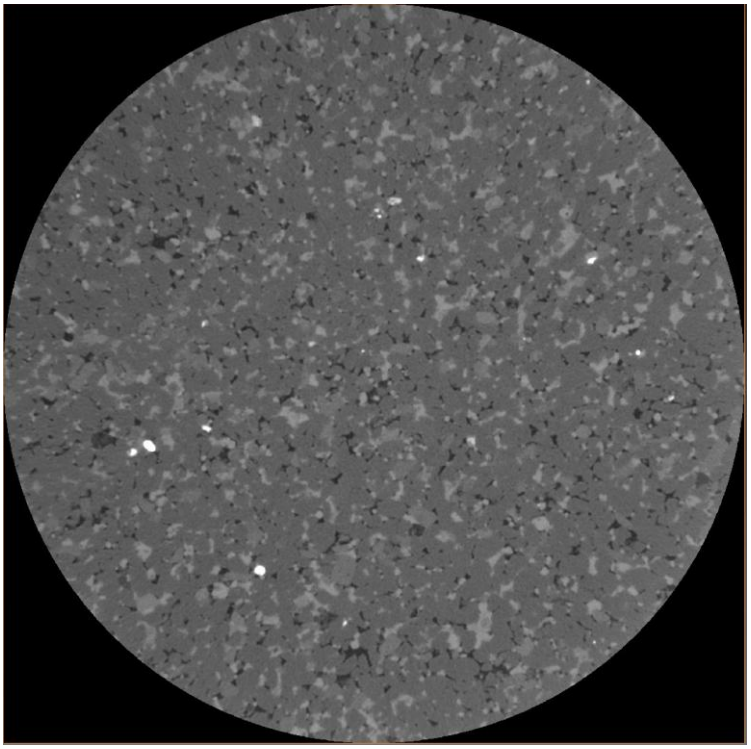

Figure-59: 'Spotty' carbonate deposition (light grey, CNV60)

Fig.59 shows another deposition feature of the carbonate. Fig.57 showed blobby deposition structure, while fig.59 shows more 'spotty' carbonate deposition. Almost all big pores are filled with carbonate and some smaller pores are left open. In contrast to fig.57, where the carbonate deposition was more regional (middle part), fig.59 shows more overall carbonate deposition. The deposition structure of heavy minerals is randomly.

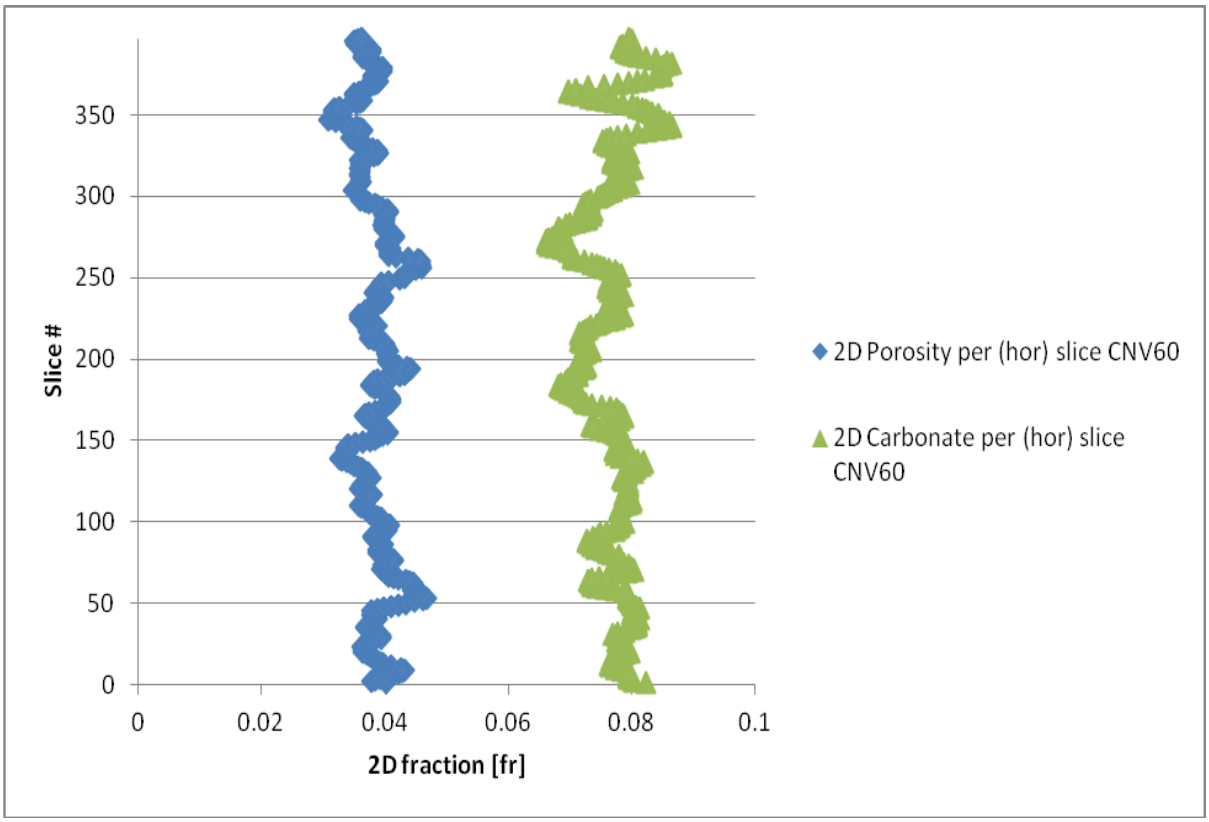

Figure-60: 2D porosity and carbonate profile (CNV60) for spotty carbonate deposition

If analyzing the 2D porosity and carbonate profile of the sample in fig.59 (CNV60), then the spotty deposition of carbonate is also illustrated in fig.60. No highly irregular features or discontinuities are present in the profiles. At some peaks in the profiles, the porosity is decreased whereas the carbonate is increased, implying pore space filled by carbonate.

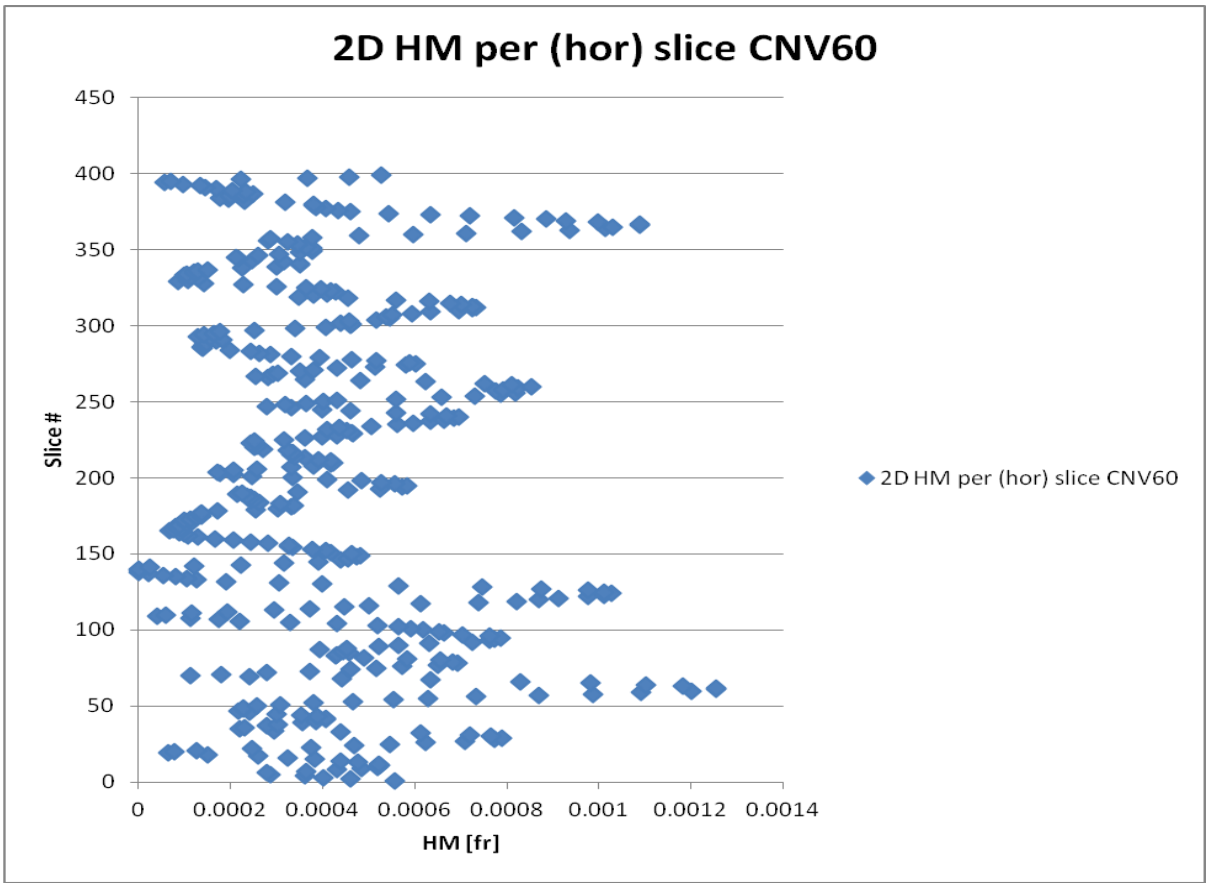

Figure-61: 2D heavy mineral profile (CNV60) for spotty carbonate deposition

Fig.61 shows the random deposited structure of the heavy minerals. The profile is highly variable and shows features of heterogeneity/ layering in the sample.

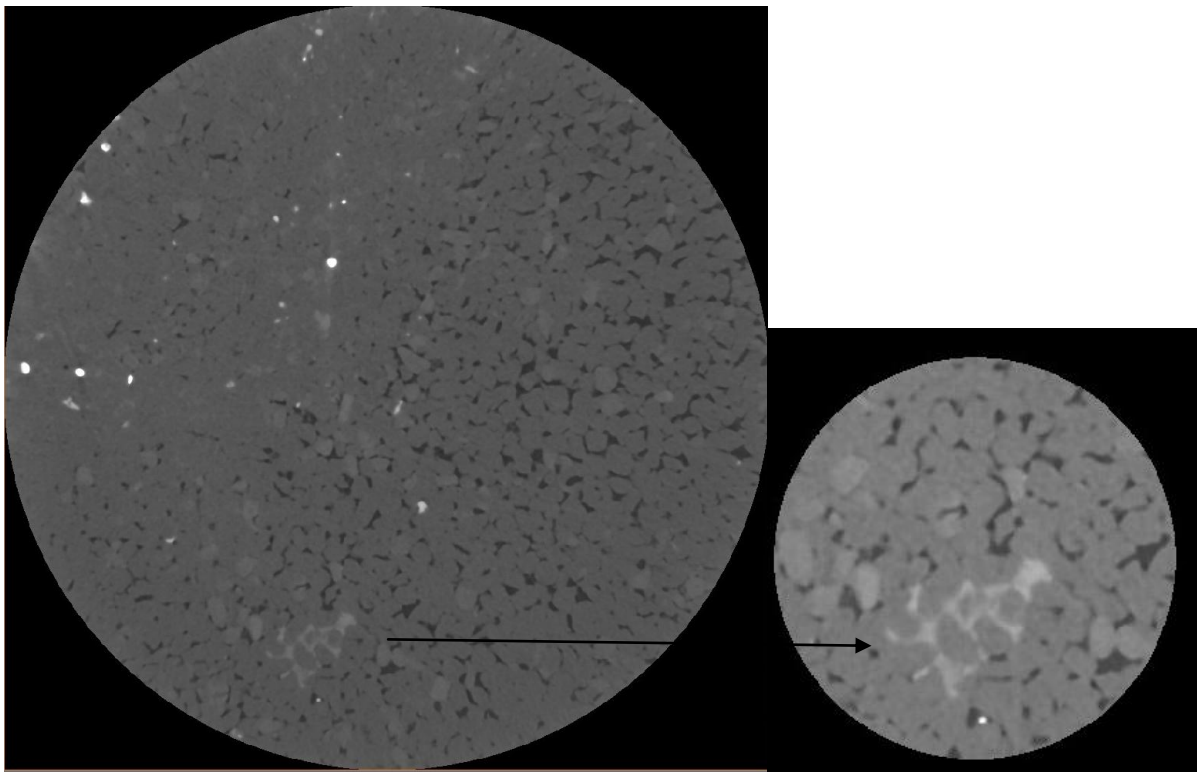

Figure-62: 'Blobby' carbonate deposition (light grey, CNV65)

Fig.62 shows a very regional deposition structure for the carbonate. The pores in the upper left part of the slice are almost completely filled with carbonate and regionally some heavy minerals, whereas the right part is not filled at all by carbonate or heavy minerals. The in zoom shows a blobby carbonate depositional structure. By comparing fig.56 (no carbonate deposition), 59 (spotty carbonate deposition) and 62 (blobby carbonate deposition) with each other, the porosity variation is clearly seen.

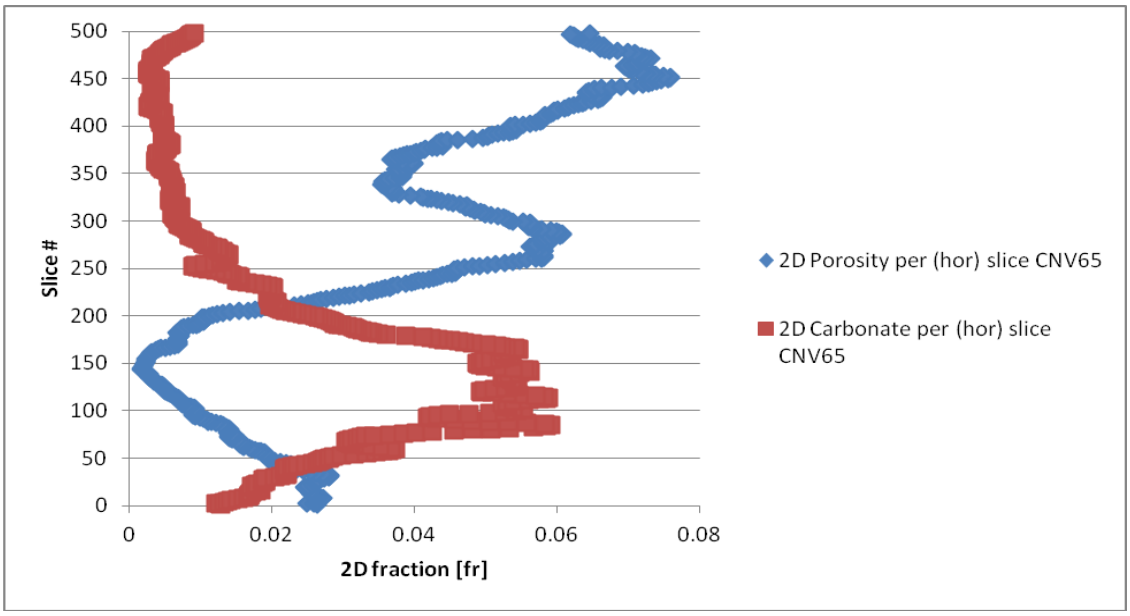

Figure-63: 2D porosity and carbonate profile (CNV65) for blobby carbonate deposition

Fig.60, which applies to spotty carbonate deposition and showed no irregularities and was reasonably constant, is not the case for fig.63. Fig.63 applies to the blobby/ regionally deposited carbonate structure as seen in fig.62. In fig.63 the pore space filling by carbonate is highly noticeable. Low carbonate values agree with high porosity values, whereas high carbonate values agree with low porosity values (between slices 50 and 200). This strongly emphasizes the replacement of pore space by carbonate filling and is much more dominant present if compared to spotty carbonate deposition. This phenomenon also applies for the heavy minerals deposition (see fig. 64).

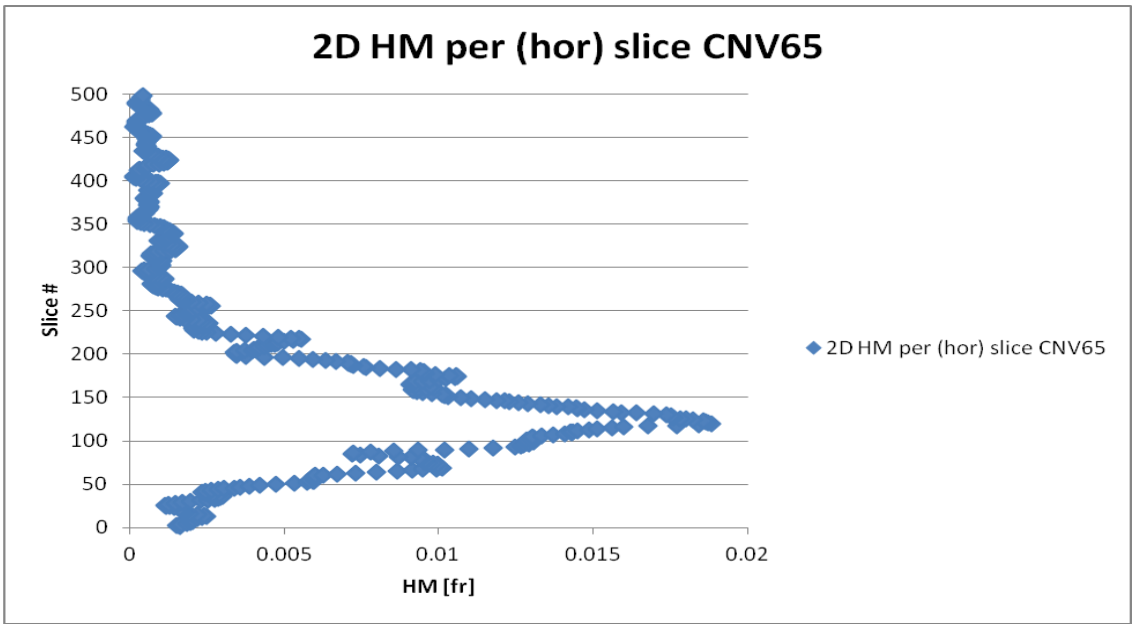

Figure-64: 2D heavy mineral profile (CNV65) for blobby carbonate deposition

3.3.2: Carbonate and heavy mineral volumes

In this section carbonate and heavy mineral profiles and comparisons are documented.

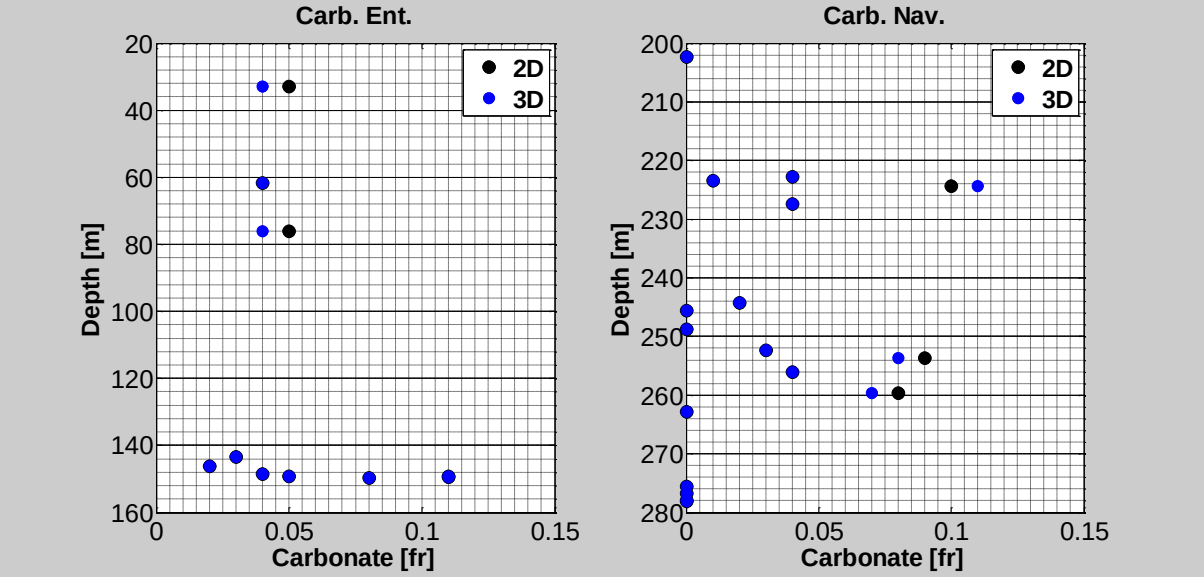

Figure-65: 2D & 3D carbonate profiles for Entrada and Navajo formations

If analyzing the profiles for carbonate for the Entrada and Navajo formations (fig.65), then no abundant trend can be seen. The carbonate deposition appears to be highly heterogeneous. The same conclusion applies for fig.66, which is for heavy minerals instead of carbonate. Note that the majority of the data points appear to be zero, but they are close to zero.

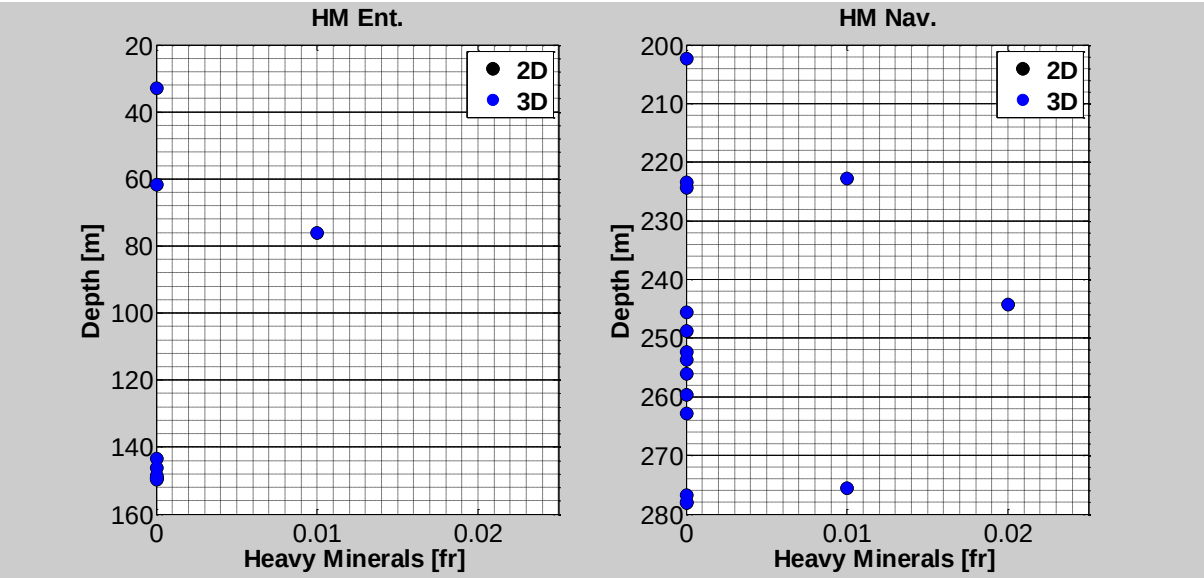

Figure-66: 2D & 3D HM profiles for Entrada and Navajo formations

As has been stated before, the results of carbonate and heavy minerals in 2D and 3D generate the same results (see fig.53 in section 3.1). This is illustrated by fig.67. The main difference lies in the dimension, meaning objects measured in area (2D-slices) and volume (3D-volumes). The lab methods like Pycnometer, Hg Shell test and Wet test are not capable of measuring carbonate and heavy mineral content, meaning that for these 2 components only image results are available.

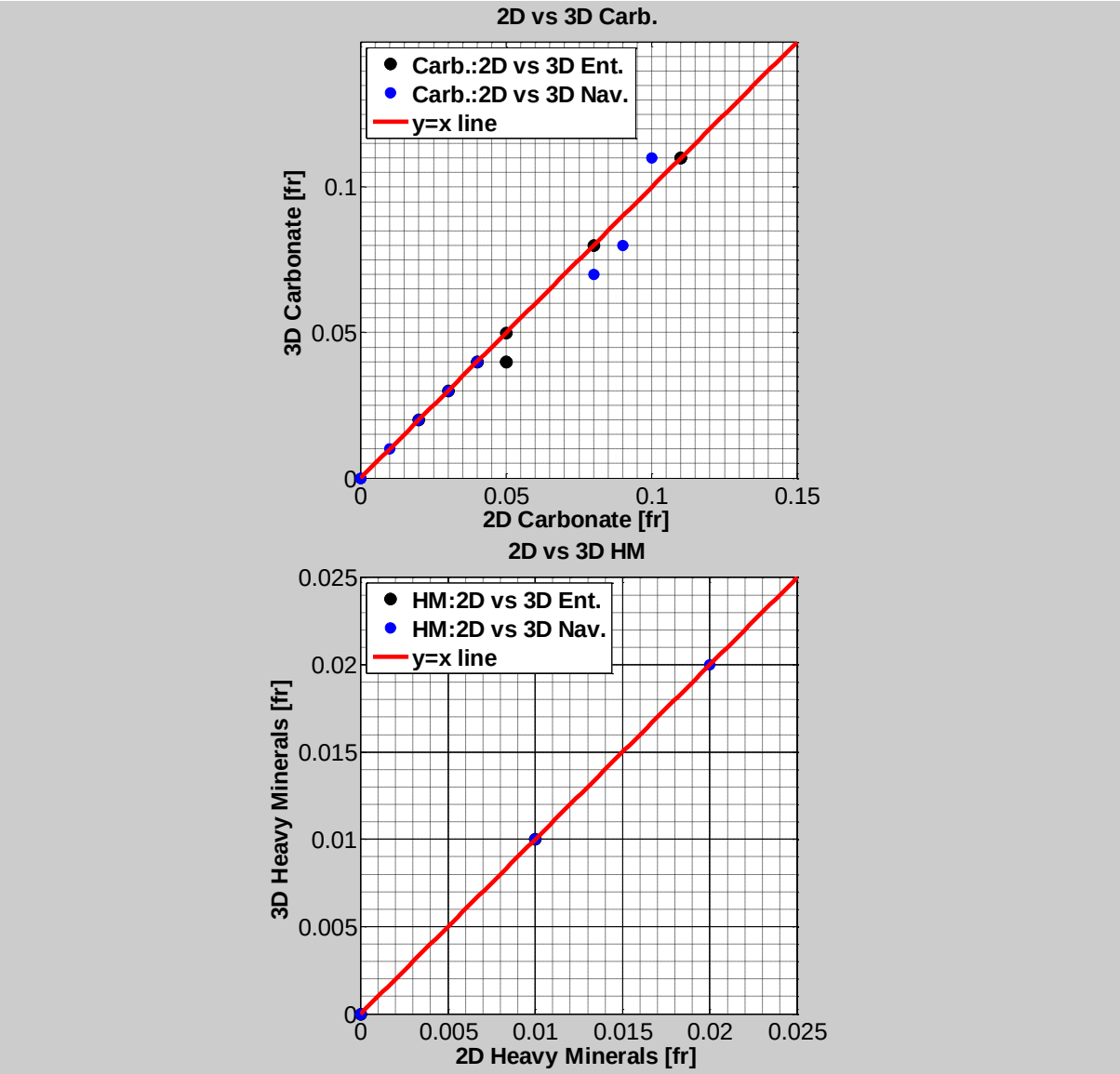

Figure-67: Heavy minerals comparison 2D & 3D

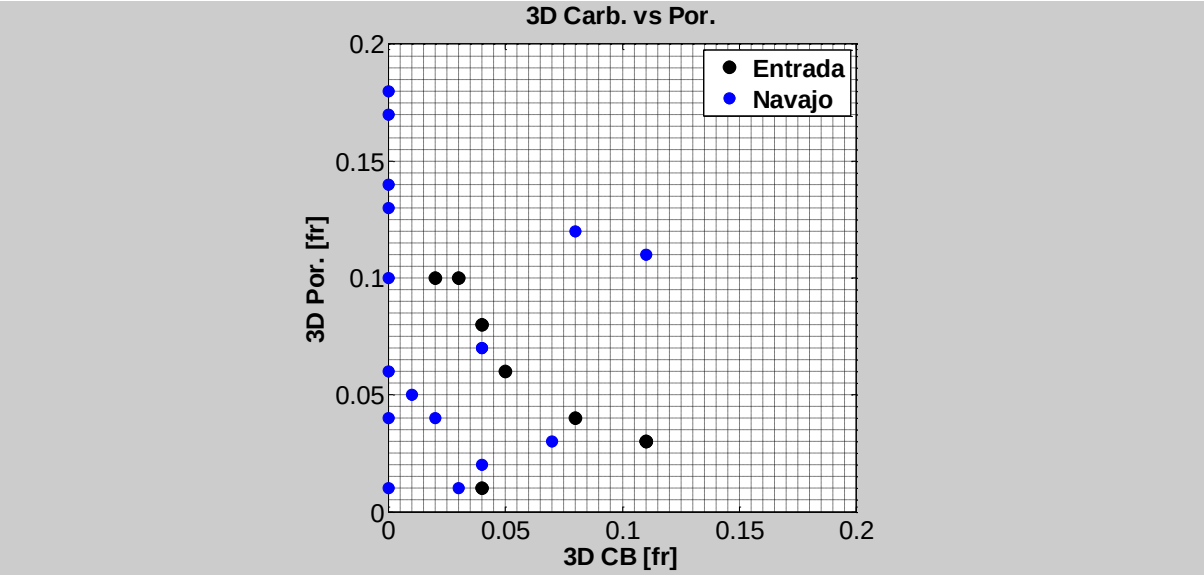

Figure-68: Porosity vs. carbonate for Entrada and Navajo formations

Fig.68 shows a slight correlation for the Entrada formation (black spots). It shows that for increasing carbonate fraction, the porosity decreases. This phenomenon is actually logical and expected if assumed that possible carbonate deposition in the original pore space will decrease the pore space. This phenomenon is not seen in the Navajo formation. The samples of the Entrada formation are situated in the deeper part of the Entrada, thus close to the fractured area, whereas this is not the case for the Navajo samples. This implies that the Entrada samples may have been affected by the nearby fracture zone, leading to significant carbonate deposition in contrast to the Navajo samples.

3.3.3: Connectivity

The main purpose of this section is to calculate the number of particles per volume for pore space and carbonate. The number of particles per volume is an indicator of the connectivity. High amounts of particles per volume indicate that the particles are not connected to each other.

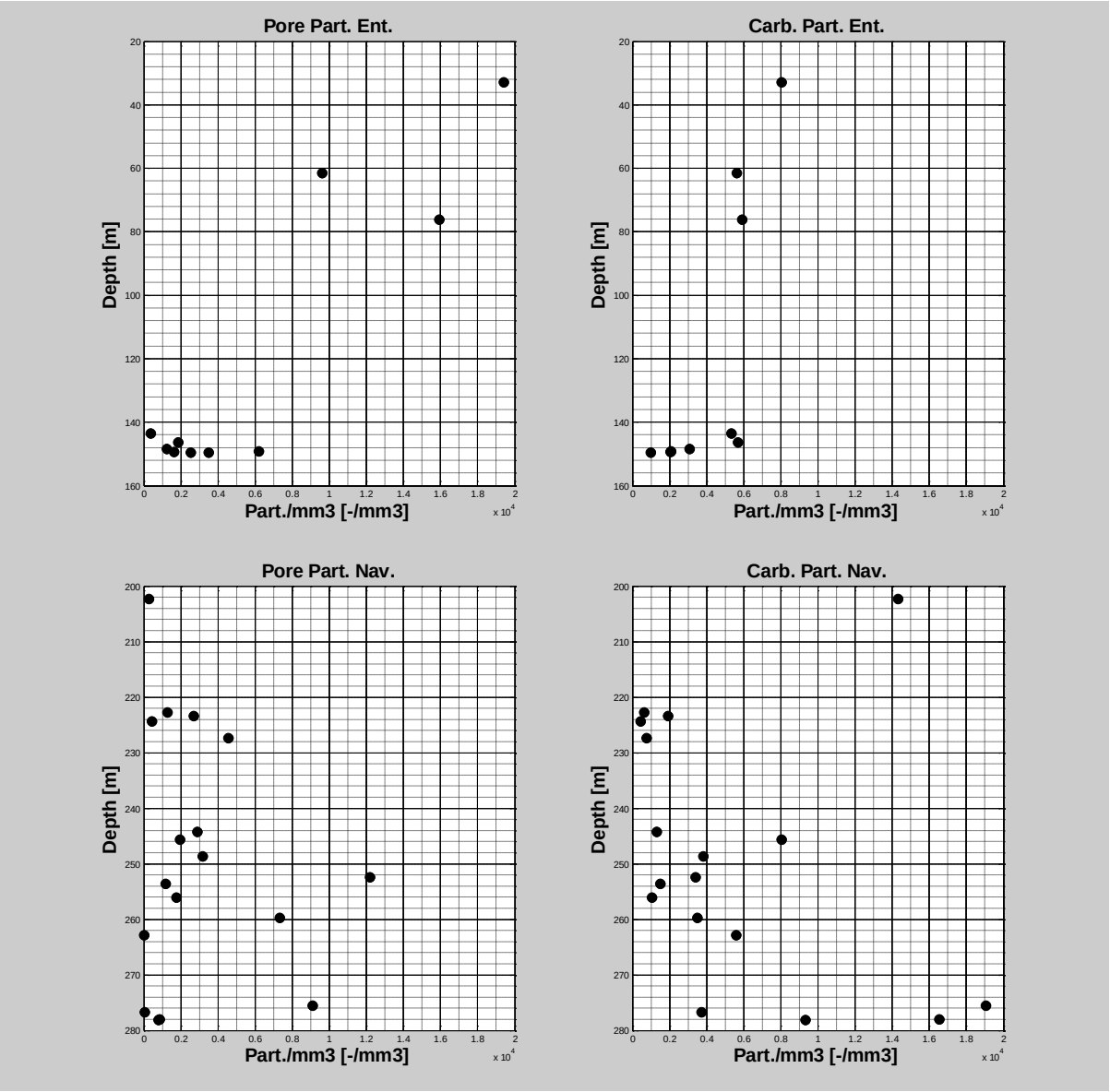

Figure-69: Pore and carbonate particles per depth (Entrada & Navajo formation)

Fig.69 illustrates the pore and carbonate particles profiles for the Entrada and Navajo formation. As is seen in the Entrada profiles, the shallow samples have high amounts of particles than the rest of the samples, indicating a low connectivity. The Navajo formation samples show no abundant trend, indicating high variability/ heterogeneity.

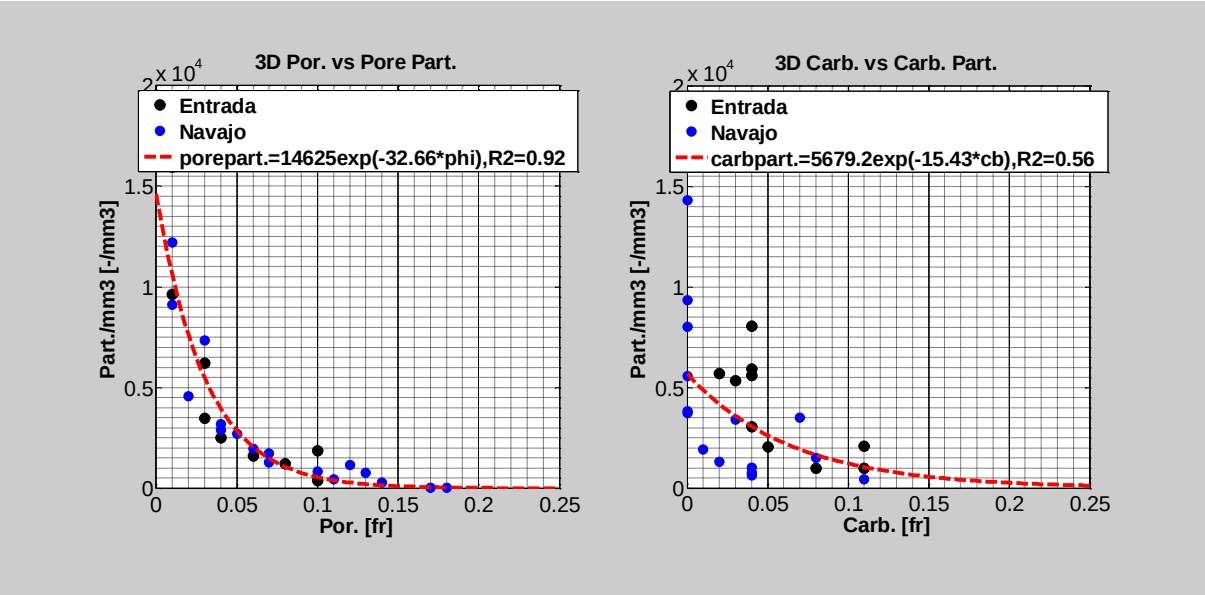

Figure-70: 3D fraction vs. particles for porespace and carbonate

Clear acquired correlations in this section are 3D carbonate fraction versus carbonate particles per volume and 3D porosity versus pore particles per volume (fig.70). Based on this figure, the relationship between particles per volume and 3D fraction for porosity and carbonate is exponential. Meaning that the more particles per volume, the lower the fraction is and so the lower the number of particles, the higher the fraction is. The relationship between particles per volume and porosity is disproportional. Essentially, this indicates that the higher the porosity, the higher the connectivity is and vice versa. The fitting for porosity is almost perfect (0.92), whereas for carbonate is less good (0.56). These trend lines have been selected after testing a number of relationships and appear to be the optimal trend lines.

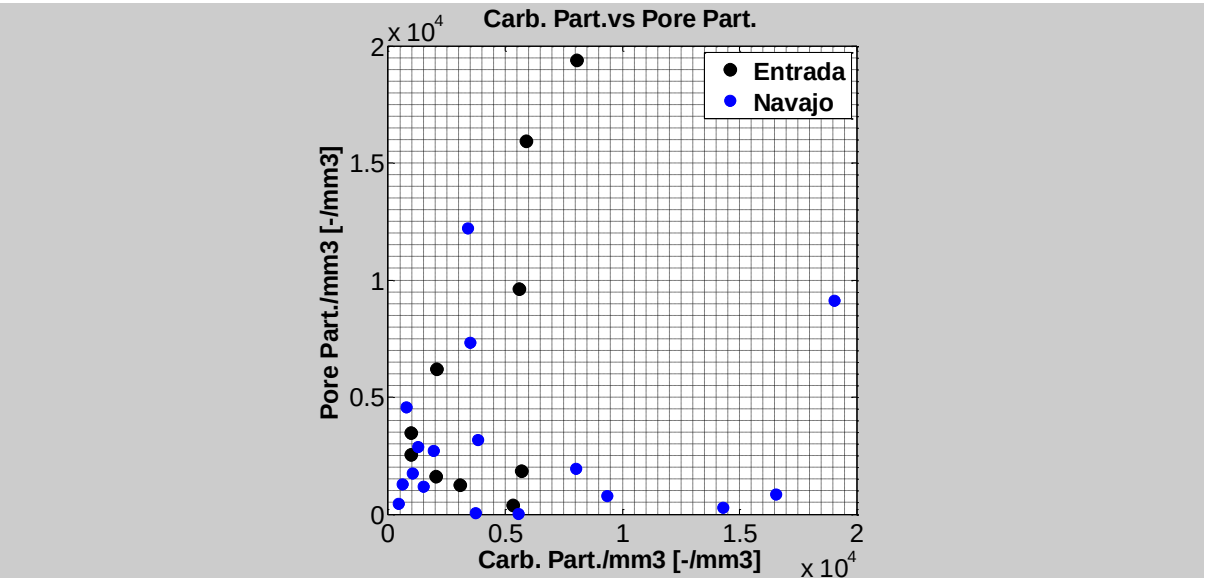

Figure-71: Pore particles vs. carbonate particles

Correlating the pore particles to the carbonate particles no essential trend can be seen. However, for the Entrada formation it may be possible to see an increase in carbonate particles and pore particles for the upper part of the graph. This means that the more pore particles, the more carbonate particles occur, implying that when carbonate is replacing pore space, the pore space is divided creating more loosened pore particles. This phenomenon agrees with the explanation in section 3.3.2, fig.68.

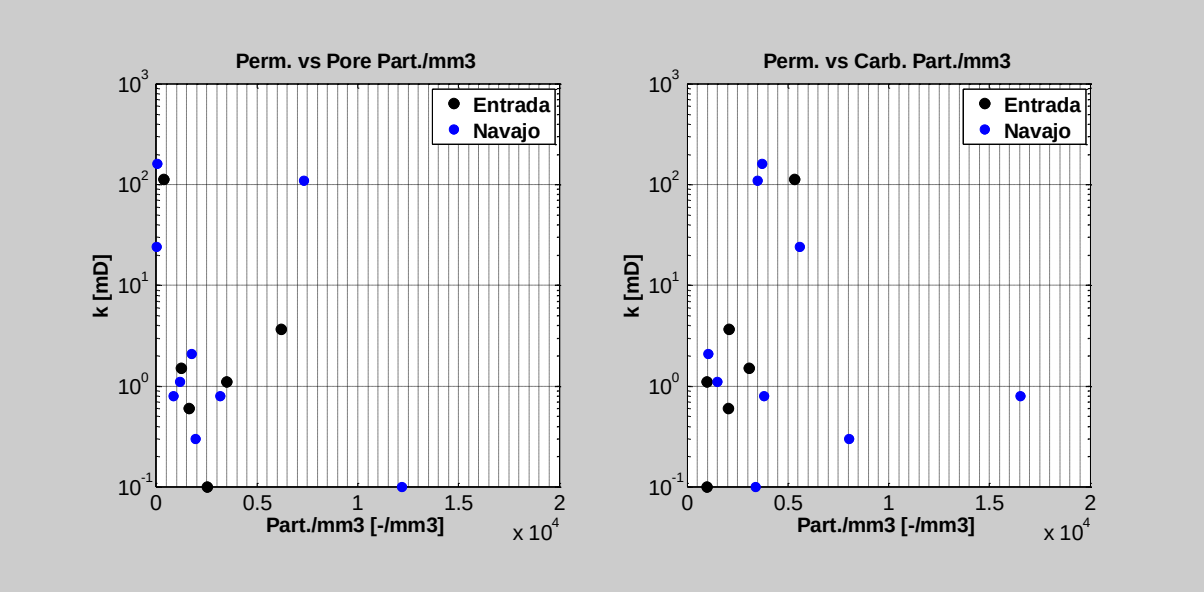

Figure-72: Correlation between permeability and pore/ carbonate particles

The relationship between permeability and pore particles as for permeability and carbonate particles per volume is not present. Generally, the high amount of particles per volume suggests a low connectivity, which is equivalent to a low permeability and vice versa. There should be a disproportional relationship between pore particles per volume and permeability. Fig.55 in section 3.2 suggests that image based permeability methods would more likely correlate to the image based porosity and thus also to the pore and carbonate particles per volume.

3.3.4: Carbonate Irregularity

The main purpose of this section is to quantify the various carbonate depositional structures by 3D grain analysis. Based on the carbonate deposited structure, grain analysis can be conducted in order to quantify de various carbonate depositional structures. The quantification can be done in 3D (volume and surface area).

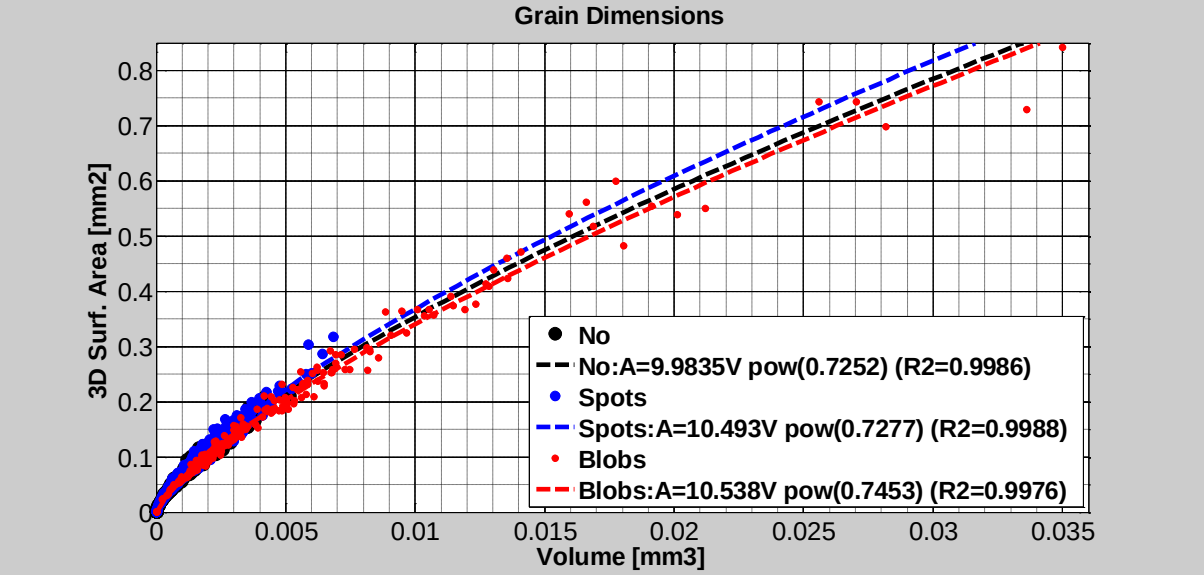

Figure-73: Silica grains dimensions (3D surface area vs. volume per grain) for 3 scenarios

This graph represents the 3 scenarios for carbonate precipitation. The 3D surface area and volume for all 3 scenarios are compared to each other. A power regression between area and volume is the best representation (fitting coefficient: 0.99). In the case of no carbonate precipitation, the maximum area and volume are respectively 0.2142 mm^2 and 0.0051mm^3. In the case of spotty carbonate precipitation, the maximum area and volume are respectively 0.3182 mm^2 and 0.0068 mm^3. In the case of blobby carbonate precipitation, the maximum area and volume are respectively 0.8418 mm^2 and 0.035mm^3. This shows that for blobby carbonate precipitation, the grains are affected to get 'bigger', whereas for no carbonate precipitation the grains appear to be smaller. The spotty case is in between. This indicates that carbonate precipitation affects the grain structure. Because of the precipitation between grains, these grains tend to 'deform'. This 'deformation' creates more irregularity of the grains and therefore higher surface area and volume.

Paragraph-3.4: Effect of fracturing

Fracture and connectivity profiles

Fractured samples contain a fracture plain. By analyzing this fracture plain for various components (porosity, carbonate and heavy minerals), the effect of the fracture on these components can be quantified. The same can be done for bleached samples. Additionally, the fractured and bleached samples are also analyzed in 3D in order to quantify the connectivity. As was done in section 3.3.3, the number of particles gives information regarding the connectivity. The main purpose of this section is to quantify the effects of bleaching and fracturing on porosity, carbonate and heavy minerals.

The results of the fractured samples (10) can be divided into 3 categories, based on fracture/ bleaching illustration/ dependence:

- Cat-1: fracture illustration(CAR-614-FR)
- Cat-2: bleaching on a Entrada sample (ENT-108-BL)
- Cat-3: no clear fracture presence (NAV-730-FR, NAV-733-FR, NAV-746-FR, NAV-801-FR, NAV-912-FR, ENT-202-FR, NAV-736-FR, ENT-108-FR, NAV-663-FR)

Cat-1:

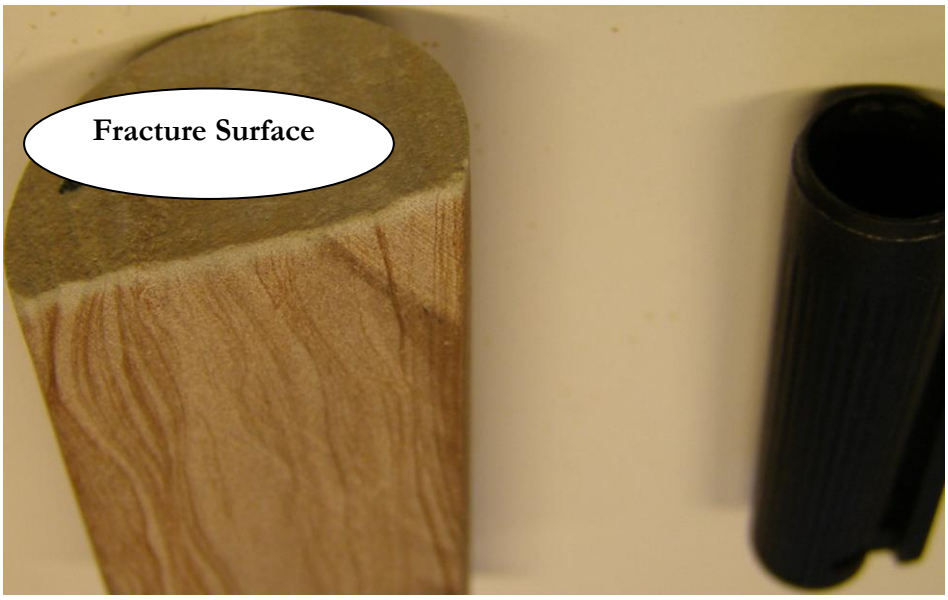

Figure-74: Carmel (CAR-614-FR) sample with fracture plane

Fig.75 shows a 3D image of the Carmel sample for carbonate occurrence. The orientation is equivalent to fig.74. From the top to the bottom the (occurrence) density of carbonate decreases. This nicely correlates to fig.77, which shows the 2D component profiles for this sample. The orientation of fig.77 is also equivalent to fig.74.

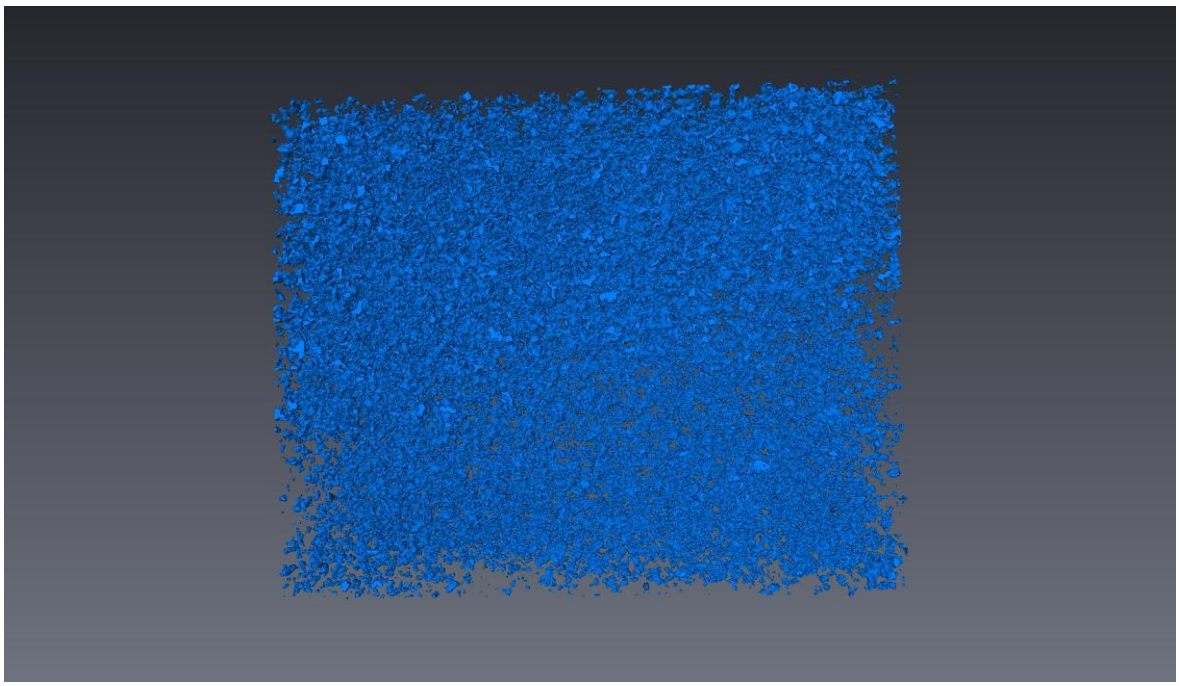

Figure-75: Micro CT representation of carbonate occurrence of Carmel (CAR-614-FR) sample

Fig.76 shows a 3D image of the Carmel sample for heavy minerals occurrence. The orientation is equivalent to fig.74. From the top to the bottom the (occurrence) density of heavy minerals decreases slightly. This nicely correlates to fig.77.

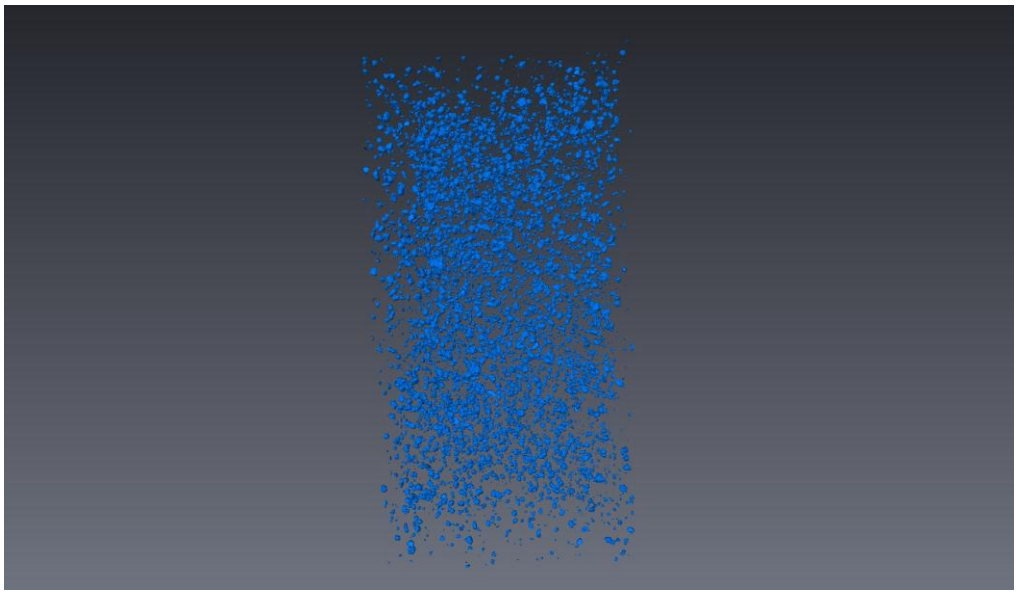

Figure-76: Micro CT representation of heavy minerals occurrence of Carmel (CAR-614-FR) sample

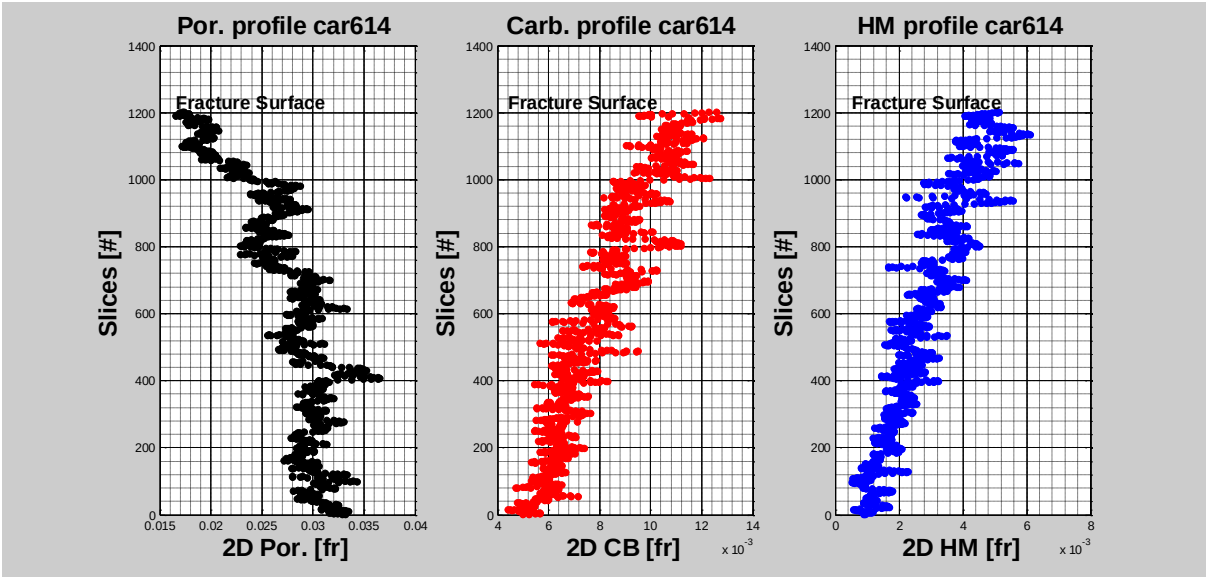

Figure-77: Cat-1: porosity, carbonate and heavy minerals profile for Carmel sample

In cat-1 the fracture dependence is nicely illustrated. At the fracture plain the porosity is at its minimum, while the carbonate and heavy minerals deposition at the maximum is. Parts of the porespace are replaced by carbonate and heavy minerals. If going away from the fracture, the porosity increases, while the depositional components decrease. This indicates the presence of the fracture.

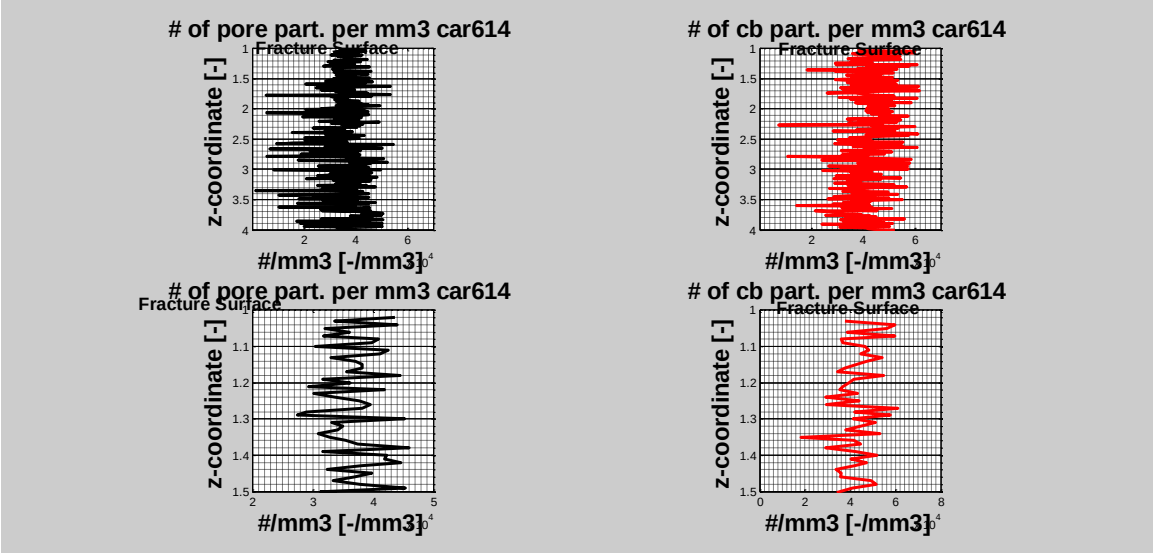

Figure-78: Cat-1: # of pore and carbonate particles per mm^3 with zoom in for Carmel sample

Based on the connectivity results, no trends are seen. There seems to be no influence of the fracture presence on the connectivity. Based on fig.75-77, there is difference in 2D component fractions. However, the reduction in porosity and the increase in carbonate and heavy minerals (from top to bottom) are relatively small (max 0.5%). Generally, connectivity profiles will only differ if there is a high anomaly (for example porosity difference between shales and eolian sandstones-> approx. On average 20%) in pore space i.e. sandstone on top of a shale will create a great anomaly in connectivity.

Cat-2:

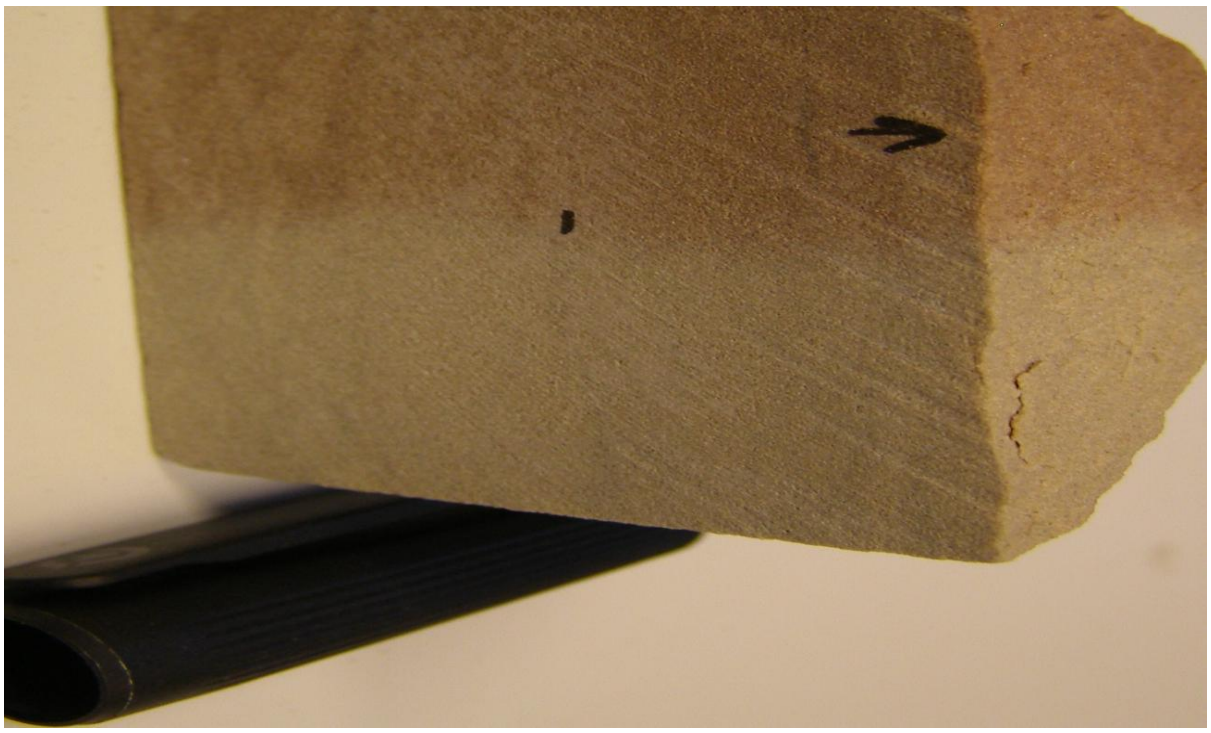

Figure-79: Cat-2; Entrada (ENT-108-BL) bleached sample

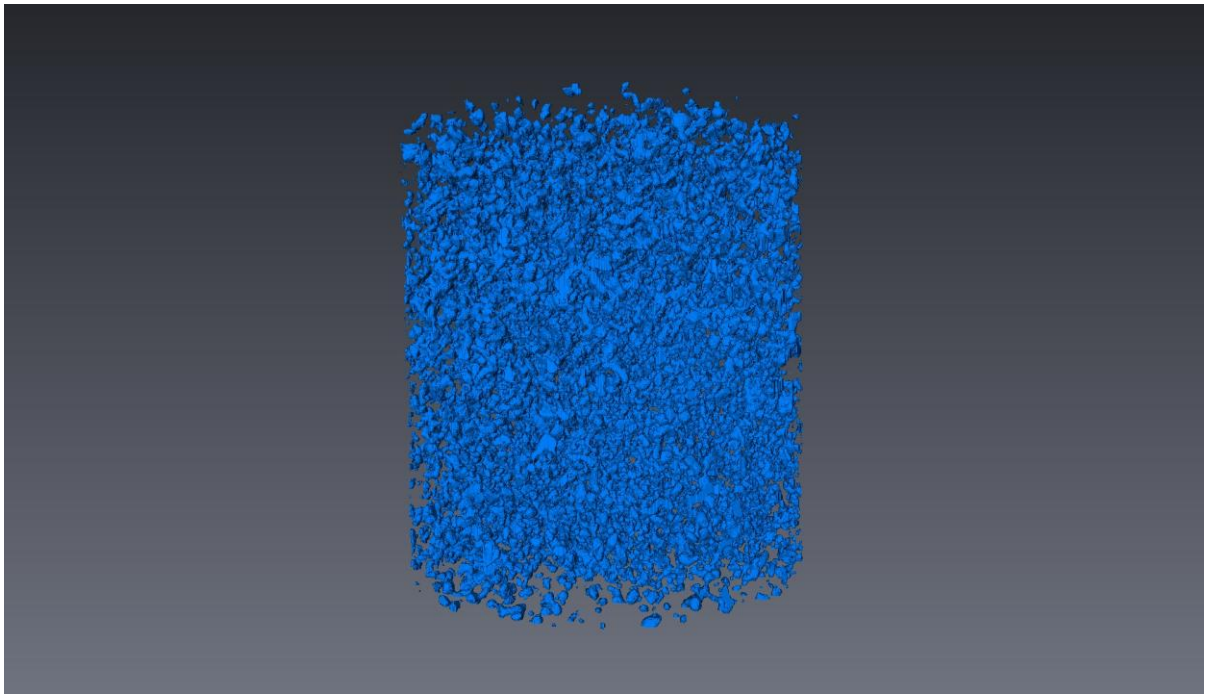

Figure-80: Micro CT representation of carbonate occurrence of Entrada (ENT-108-BL) bleached sample

Fig.80 shows a 3D representation of carbonate occurrence of the bleached sample. The orientation is equivalent to fig.79. It is not easy to see a trend or increase/ decrease in carbonate occurrence in fig.80. This same conclusion applies to fig.81, which shows a 3D representation of heavy minerals for the bleached sample.

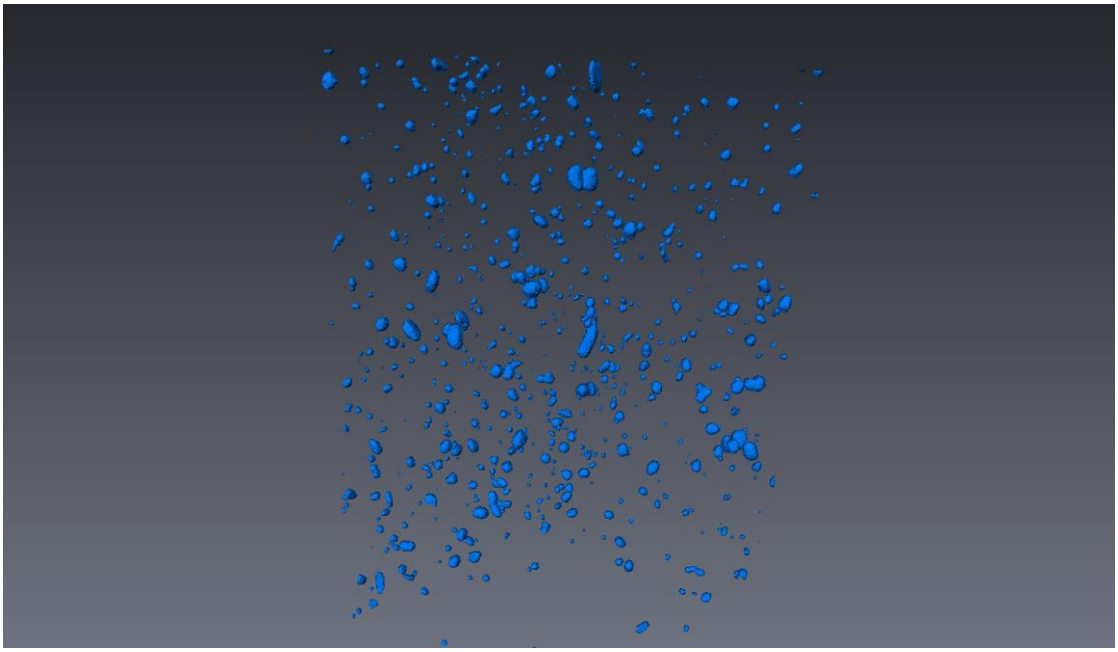

Figure-81: Micro CT representation of heavy mineral occurrence of Entrada (ENT-108-BL) bleached sample

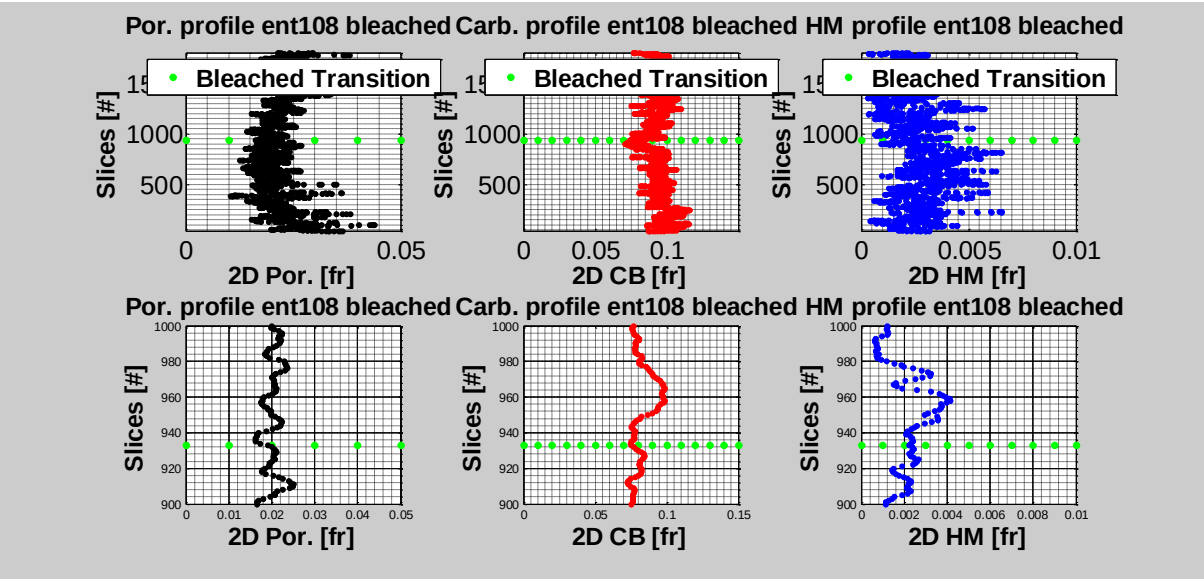

Figure-82: Bleached zone transition (ENT-108-BL); porosity, carbonate and heavy minerals profile with zoom in

The conclusions based on fig.80 and fig.81 correlate to the profiles in fig.82. The profiles from top to bottom represent oxidized (red) to bleached. Bleaching means that water flow with carbon

dioxide solution enables iron minerals to flush out of the rocks. 'Downstream' several geysers are identified which show high concentration of iron minerals (Bickle et al. (2009)). This transition cannot be seen in the profiles of porosity, carbonate and heavy minerals; the profiles show no clear trend. Based on this, the conclusion can be drawn that the bleaching which is clearly seen on the surface of the sample has no essential effect on the analyzed components.

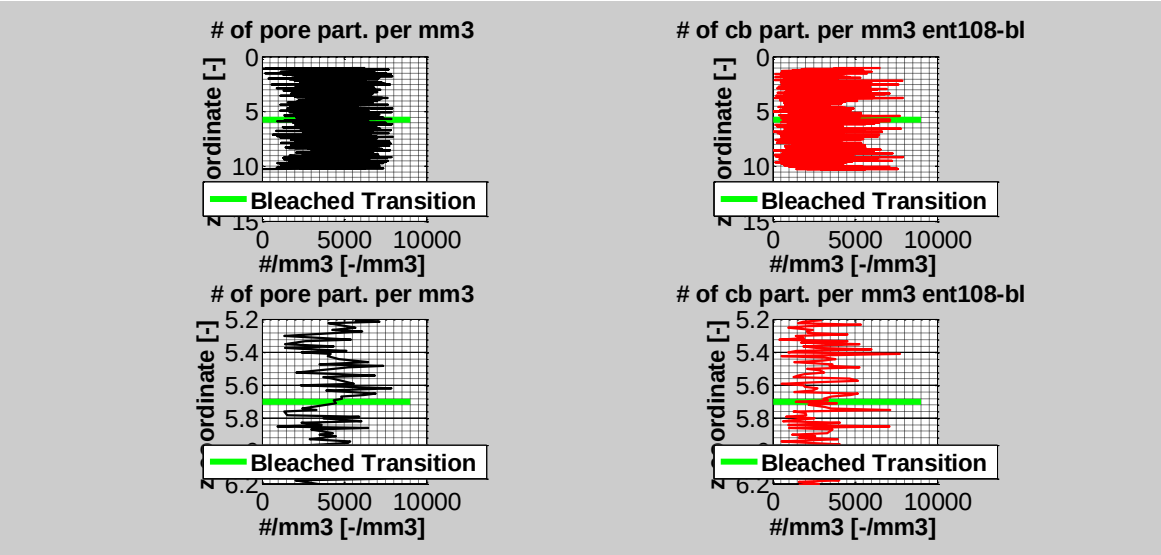

Figure-83: Bleached zone transition (ENT-108-BL); # of pore and carbonate particles per mm³ with zoom in

The profiles from top to bottom represent oxidized (red) to bleached. If searching for the effect of the bleaching in terms of connectivity, the conclusion can be drawn that there is no clear trend for carbonate particles, however pore particles from the oxidized to bleached zone decrease. This means that the connectivity from oxidized to bleached increases. The increase in connectivity may be explained by the bleaching, which gets rid of heavy minerals and slightly increases the porosity (the porosity increase can be seen in fig.82)

Cat-3:

NAV-663-FR and NAV-733-FR of cat-3 have been selected and represents the rest of the remaining samples. Cat-3 implies no clear fracture dependence.

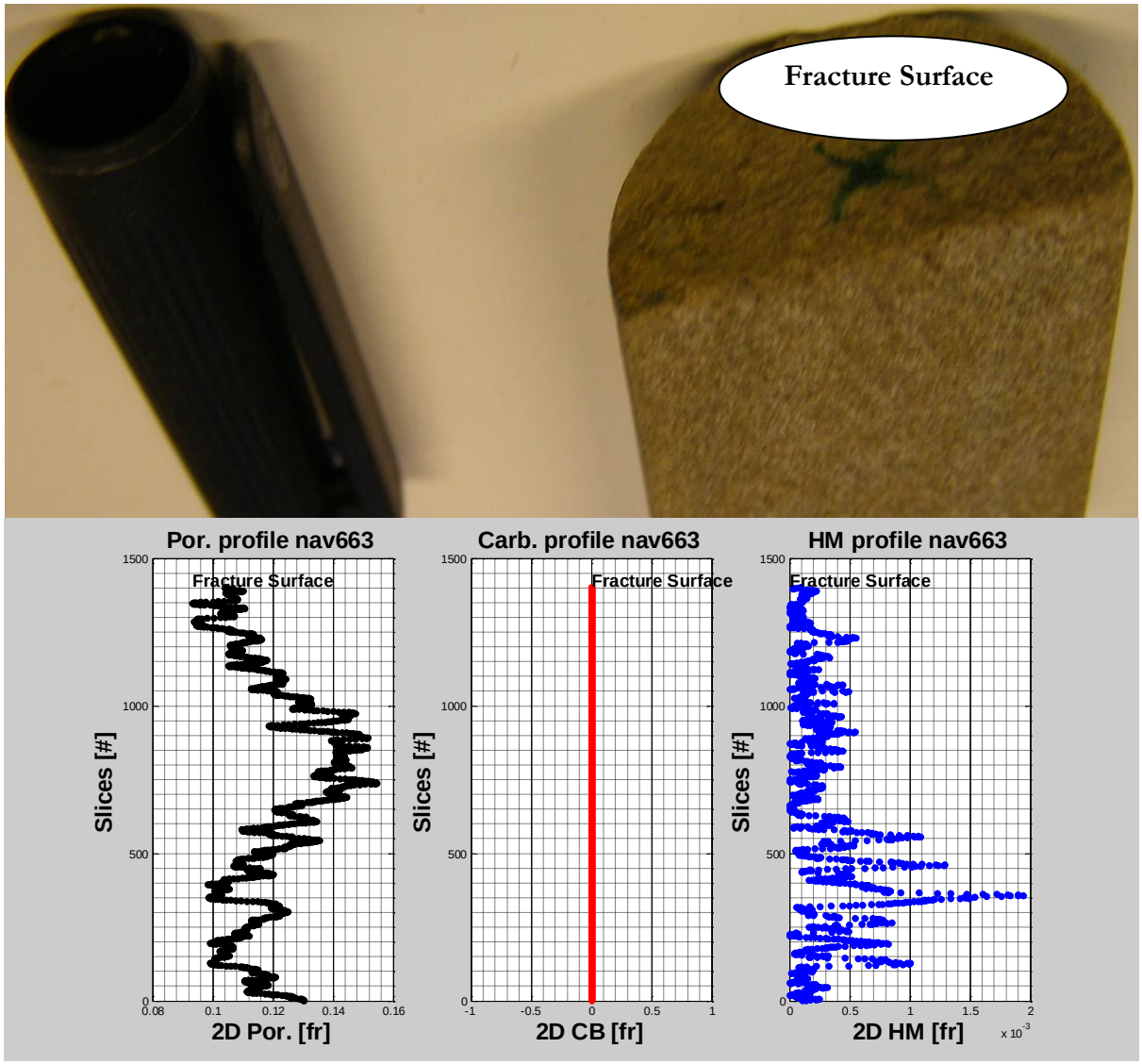

Figure-84: Cat-3: porosity, carbonate and heavy minerals profile

In fig.84 the fracture dependence is not present as was the case in cat-1. Carbonate deposition is zero, so no carbonate deposition at all. This counter correlates to the presence of a fracture. Fig.85 shows the measurable micro CT pore space representation. As can be seen in fig.85, the pore space shows high variability. On some levels, the pore space is very dens present and on other levels the pore space is less dens present. This feature correlates nicely to the porosity profile in fig.84.

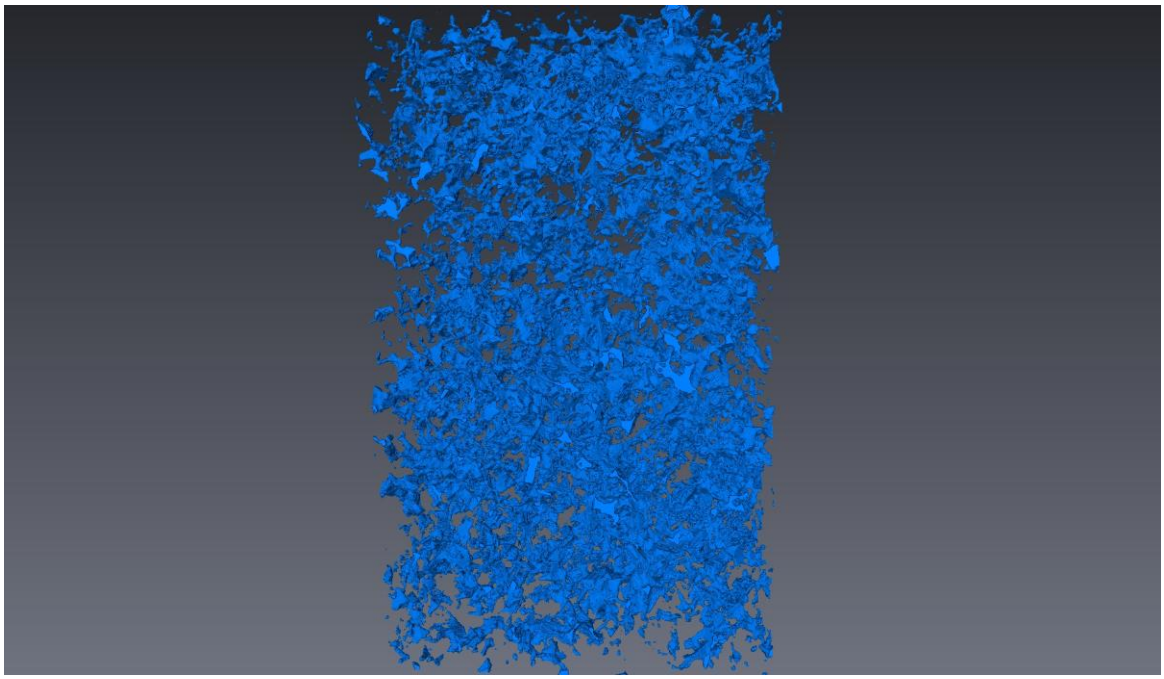

Figure-85: Micro CT representation of porosity occurrence of NAV-663

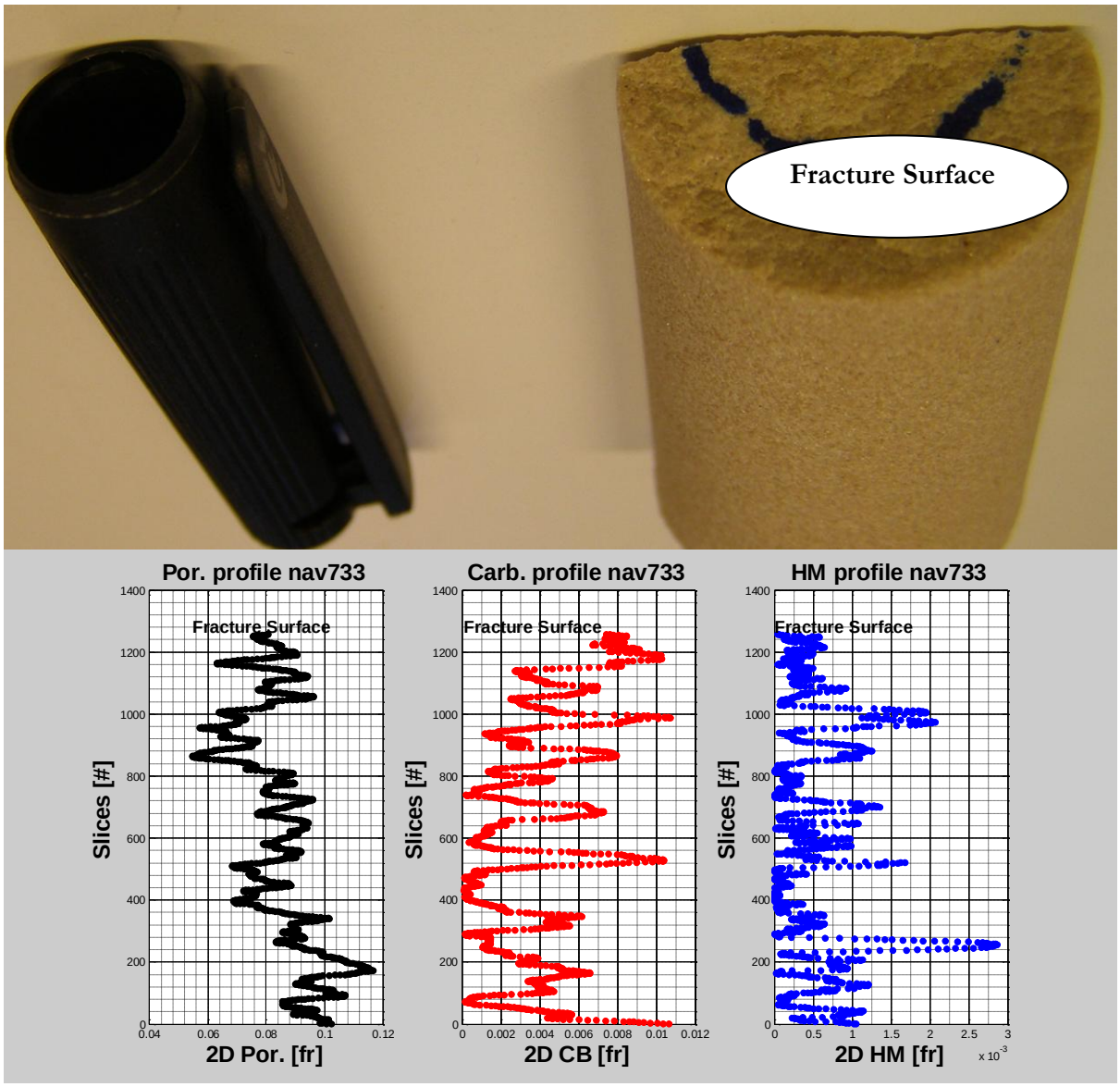

Figure-86: Cat-3: porosity, carbonate and heavy minerals profile for NAV-733

In fig.86 the fracture dependence is also not present as was the case in cat-1. All three components show variability in the profiles and do not indicate a direct fracture dependence.

The counter correlation of the components with respect to the fracture needs an alternative explanation. The fracture cannot be the cause that away from the fracture the carbonate/ heavy minerals depositions increases. An alternative explanation can be that older/ other fractures/ phenomenon and high heterogeneity are the cause of these depositions (fig.85 shows the variability in pore space, which is reflected in the porosity profiles in fig.84 and 86).

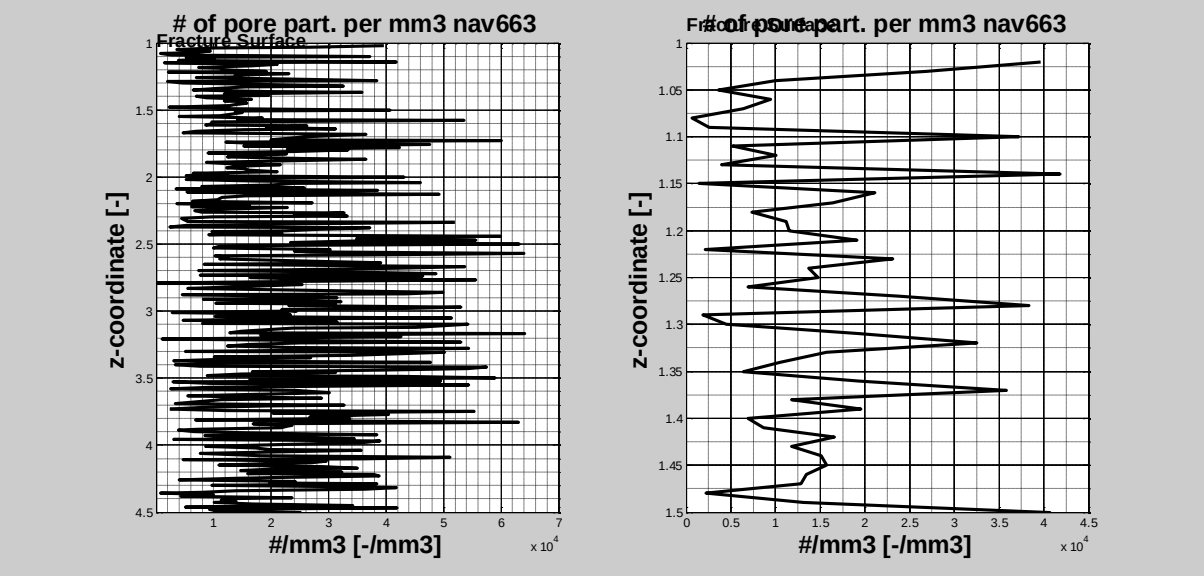

Figure-87: Cat-3: # of pore particles per mm³ with zoom in for NAV-663-FR

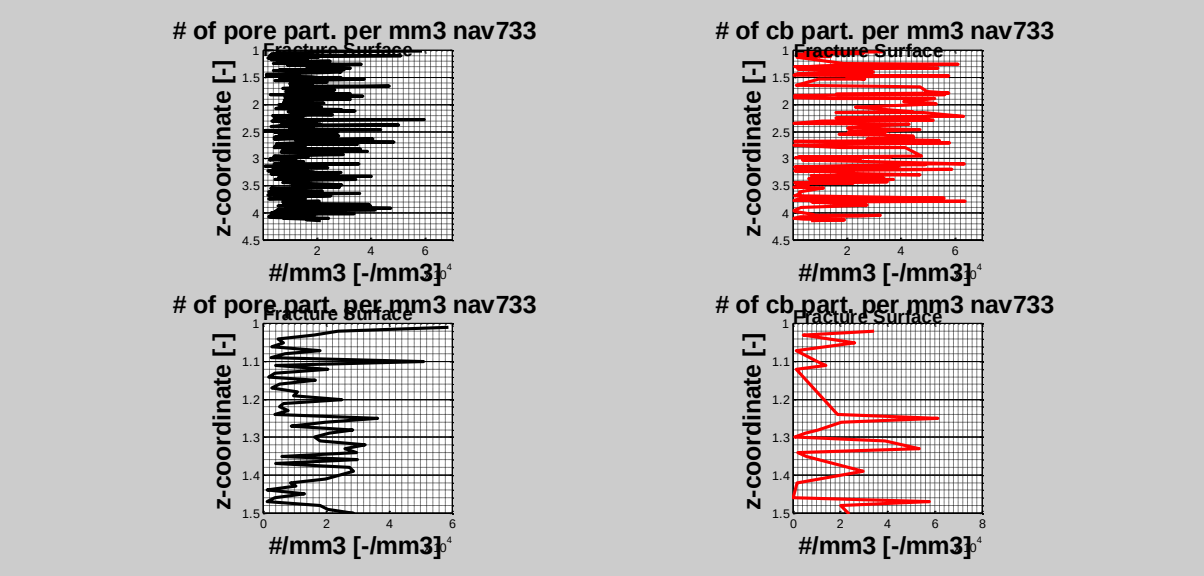

Figure-88: Cat-3: # of pore and carbonate particles per mm³ with zoom in for NAV-733-FR

Based on the connectivity results, no trends are seen. There seems to be no influence of the fracture presence on the connectivity. This result correlates to the result acquired in the previous paragraph. Generally, connectivity profiles will only differ if there is a high anomaly in pore space i.e. sandstone on top of a shale will create a great anomaly in connectivity.

Extra

Non-fractured related, fig.89 shows a micro CT representation of natural heterogeneity. Natural variability in layering can be the cause of porespace variability. Fig.89a shows sedimentary based heterogeneity and fig.89b shows compaction bands, where pore space is not present in compacted areas in comparison to not-compacted areas.

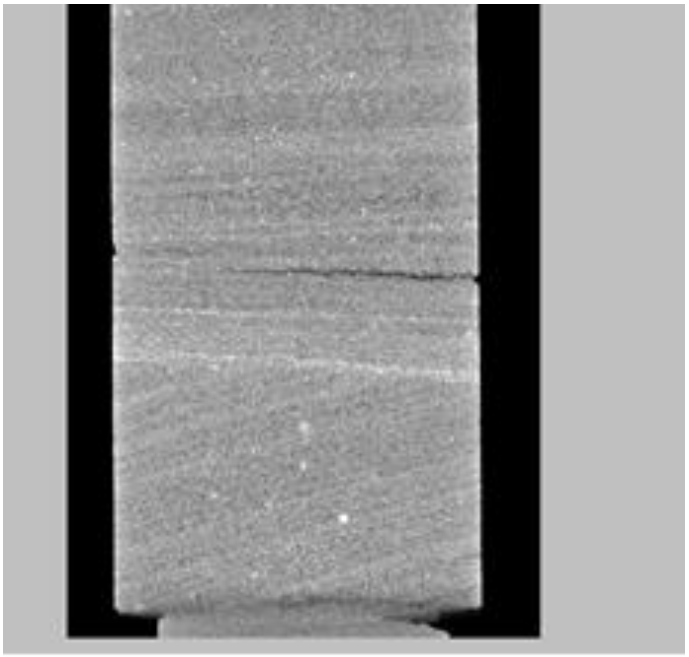

Fig.89a: natural heterogeneity in layering

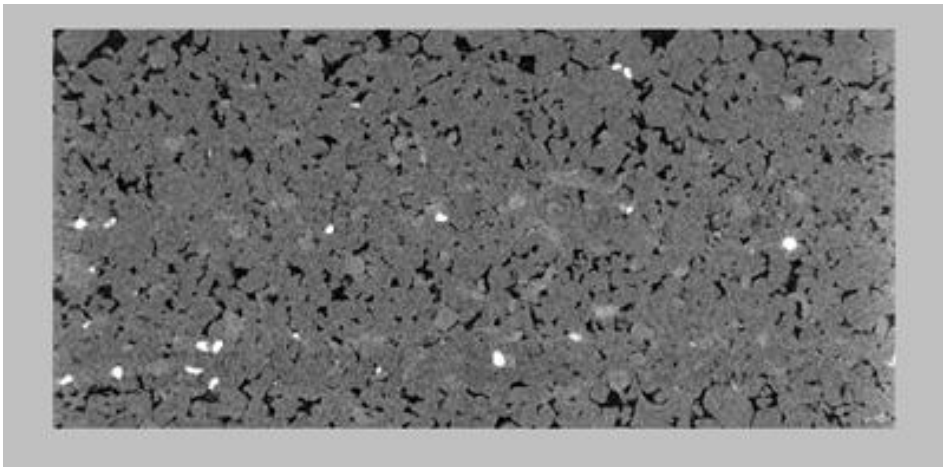

Fig.89b: natural heterogeneity in layering (compaction bands)

Discussion

Resolution, lab versus image methods

Porosity has been acquired in the lab and with use of Micro CT technique. Lab based porosity (Pycnometer, Wet Test & Shell) results and image based porosity (Micro CT) results are not in agreement with each other. The image based results are generally underestimated in comparison to the lab results. Two main reasons may be sample volume differences and resolution features. The volume used in the lab methods is much bigger (~25 times) than the volume used in the image method, which may lead to picking of highly heterogeneous sample volumes for the image method. The large volume difference has to do with the fact that the bigger the sample is, the better its representation in lab methods, whereas the smaller the sample is for image methods, the more detail can be captured. Furthermore, all pore features below 2.5 microns resolution may not be captured by the image method. 2.5 microns will not be robust/ reliable enough to quantify shales; a higher resolution will be needed for shales. By lowering the resolution the robustness of the 2.5 microns resolution has been tested positive, because 5 and 10 microns generally show the same results (see fig.90). Generally, if lowering of resolution generates same results, the original resolution (2.5 microns) will be robust. If 5 and 10 microns would show different results, then the 2.5 microns resolution would not be robust. A correlation between lab based and image based results show no reasonable fitting (see fig.91).

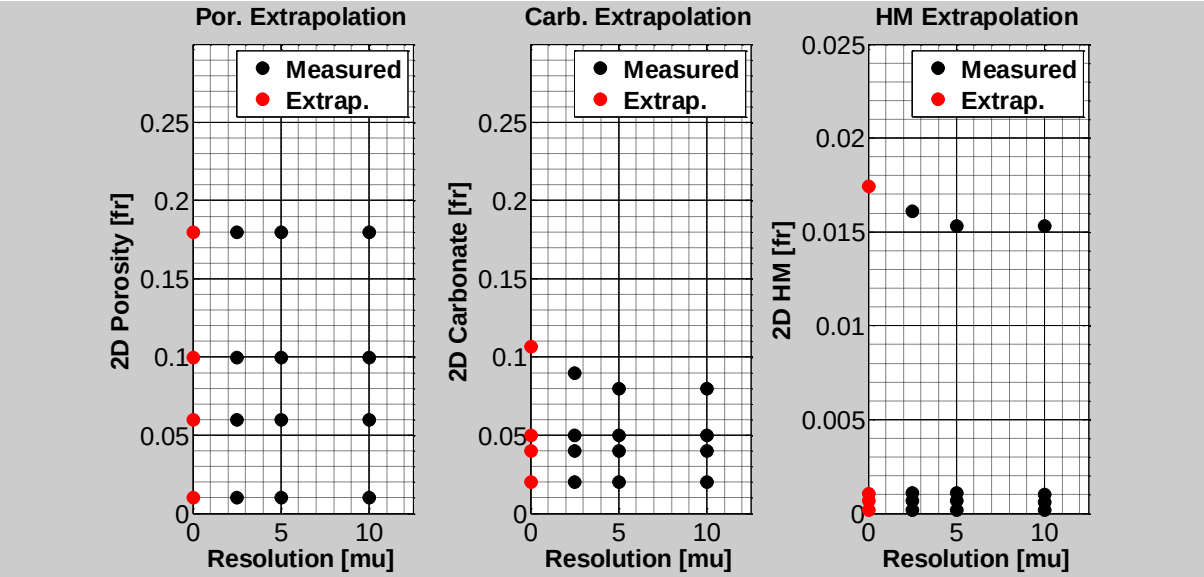

Figure-90: 2D components as function of resolution

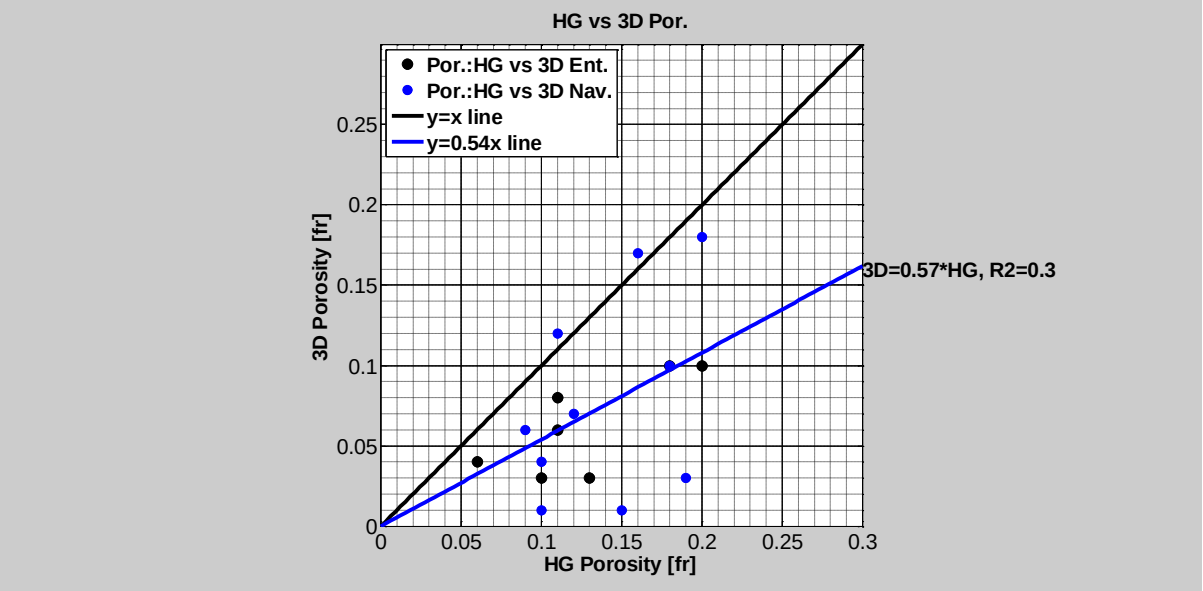

Figure-91: Porosity comparison Hg & 3D (lab and image)

Blunt et al. (2012) conducted Micro CT and lab tests on rock samples (Fontainebleau sandstone, Berea sandstone and Saudi Aramco samples). The objective was to petrophysically determine porosity and to correlate the lab methods to the Micro CT method. They found that the difference between their Micro CT and lab based methods was on average 2 % porosity, meaning that the Micro CT method is 0.87*lab method. If comparing this to the relationship acquired in fig.91, there is a difference in the factor (0.57 vs. 0.87). The samples used by Blunt et al, 2012 were clean sandstones (no carbonate deposition in the pores) in contrast to samples used in this report. It is therefore more likely that clean sandstones (no pore filling) may produce much better correlations between lab and Micro CT methods.

Permeability

Shell, as one of the stakeholders, has conducted permeability measurements in the lab. Permeability is a very sensitive parameter to the smoothness of the cores, the pores which are not connected to the gas pathways are not measured, the smoothness of the sleeve containing the core (sufficient radial pressure) and non leaking flow lines. The correlation of lab based permeability to lab based porosity is present (see fig.92). Correlating the lab based permeability to the image based porosity, the correlation will not be reasonable (see fig.92). This is because of the underestimation of the image porosity due to volume and resolution features. It will be more likely that image based permeability will fit image based porosity.

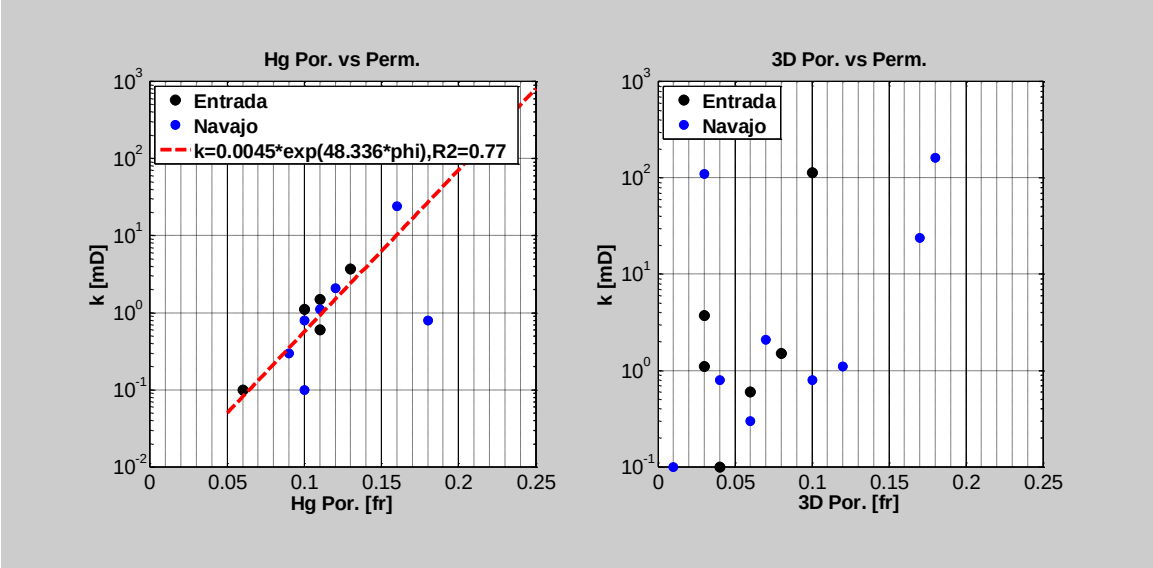

Figure-92: Correlation between permeability and porosity for lab and image methods

Mostaghmi et al. (2012) have conducted porosity and permeability measurements by use of Micro CT technique. One of the objectives was to use Micro CT technique to determine porosity permeability relationships. The permeability is a numerical Stokes flow based image technique with no flow conditions at the solid boundaries. Basically, the permeability uses the pore space which has been detected based on grey values. Fig.93 shows the reasonably good fit for porosity versus permeability based on Micro CT flow simulations. Comparison to fig.91 (0.3 vs. 0.9) is evident for fitting coefficients.

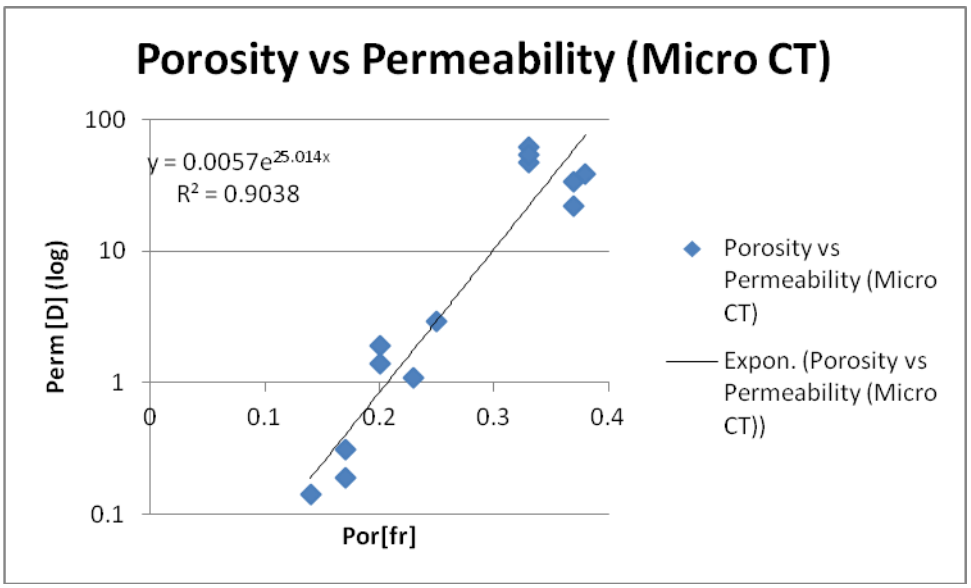

Figure-93: Porosity vs. permeability Micro CT based (Mostaghmi et al., 2012)

In this report, the lab based porosity is found to be larger than the image based porosity. This was also one of the findings of Blunt et al. (2012). Based on these findings and the fact that lab based porosity- permeability and image based porosity- permeability relationships are reasonable,

it is likely that the image based permeability will be smaller than the lab based permeability. This has also been found by Kaczmarczyk et al. (2011). They conducted evaluation of carbonate rock permeability with use of Micro CT. For various samples it was found that the lab based permeability is always higher than the image based permeability and that the difference between lab and image based permeability can be between 2.5%- 50%.

Carbonate precipitation

Carbonate precipitation is one of the most interesting phenomena in this research, because it may give an indication of the result of CO_2-brine fluxes through sandstones. For the Entrada formations some correlations are found like carbonate replacing pore space meaning that the higher the carbonate fraction gets, the lower the porosity gets and the larger the number of carbonate particles per volume get, the larger the number of pore particles per volume get (see fig.94 & 95).

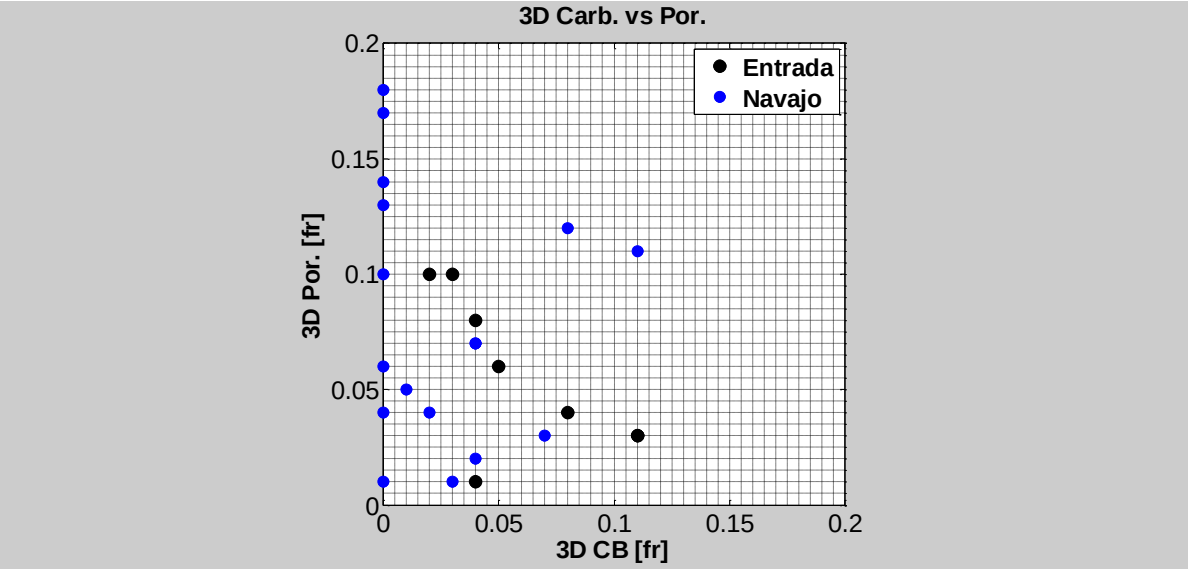

Figure-94: Porosity vs. carbonate for Entrada and Navajo formations

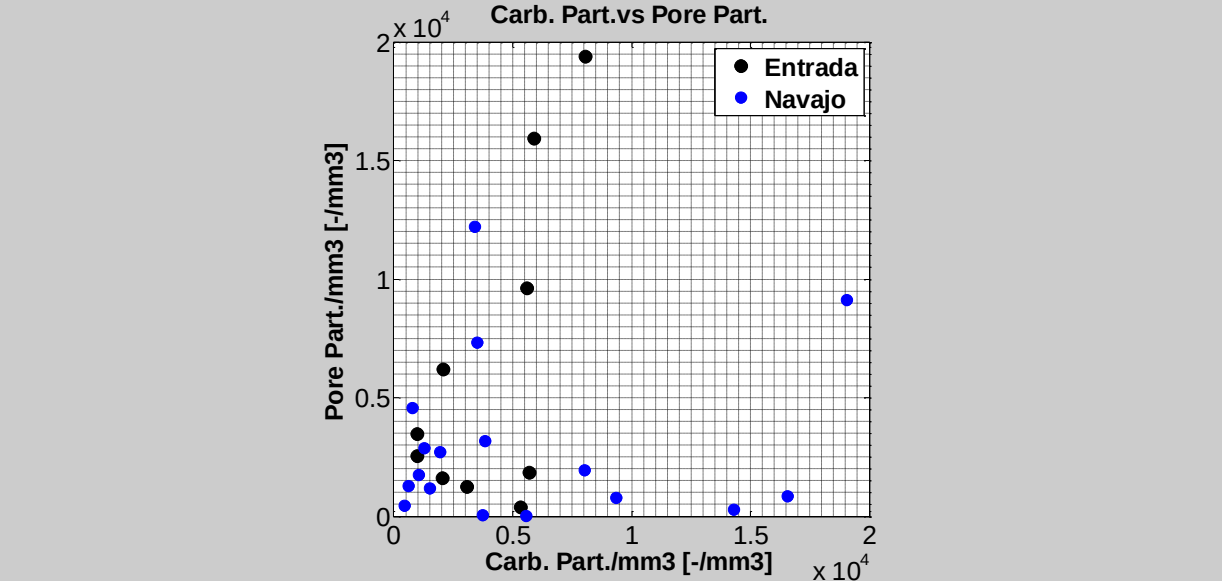

Figure-95: Pore particles vs. carbonate particles

The few samples of the Entrada formation show some features of carbonate replacing pore space. These samples are indeed in lower part of the Entrada formation, meaning close to the fracture zone in contrast to the Navajo samples. The fracture may have been the supplier of carbonate in the deeper part of the Entrada formation. However, this feature may also be an older sedimentary process. This doubt is caused due to section 3.4, where the fracture presence is not seen at all in the Entrada samples. They show no fracture presence and are more likely affected by high heterogeneity and variability caused by other/ older depositional/ sedimentary features. This is also the case for the Navajo samples. The Carmel sample on the other hand clearly contains a fracture filled with carbonate and heavy mineral precipitation. This is the only sample which shows carbonate deposition due to a fracture (see fig.96). Based on the number of slices and the resolution, the carbonate precipitation on the Carmel sample is not more than 4 mm thick. Based on these findings, the exact influence of a fracture on carbonate precipitation can be summarized to be minimal. In the case of sample car614 the influence is clearly seen, but in all other samples the fracture seems to have had no influence or overruled by other (depositional) phenomena.

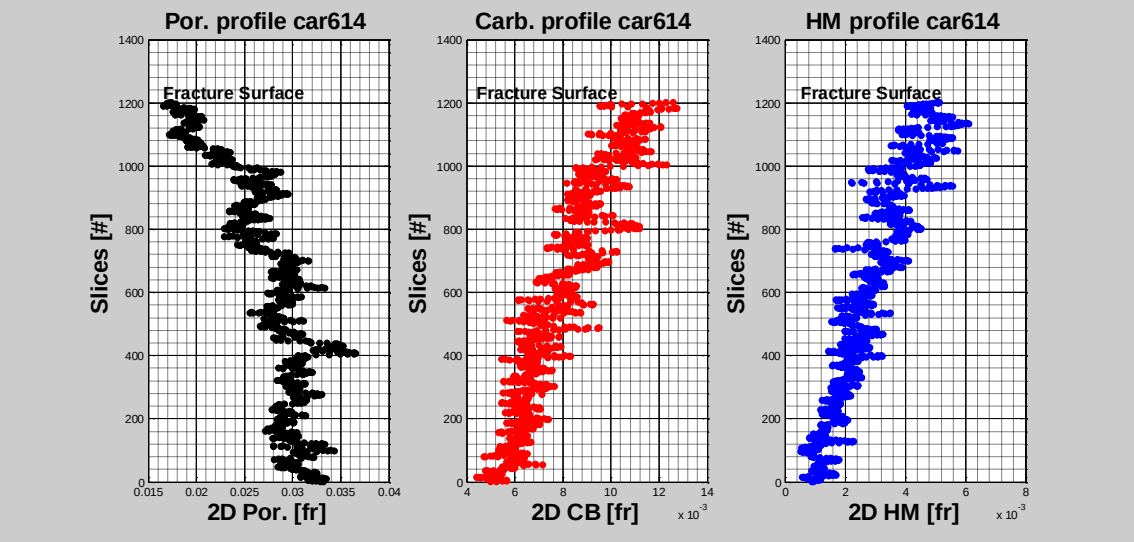

Figure-96: Cat-1: porosity, carbonate and heavy minerals profile

Wigley et al. (2012) state in their paper that red sandstones have been bleached by diagenetic CO_2 –charged brine fluids. Mineralogical and chemical methods provide profiles from unbleached to bleached sandstone which imply that a band of 1-2 cm of carbonate and an iron rich mineral is generated at the reaction front. The used method is spectroscopy. If comparing the main result of this paper to the Carmel sample (fig.96), the results are similar, where the reaction front is the fracture surface in fig.96. If comparing this result with the bleached Entrada sample in fig.97, the results are not the same. The profiles in fig.96 from top to bottom represent oxidized (red) to bleached. This transition cannot be seen in the profiles of porosity, carbonate and heavy minerals; the profiles show no clear trend. Based on this, the conclusion can be drawn that the bleaching which is clearly seen on the surface of the sample has no essential effect on the analyzed components.

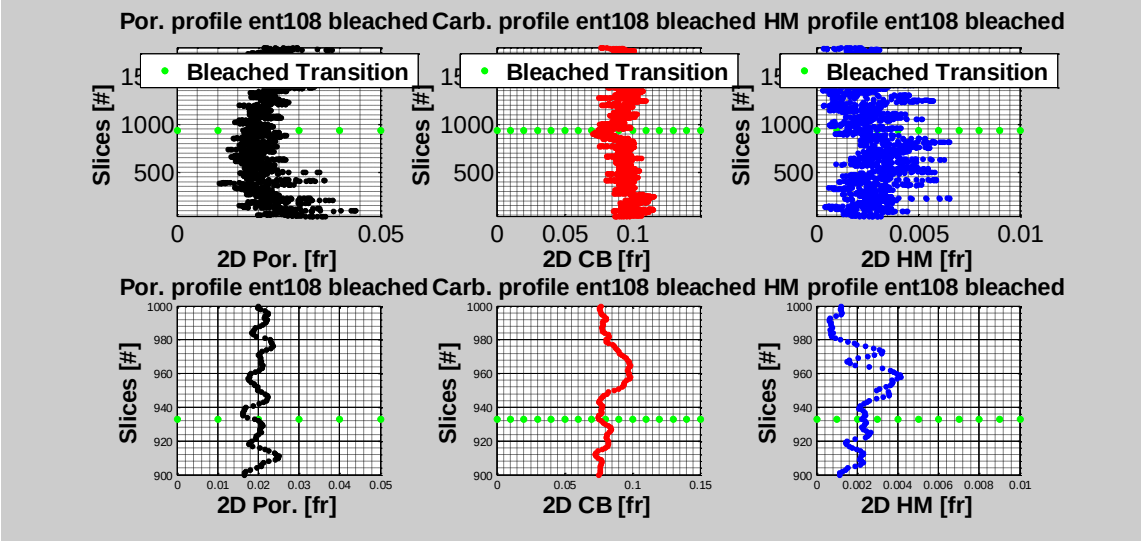

Figure-97: Bleached zone transition (ENT-108-BL); porosity, carbonate and heavy minerals profile with zoom in

Conclusions

- All 3 lab based methods (Pycnometer, Wet Test & Shell) for porosity agree with each other
- 2D and 3D image results agree with each other
- Lab based results and image based results do not agree with each other
- 2.5 microns is a reasonable resolution to quantify components
- The smaller the sample, the easier it is to obtain high resolutions
- Beam hardening correction is not a 100% perfect correction. By cutting out the edges of the sample, remaining beam hardening effects are helped to vanish.
- Lab based porosity permeability relationship is exponential and generates nice fitting coefficient
- Lab based permeability does not fit image based porosity. More likely that image based permeability will better fit image based porosity
- For the Entrada formations some correlations are found like carbonate replacing pore space meaning that the higher the carbonate fraction gets, the lower the porosity gets and the higher the carbonate particles get, the higher the pore particles get. Furthermore, the particles versus fractions generate exponential fitting.
- Blobby carbonate precipitation deforms the silica grains and increases the surface area and volumes.
- The Carmel sample clearly shows a fracture presence (carbonate and heavy mineral precipitation)
- The visibly bleached sample shows no effect on components/ microstructure
- All remaining samples show no fracture presence and are more likely affected by high heterogeneity and variability caused by other/ older deposited/ sedimentary features.
- Generally, connectivity profiles will show high anomalies if the permeability is drastically different.
- The exact influence of a fracture on carbonate precipitation can be summarized to be minimal. In the case of sample car614 the influence is clearly seen, but in all other samples the fracture seems to have had no influence or overruled by other (deposited) phenomena.

Recommendations

Various experienced difficulties and solutions which have been met during this research may help following researchers in this field:

- More calibration research should be done on micro CT technique. Nowadays, if one sample is scanned the pore space which is black is assigned to a certain grey value. However, if the same sample is scanned again or another sample is scanned, the pore space is assigned to another grey value. To optimize the detection workflow, this difference in grey values for the same components should be eliminated by for example scanning some pure components together with the samples. To know the needed pure components, an XRF/ XRD analysis would be preferable. These pure components can be placed under the sample and can be used as reference/ calibration.

- Beam hardening effects play an important role in micro CT scanning. Apart from the beam hardening correction used in the Phoenix Datos reconstruction software, another additional task can be conducted to leave out beam hardening effects which may not entirely vanish by the beam hardening correction. This is simply by cutting out the border of the sample, because the border is sensitive to the beam hardening effects.

- Generally all pore features below the highest used resolution may not be captured by the image method. It is essential to test the used resolution for robustness. By lowering the resolution the robustness can be tested. If lower resolution points generate same results as the highest used resolution, then the highest used resolution is robust. If the lower resolution points generate other results, then the chosen used resolution is not high enough and should therefore be improved before application.

- For thresholding silica grains in sandstones, an indirect method should be used. Because of the millions of silica grains in sandstones, not all of the grains have a constant density, resulting in various grey values. This hinders a good thresholding of grains. Carbonate, heavy minerals and pore space on the other hand are easier to threshold. By summing the binaries of these components and colour inverting the result, a binary of silica grains is obtained.

- If a transition zone or fracture surface is to be imaged, making a physical mark on the sample to indicate the particular surface helps a lot. Colouring will not work, because the sample is reconstructed in grey values.

- To exactly know where a particular transition zone is in a sample, make sure to cut out a symmetrical part with the transition zone in the middle. By doing this, at the end of imaging the exact position (at half of the slice numbers) is known.

- Comparison of image and lab based samples can be optimized to use the exact same sample for both methods. This means that lab methods like Pycnometer should be designed to be used on small (5 mm diameter) samples.

- The exact carbonate deposition process can be an interesting project for further analysis, especially where and how the first deposition takes place in the pore space.

- Development or adaption of Micro CT technique in order to quantify the relative 'age' of depositional carbonate to each other. This would be interesting to see which deposited material is due to fracturing and which is due to other (depositional) phenomena. This can for example be done with illumination fluids.

Bibliography

References:

- **Avizo Fire manual**
- **Barke, Gunther, Siegbert 2012. *Essentials of Chemical Education*. ISBN 978-3-642-21755-5**
- **Benson S, Cook Peter 2003. *Underground geological storage*. IPCC special report on carbon dioxide capture and storage Part-5.**
- **Bickle et al., 2014. *Drilling and sampling a natural CO_2 reservoir: Implications for fluid flow and CO_2-fluid-rock reactions during CO_2 migration through the overburden.* Volume 369, 51-82, Chemical Geology.**
- **Busch Andreas, Royal Dutch Shell, Rijswijk.**
- **co_2-cato.nl**
- **gasopslagbergermeer.nl**
- **globalccsinstitute.com/projects/browse**
- **Holland & Gilfillan 2002. *Application of noble gases to the viability of Carbon dioxide storage*.**
- **http://www.b-cube.ch/index.php?option=com_content&view=article&id=21&Itemid=19**
- **http://www.energy-pedia.com/news/norway/statoilhydros-sleipner-carbon-capture-and-storage-project-proceeding-successfully**
- **Jan Kaczmarczyk, Marek Dohnalik & Jadwiga Zalewska, 2011. *Evaluation of Carbonate Rock Permeability, with the use of X-Ray Computed Micro tomography.* NAFTA-GAZ KWEICIEN 2011, 4/2011.**
- **Kampman, N. , Bickle, M., Becker, J., Assayag, N., Chapman, H, 2009. *Feldspar dissolution kinetics and Gibbs free energy dependence in a CO_2-enriched groundwater system, Green River, Utah*. Earth and Planetary Science Letters 284, 473-488.**
- **Kampman, Niko (Courtesy through Auke Barnhoorn).**
- **Kampman et al, 2013. *Scientific drilling and downhole fluid sampling of a natural CO_2 reservoir, Green River, Utah.* Sci. Dril., 16, 33-43, 2013.**
- **Manual Ultra Pycnometer 1000**
- **Peterson, 2005. *Introduction to basic measure of a digital image for pictorial collections*. Prints & Photographs Division, Library of Congress, Washington, D.C 20540-4730.**
- **Peyman Mostaghimi, Martin Blunt and Branko Bijeljic, 2012, *Computations of Absolute Permeability on Micro-CT Images.* Math Geosci, DOI 10.1007/s11004-012-9431-4.**
- **Technical Summary IPCCAR4, Solomon, S., D. Qin, M. Manning, R.B. Alley, T. Berntsen, N.L. Bindoff, Z. Chen, A. Chidthaisong, J.M. Gregory, G.C. Hegerl,**

M. Heimann, B. Hewitson, B.J. Hoskins, F. Joos, J. Jouzel, V. Kattsov, U. Lohmann, T. Matsuno, M. Molina, N. Nicholls, J. Overpeck, G. Raga, V. Ramaswamy, J. Ren, M. Rusticucci, R. Somerville, T.F. Stocker, P. Whetton, R.A. Wood and D. Wratt, 2007: *Technical Summary In*: Climate Change 2007: The Physical Science Basis.

- **Van Meel, Joost, Image Analyst TU Delft.**
- **Wigley M., Niko Kampman, Benoit Dubacq, and Mike Bickle, 2012. *Fluid-mineral reactions and trace metal mobilization in an exhumed natural CO_2 reservoir, Green River, Utah*. The Geological Society of America, G32946.1.**

List of attachments:

Attachment_Final_Results.xls
Attachment_Pictures_Irregular.doc
Attachment_Scan_Settings.txt.
Attachment_Reconstruction_Settings.txt.